THE EUROPEAN
PHYSICAL JOURNAL C

Review

Shedding light on X17: community report

Daniele S. M. Alves[1], **Daniele Barducci**[2,3], **Gianluca Cavoto**[2,3], **Luc Darmé**[4], **Luigi Delle Rose**[5,6], **Luca Doria**[7], **Jonathan L. Feng**[8], **André Frankenthal**[9], **Ashot Gasparian**[10], **Evgueni Goudzovski**[11], **Carlo Gustavino**[3], **Shaaban Khalil**[12], **Venelin Kozhuharov**[13], **Attila J. Krasznahorkay**[14], **Tommaso Marchi**[15], **Manuel Meucci**[2,3], **Gerald A. Miller**[16], **Stefano Moretti**[17], **Marco Nardecchia**[2,3], **Enrico Nardi**[18], **Hugo Natal da Luz**[19], **Giovanni Organtini**[2,3], **Angela Papa**[20], **Ann-Kathrin Perrevoort**[21], **Vlasios Petousis**[19], **Gabriele Piperno**[2], **Mauro Raggi**[2,3,a] (ORCID), **Francesco Renga**[3], **Patrick Schwendimann**[20], **Rudolf Sýkora**[19], **Claudio Toni**[2,3], **Paolo Valente**[3], **Cecilia Voena**[3], **Cheuk-Yin Wong**[22], **Xilin Zhang**[23]

[1] Theoretical Division, Los Alamos National Laboratory, Los Alamos, NM 87544, USA
[2] Dip. di Fisica Sapienza Univ., p.le A. Moro 2, Rome, Italy
[3] INFN sez. Roma, p.le A. Moro 2, Rome, Italy
[4] Institut de Physique des 2 Infinis de Lyon (IP2I), UMR5822, CNRS/IN2P3, 69622 Villeurbanne Cedex, France
[5] Institut de Fisica d'Altes Energies (IFAE), The Barcelona Institute of Science and Technology, Campus UAB, 08193 Bellaterra, Barcelona, Spain
[6] Dipartimento di Fisica, Università della Calabria, 87036 Arcavacata di Rende, Cosenza, Italy
[7] Johannes Gutenberg-Universität Mainz, Johann-Joachim-Becher-Weg 45 D, 55128 Mainz, Germany
[8] Department of Physics and Astronomy, University of California, Los Angeles, CA 92697, USA
[9] Department of Physics, Princeton University, Princeton, USA
[10] North Carolina A&T State University, Greensboro, NC 27411, USA
[11] School of Physics and Astronomy, University of Birmingham, Edgbaston, Birmingham B15 2TT, UK
[12] Center for Fundamental Physics, Zewail City of Science and Technology, 6 October City, Giza 12588, Egypt
[13] Faculty of Physics, Sofia University, 5 J. Bourchier Blvd., 1164 Sofia, Bulgaria
[14] Institute for Nuclear Research (Atomki), P.O. Box 51, Debrecen 4001, Hungary
[15] INFN-Laboratori Nazionali di Legnaro, Legnaro, PD, Italy
[16] Department of Physics, University of Washington, Seattle, WA 98195, USA
[17] School of Physics and Astronomy, University of Southampton, Southampton SO17 1BJ, UK
[18] Istituto Nazionale di Fisica Nucleare, Laboratori Nazionali di Frascati, C.P. 13, 00044 Frascati, Italy
[19] Institute of Experimental and Applied Physics, Czech Technical University in Prague, Prague, Czech Republic
[20] Paul Scherrer Institute, Würenlingen, Switzerland
[21] Institute of Experimental Particle Physics, Karlsruhe Institute of Technology, Karlsruhe, Germany
[22] Physics Division, Oak Ridge National Laboratory, Oak Ridge, USA
[23] Facility for Rare Isotope Beams, Michigan State University, East Lansing, MI 48824, USA

Abstract The workshop "Shedding light on X17" brings together scientists looking for the existence of a possible new light particle, often referred to as X17. This hypothetical particle can explain the resonant structure observed at ~ 17 MeV in the invariant mass of electron-positron pairs, produced after excitation of nuclei such as ^{8}Be and ^{4}He by means of proton beams at the Atomki Laboratory in Debrecen. The purpose of the workshop is to discuss implications of this anomaly, in particular theoretical interpretations as well as present and future experiments aiming at confirming the result and/or at providing experimental evidence for its interpretation.

1 Executive summary

The Standard Model (SM) of particle physics has been highly successful in describing the fundamental particles and their interactions in experiments performed in the last decades. Nevertheless, the SM leaves unanswered questions on many aspects of fundamental physics, like dark matter, the origin of matter over anti-matter asymmetry in the Universe, the strong CP problem. It has been considered a low energy limit of a more complete theory implying a huge experimental and theoretical effort to search for new phenomena.

One of the most unambiguous signals of physics beyond the SM would be the observation of new particles, which in

[a] e-mail: mauro.raggi@uniroma1.it (corresponding author)

fact are searched for in a variety of experiments over a wide energy mass range.

1.1 Summary of the experimental status of X17 searches

In 2016, an experiment conducted at the Atomki laboratory (Debrecen, Hungary) [1] studied the nuclear reaction ^{7}Li(p, e$^+$e$^-$)^{8}Be. The experiment consists in exciting a target nucleus using the proton capture process, and measuring the distribution of $\theta_{e^+e^-}$, the relative angle between positron and electron (e$^+$e$^-$) produced in the Internal Pair Creation (IPC) in the transition from the exited to the ground state of ^{8}Be. Due to the very low energy of the emerging e$^+$e$^-$ pair, just a few MeV, the measurement of their angles is not a trivial task. This experiment was using a set of multiwire proportional counters placed in front of the ΔE and E detectors to determine the $\theta_{e^+e^-}$ angle. The very thin ΔE detectors were made of plastic scintillators and chosen to provide excellent γ suppression while the much thicker E detectors were used to determine the energy of the electron and positron separately (Figs. 1 and 2). A detailed description of the experimental setup can be found in [2]. The Atomki collaboration observed an enhancement around 140° in the distribution of $\theta_{e^+e^-}$ in contrast with the expectations that are based on the Rose theory [3].

The study of the IPC angular distributions has in fact a long tradition in nuclear physics. It has been used for more than 30 years to study the multi-polarity of nuclear transitions exploiting the different kinematics of magnetic and electric transitions at large angles.

After 2016 the Atomki collaboration improved the measurements in many ways [4–6] but the anomaly did not disappear. Moreover no nuclear physics model could explain it. This led to a fascinating explanation of physics beyond the SM, such as the creation of a light boson that decays in the observed e$^+$e$^-$ pair. This particle is now referred to as X17, because of the value of the observed e$^+$e$^-$ invariant mass excess. It should be noticed that ^{8}Be along with ^{4}He, is somehow a peculiar nucleus. They both exhibit states with excitation energy larger than 15 MeV with respect to the ground state, very uncommon in nuclear physics. This characteristic makes them particularly suited to search for new particles, being the accessible mass region quite large with respect to other studies of IPC performed on different nuclei.

In the first experiment [1] the ^{7}Li(p, e$^+$e$^-$)^{8}Be reaction was induced with a 1 μA proton beam impinging on 15 μg/cm^2 thick LiF$_2$ or 700 μg/cm^2 Li$_2$O targets. The proton beam energy was adjustable, so that it was possible to populate both the 18.15 MeV and 17.6 MeV ^{8}Be excited states. At the energy of the 18.15 MeV transition, a 6.8σ significant anomaly was observed in the e$^+$e$^-$ angular correlation, explainable with the production and the sub-
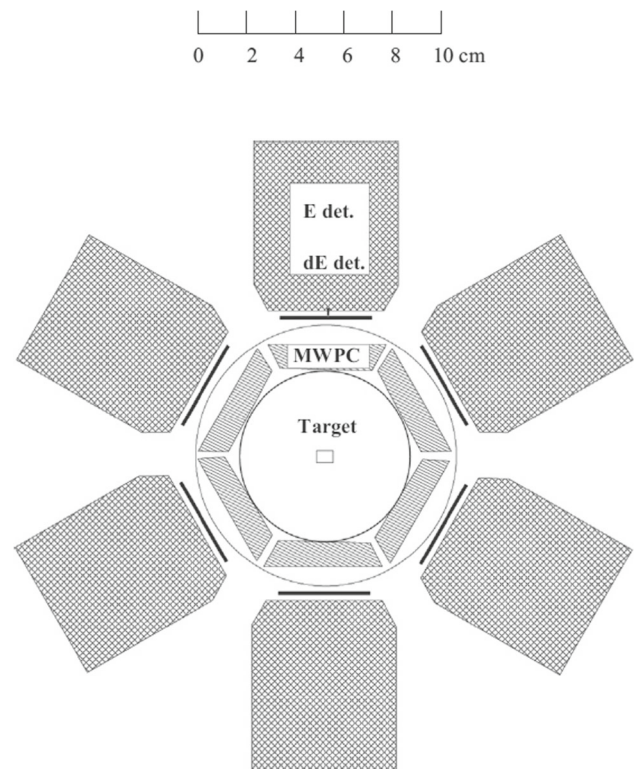
Fig. 1 The Atomki spectrometer layout

Fig. 2 The Atomki 5 arms spectrometer used in the first ^{8}Be measurement in 2016

sequent decay of a new particle with mass 16.7 MeV. The anomaly was defined as the difference of the experimental data distribution with respect to the expectation of a mixed E1+M1 angular correlation, according to the Rose theory. No anomaly was observed in the 17.6 MeV/c^2 transition. Several independent checks ruled out any instrument-related systematic effect.

The anomaly was re-investigated and confirmed in the same nuclear reaction in 2017 with a new and more stable accelerator and an improved tracking detector [4] and in 2018 with a further improved experimental apparatus and a new analysis method to subtract the background from cosmic rays [5]. The best estimate of the hypothetical particle mass was found to be 17.01(16) MeV/c^2.

Since 2019 the same collaboration studies the ^{3}H(p, γ)^{4}He reaction induced with different proton energies. A similar anomaly was observed in the 21.01 MeV $0^- \to 0^+$ transition of ^{4}He [6]. The experimental apparatus was not changed with respect to the previous ^{8}Be measurement except for the ^{3}H target. Also in this study an evident peak around $\theta = 115^o$ was found that could not be explained with the IPC background simulations and measurements. The effect was observed with a high statistical significance (greater than 6.6 σ) at the same invariant mass.

Several experimental aspects support the hypothesis that the Atomki anomaly is a genuine effect:

- The statistical significance of the observations is always >6 standard deviations.
- The anomaly has been observed in ^{8}Be using two different experimental setups: 5 and 6 arms spectrometers.
- The anomaly has been observed using different position sensitive detectors: multiwire chambers and silicon strip detectors.
- The anomaly has been observed in two different target nuclei ^{8}Be and ^{4}He and shows up at different value of the angle.
- The anomaly has been observed with different proton beam energies.
- The anomaly has not been observed in calibration atoms i.e. ^{16}O during the same data taking period.
- The anomaly has not been observed in events with asymmetric momentum e^+e^- pairs.

However, despite the consistency of the several observations at Atomki, more experimental data are needed to understand the nature of this anomaly. For this reason many experiments all over the world looked for such particle in different channels, or are planning to do so. Many of these experiments already put constraints on the coupling of this hypothetical particle with ordinary matter, while others are still in the R&D phase, but they will soon contribute a deeper understanding of this phenomenon.

An important aspect of the experimental effort is the direct confirmation of the Atomki measurement. While it was shown that the same detector gives the same result, it still has to be proven that the anomaly is not an artefact of the detector geometry, as suggested in [7]. Also measuring the e^+e^- invariant mass at the X17 observed peak with a better precision can add information. For example, if the width of the peak remains unchanged even though the resolution gets better, this would rule out the existence of the hypothetical particle, that has a much narrower predicted width (order of 10^{-5} eV [8] than the experimental resolution).

Therefore there are numerous experiments that want to look for the hypothetical X17 in IPC from nuclear transitions, as the experiment at Atomki did.

The MEG II experiment [9] at the Paul Scherrer Institute in Switzerland, whose principal goal is to search for the lepton flavor violating decay $\mu^+ \to e^+\gamma$, plans to repeat the ^{7}Li(p, e^+e^-)^{8}Be measurement. A Cockroft–Walton accelerator is available to produce a 1–100 µA beam of up to 1.1 MeV protons. MEG II aims at obtaining an improved invariant mass resolution and extending the study to larger angular acceptance, thanks to its spectrometer composed of a high resolution drift chamber tracker in a non-uniform magnetic field.

The Institute of Experimental and Applied Physics (IEAP [10]) at Czech Technical University (CTU) in Prague is designing a new experiment to measure IPC in different nuclear reactions. The IEAP proposed the COmpact Positron Electron spectrometer (COPE) to have a full measurement of the X17 decay products. This detector will allow to measure with high precision the pairs from IPC integrating a silicon based Timepix detector in vacuum with gas detectors.

The Laboratori Nazionali di Legnaro (LNL [11]) are equipped with a 2 MV Van de Graaff accelerator that can deliver a proton beam current of 1 µA. The protons from this accelerator can be used to excite the nuclear states from which an X17 can be emitted, so a e^+e^- scintillator-based modular detector has been proposed to perform a measurement very similar to the Atomki one. The goal is to measure the X17 decay products in the ^{8}Be and ^{12}C de-excitation with a very good angular resolution thanks to the low material budget and a good angular coverage to reach the goal of 1% invariant mass resolution. A prototype module has been built and calibrated with a radioactive sources recently.

Given the observation of the anomaly in a proton induced nuclear reaction a proposal of using a neutron beam to induce the ^{3}He(n,X)^{4}He reaction is thought to be complementary. The ^{4}He de-excitation has been proposed to be studied at the nToF [12] facility at CERN. The nToF in fact provides a pulsed neutron beam with an energy up to $E_n = 100$ MeV.

The ^{4}He de-excitation might also be explored at the LUNA-MV facility [13] at Laboratori Nazionali del Gran Sasso (LNGS). LUNA-MV is a high intensity proton beam

accelerator that can provide a proton beam with a maximum current of $100\,\mu A$, thus being able to produce the $^3H(p,X)^4He$ reaction. This might shed some light on the hypothesis that the X17 might be the carrier of protophobic interaction.

Finally, the UdeM 6 MV Tandem Van de Graaff Facility at CCPAC [14] in Montreal is able to produce a ^3He beam, and has a beamline dedicated to the X17 measurement in the reaction $^7Li(^3He, \gamma)^{10}Be$. Its goal is to measure IPC in ^8Be and ^{10}B nuclear reactions with a 95% angular acceptance to remove any possible bias introduced by the experimental apparatus.

Besides these tests of direct confirmation of the Atomki results a search of X17 can be conducted also at higher energy accelerators. If the X17 exists, it might be produced in the $e^-Z \to e^-ZX$ Bremsstrahlung reaction, that can be obtained from a high energy electron beam impinging on an active target. The NA64 experiment at CERN was able to perform this measurement in 2017–2018 collecting a statistics of 8.4×10^{10} electrons. The NA64 collaboration did not find any evidence of the existence of the X17 particle, but managed to set constraints to its coupling to electrons. They set a limit on the coupling of the X17 with electrons to be less than 6.8×10^{-4} for a mass value of 16.7 MeV [15].

Another experiment at the CERN SPS, NA48/2, collected in 2003–2004 a sample of π^0 from $\sim 2 \times 10^{11}$ charged kaon decays in flight [16]. The decay of π^0 mesons produced in the kaon decays is a good tool to search for a hypothetical dark boson, expected to be produced in $\pi^0 \to \gamma X$, $X \to e^+e^-$. In the X17 mass range the NA48/2 experiment obtained an upper limit on ϵ^2, the vector coupling of dark photon to Standard Model particles, of order of few 10^{-7} [17], improving existing limits from other experiments. The upgraded experiment NA62, which is currently running, will achieve larger statistics with an improved e^+e^- invariant mass resolution and a better background rejection.

A study of the resonant production of the X17 with a positron beam would be highly desirable. The Positron Annihilation into Dark Matter Experiment PADME [18], at Laboratori Nazionali di Frascati (LNF) is well suited to explore this. The LNF linear accelerator used in this experiment can in fact deliver a positron beam with energy in the range 250–550 MeV/c^2 to a 100 µm diamond target to produce X17 from a e^+e^- annihilation.

A search for the dark photon A′ is foreseen also at the Mu3e experiment [19] at Paul Scherrer Institut (PSI). The experiment is built to look for charged Lepton Flavor violation in the $\mu^+ \to e^+e^-e^+$ channel, but can also be used to search for dark photons in the mass range 10–80 MeV/c^2 in the decay $\mu^+ \to e^+\nu_e, \bar{\nu}_\mu A'$, with A′ $\to e^+e^-$. It can explore the kinetic-mixing parameter region up to $\epsilon^2 \sim 10^{-8}$.

Other experiments where it will be possible to search for the X17 are FASER [20] at CERN, DarkLight [21] and

HPS [22] at JLAB, VEPP-3 [23] at Novosibirsk and the MAGIX and DarkMESA experiments foreseen at the MESA accelerator complex at Mainz [24].

Also searches in charmed meson and J/Ψ decays have been proposed [25,26], that can be explored at BelleII (SuperKekB), BESIII (BEPCII) and LHCB (CERN).

The anomalous signals observed by the Atomki collaboration in multiple experiments analysing the $^8Be^* \to {}^8Be + e^+e^-$ and $^4He^* \to {}^4He + e^+e^-$ transitions call for an explanation. Given the level of significance of these measurements, both around the 7σ value, the option of a statistical fluctuation is excluded. To date it is fair to conclude that no plausible experimental source of error has been identified. The compatibility of the observed angular anomalies in the different target nuclei with the same new particle mass, strongly supports the hypothesis of a new effect. At the same time, however, the Atomki results requires an independent experimental confirmation in order to be firmly established beyond any reasonable doubt. Strong effort is foreseen in the next few years to confirm the Atomki results in different international laboratories.

1.2 Summary of the theoretical perspectives on the X17

From the theoretical side if one assumes the robustness of the experimental results the anomaly may be explained by[1]

(i) A SM and/or nuclear physics effect that has not been accounted for
(ii) A beyond the SM effect, given by a new unknown degree of freedom beyond the SM particle content.

Both options have received considerable attention in the literature, admittedly more regarding (ii) than (i). This is not only due to the possible existence of the long sought physics beyond the SM, although the possibility of simultaneously explaining in a common framework the Atomki measurement and other open questions of the SM is definitively intriguing and acts as a trigger for many theoretical works. It is the characteristic feature of the anomalous signals itself that makes these results fascinating from a new physics perspective. The anomalies show simple but well defined properties, which are

– the excesses are resonant bumps located, within the experimental errors, at the same e^+e^- invariant mass both in the ^8Be and in the ^4He transition;
– the e^+e^- opening angles of the anomalous peaks in the two transitions, that have different available energy in their decay, vary in a way which is compatible with the kinematic of a 17 MeV boson decaying into a lepton pair;

---

[1] Obviously, there is also the possibility of a combination of the two effects.

– the anomalous signal in the ^{8}Be transition has been observed only inside the kinematic region given by $|y| < 0.5$, where y is the energy asymmetry of the lepton pair (i.e. the ratio of the difference and the sum of their energies).

The X17 hypothesis would naturally explain such non-trivial features of the observed signal.

Before introducing and commenting upon the more compelling, yet speculative, possibilities in terms of physics beyond the SM that has been proposed in the literature, let us review the options that have been pushed forward for the case of an unaccounted SM and/or nuclear physics effect. These may either completely explain the experimental measurements or reduce their statistical significance to a more modest level, compatible with a fluctuation which might disappear with more data. Given the nature of the anomaly, which is measured in low energy nuclear transitions, various works have studied the possibility of some neglected or poorly understood nuclear physics effects. Along this line of reasoning the first step has been taken in [27]. Here the Authors improved upon the nuclear physics modelling of the reaction in multiple directions by using an effective field theory framework and conclude that the probability of unknown nuclear effects explaining the Atomki anomalies are very low. They found that the length scale of the nuclear form factor needed to explain the anomalous signal is larger than the one observed in nuclear scattering experiments. We refer to their contribution in Sect. 3 for more details. Some years later in [28] the possibility that the anomalous signal could be given by a nuclear decay chain with the subsequent conversion of two highly energetic γs into an e^+e^- pair has been investigated. While both the rates and the kinematic fits nicely agree with the experimental results the Author himself concludes that "*The assumed nuclear chain reaction is not favoured in the established nuclear models and no explanation for the isospin structure of the signal can be given. Thus, it has to be concluded that the process studied in this paper does not give a completely satisfying explanation of the X17 puzzle.*". For what concerns possible SM explanations, various Authors have proposed that the X17 resonance may be a new exotic QCD bound state. In [29] it has been proposed that the X17 resonance might be identified with a tetraquark, i.e. a four quarks QCD bound state, made up by first generation quarks. The proposed explanation predicts however a second degenerate resonance with a different width, but unobserved. More recently in [30] the even more exotic possibility of an hexadiquark, i.e. a 12 quarks bound state, has been advanced, albeit in this framework only the ^{4}He anomaly can be addressed. Another exotic explanation in terms of a composite system of a light quark and a light antiquark confined by the QED interaction has been proposed in [31] and we refer to the Author's contribution

in Sect. 3 for this latter option. Finally, on less exotic lines, the Authors of [7] have instead claimed that the experimental results can be reproduced within the SM by carefully considering the full set of next to leading order corrections and the interference terms to the Born-level decay amplitudes, also proposing some experimental improvements in order to test this hypothesis. All together it is fair to say that no firm explanation of the Atomki measurements in terms of SM effects has been established. While this automatically pushes forward the possibility of beyond the SM physics, more work on possible SM explanations should be pursued in order to conclusively reject this hypothesis.

Moving on the more speculative side of the existence of a new dynamical degree of freedom beyond the SM, many more scenarios have been advanced.[2] The lightness of the putative X17 resonances is particularly intriguing, in that it could be interpreted within the framework of a light and weakly coupled dark sector with possible connection with Dark Matter physics. It could also leave its imprint in other astrophysical and cosmological observables, providing additional handles to disentangle its nature. This is an area of research which has gained increasing attention in the last years from both the theoretical and experimental side, clearly motivated by the lack of TeV scale new physics in high p_T experiments at the LHC. Intriguing connections with the solution of the strong CP problem and axion physics have also been made [32,33] and will be presented in Sect. 3. A light resonance could also be of relevance for the explanation of other experimental anomalies reported in recent years. This is the case, e.g., of the anomalous magnetic moment of the muon [34], the neutron lifetime anomaly [35] and the NuTeV anomaly [36].

It remains however a concrete possibility that the X17 resonance is not related to the resolution of any of the SM shortcomings nor to other experimental anomalies, but is the manifestation of truly unexpected new physics. Needless to say this is an exciting possibility, which however raises more questions than answers. The mere observation of the ^{8}Be and ^{4}He transitions restrict the X17 boson to be either a vector, an axial vector or a pseudoscalar, under the assumption of definite parity. These possibilities have been all investigated in the recent literature. Solutions with mixed parity, even if possible, have been less explored so far. Feng and coworkers were the first to consider the X17 hypothesis and mainly focused on the pure vector scenario [37–39]. They found that the main experimental constraint of such a scenario comes from the search of the pion decay $\pi^0 \rightarrow \gamma(X \rightarrow e^+e^-)$ by the NA48/2 collaboration, whose null results require the

---

[2] It is not the purpose of this Introduction to review or enumerate all proposed theoretical explanations for the Atomki anomalies. We refer to https://inspirehep.net/literature/1358248 for a full updated reference list.

new particle to be "protophobic", i.e. to have a suppressed coupling to the proton. Working in an effective field theory framework, they claim a protophobic vector boson could simultaneously explain both the anomalies in the ^{8}Be and ^{4}He transitions. Later on, however, Zhang and Miller [40] pointed out that the contribution from the direct proton capture for a protophobic vector boson with mass around 17 MeV would be dominant with respect to the contribution from the ^{8}Be(18.15) resonance, in contradiction with experimental observation that the anomaly disappears off the nuclear resonance.

Kozackzuk and coworkers investigated instead the case of an axial vector [41]. The authors applied a multipole expansion method to the anomalous nuclear decay rates and evaluated the related nuclear matrix elements by ab-initio calculation using realistic nuclear forces. Their estimation concludes that the X17 axial coupling to quark should be order $\mathcal{O}(10^{-4}-10^{-5})$ to explain the anomalous signal in the ^{8}Be transition. Apparently an axial boson of 17 MeV with such range of couplings is still viable and not excluded by experimental research.

The last scenario, relative to a light pseudoscalar, has been analyzed by Ellwanger and Moretti [42]. The authors made a rough estimation of the range of the values of the Yukawa couplings, assuming a nuclear shell model for the ^{8}Be nucleus. The strongest constrains they reported comes from the flavour changing neutral current interactions due to a light pseudoscalar, especially from $K \to \pi + X$ decays.

Beyond such generic studies of the X17 properties, for which we refer to [43] for a recent study, some work has been done on BSM models which could include a 17 MeV boson. In particular, Delle Rose and coworkers have considered extensions of the Standard Model with a gauged $U(1)'$ symmetry [44]. The authors identify various scenarios able to provide a light Z' boson with interactions explaining the anomalous signal of Atomki searches, even including in the discussion the possibility of an additional Higgs doublet or more complicated Yukawa structures.

Altogether the anomalous signal measured by the Atomki collaboration shows particular features, which could be explained by assuming the existence of a new particle with a mass around 17 MeV. Trivial theoretical considerations require the new particle to be a neutral boson and restrict its spin-parity assignments to be a vector, an axial vector or a pseudoscalar, if one assumes definite parity. A pure scalar solution is excluded by parity conservation, given the observation of the anomalous signal in the ^{8}Be transition. Other than the intriguing solution of a new particle, however, alternative explanations relying, e.g., on underestimated experimental systematic effects or some yet unidentified additional SM contribution, are still possible and ask for further investigations. To conclude, there are many theoretical attempts to understand the observed signal. No unique explanation exists, however the claim of a new particle hinting at physics beyond the Standard Model is an intriguing possibility.

1.3 The Shedding light on X17 workshop

This volume summarises the contributions presented at the "Shedding light on X17" workshop held at the Centro Enrico Fermi in Rome form September 6th to September 8th 2021 which brought together in Rome nuclear, theoretical, and experimental particle physicists, interested in discussing the origin of the anomaly observed at the Atomki Laboratory, its interpretation and future experimental efforts to confirm and explain this observation.

The conference was divided into tree main sessions:

– Experiments on Internal Pair Creation
– Theoretical interpretations
– Beyond the Standard Model experimental searches for X17.

In the "Experiments on Internal Pair Creation" sections the most recent experimental results obtained at the Atomki Laboratory and the techniques they used are presented. Possible theoretical interpretations are discussed in the "Theoretical interpretations sections". Finally in the "Beyond the Standard Model searches for X17" section we will review the status of past, present and future experiments aiming at detecting a possible X17 particle not related to IPC measurements.

The Shedding Light on X17 participants at the entrance of the historical building of the "Istituto di Fisica" di via Panisperna in Roma.

2 Experiments on internal pair creation

2.1 X17: status of the experiments on ^{8}Be and ^{4}He

Attila J. Krasznahorkay

Institute for Nuclear Research (ATOMKI), P.O. Box 51, H-4001 Debrecen, Hungary

Abstract The angular correlation of e^+e^- pairs produced in the $^7\text{Li}(p, \gamma)^8\text{Be}$ and in the $^3\text{H}(p, \gamma)^4\text{He}$ reactions have been studied at several proton energies and significant deviations from the standard theoretical expectations were observed at large angles, between $110° \leq \theta_{e^+e^-} \leq 150°$ (where $\theta_{e^+e^-}$ is the angle between e^+e^- momenta) supporting the formation and the subsequent decay of a hypothetical particle, recently named X17. We found that the particle is created most probably in the direct proton capture, and not in the M1 decay of the 18.15 MeV $J^\pi = 1^+$ state as previously supposed. As a consequence, our present results strengthen the vector boson interpretation of the data.

A very challenging experimental campaign was initiated in the late seventies to search for a new particle, the QCD axion, which was predicted by Weinberg [45,46] and which is one of the most compelling solutions to the strong CP problem [47,48]. Donnelly et al. [49] proposed to study the angular correlation of the e^+e^- pairs created in $1^+ \rightarrow 0^+$ nuclear transitions by tracking the signatures of the two-body decay of the axion. However, the axion was rapidly ruled out in the MeV/c^2 mass regime casting a shadow on these experiments.

The hunting for heavier particles, in particular around 9 MeV/c^2, was originally suggested by de Boer and van Dantzig [50]. They performed a series of experiments at the University of Frankfurt, which was discontinued after the shutdown of their accelerator [51]. Soon later, their e^+e^- spectrometer [52] was transferred from Frankfurt to Debrecen and the search for the 9-MeV/c^2 particle could be restarted at the ATOMKI accelerator facilities. However, the low efficiency of the spectrometer and the observed large background did not allow the detection of the expected weak signal of the decay of such a particle.

To improve the sensitivity of the apparatus, we developed a new spectrometer [2] with an almost three order of magnitude higher efficiency. Using this upgraded spectrometer, we re-investigated the reaction of $^7\text{Li}(p, \gamma)^8\text{Be}$ first studied by de Boer, but no signatures of the 9 MeV/c^2 particle was found. As a next step, our spectrometer was again modified and adapted to study the e^+e^- angular correlation in a wider angular range up to 180°, and thus the mass range sensitivity was extended to search for particles heavier than 9 MeV/c^2.

In 2014, the $^7\text{Li}(p, \gamma)^8\text{Be}$ reaction was reinvestigated, and the angular correlation of the e^+e^- pairs formed in the 17.6 MeV and 18.15 MeV $1^+ \rightarrow 0^+$ transitions was measured. In the 18.15 MeV transition, a significant anomaly was observed at large angles ($\theta_{e^+e^-} = 140°$) signalling the formation and the subsequent decay of a 16.7 MeV/c^2 particle, called later on the X17 particle. At the same time no anomaly was identified in the 17.6 MeV transition. The angular corre-
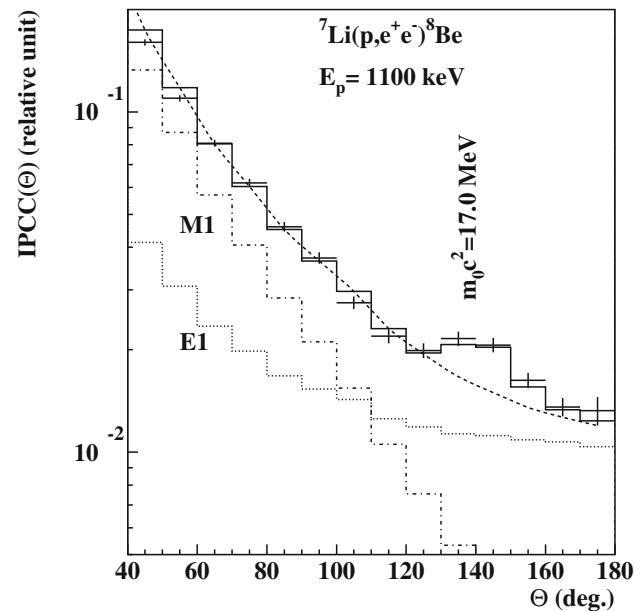


Fig. 3 Comparison of the experimental results obtained for the 18.15 MeV transition of ^8Be (dots with error bars) and the simulated angular correlations of the e^+e^- pairs assuming E1 (dotted line) and M1 (dashed dotted line) multipolarities. The best fit (black histogram) is a sum of the simulated backgrounds (dashed line) and the simulated contribution of the hypothetical X17 boson

lations obtained at $E_p = 1100$ keV, and at $E_p = 450$ keV are presented in Figs. 3 and 4, respectively. Before publishing our results [1], we performed several independent measurements to make our results solid by ruling out any instrument-related artifacts.

In the data analysis of our measurements, a complex, but straight-forward fitting procedure was applied to derive the mass of the decaying hypothetical particle [53]. As a first step, the E1 and M1 internal e^+e^- pair angular correlations are simulated with GEANT3, and their combination was fitted to the measured angular correlation data in the $40° \leq \theta_{e^+e^-} \leq 130°$ angular range to extract the mixing ratio of I(M1)/I(E1). The anomaly was then defined as the difference of the experimental and simulated distributions and fitted in the full angular range with the simulated contribution of the e^+e^- decay of X17 on top of the mixed E1+M1 angular correlation. In all cases, the fit of the original experimental data was performed with the RooFit toolkit [54,55].

The possible relation of the X17 boson to the dark matter problem has triggered an enormous interest in a wider physics community [56]. The first theoretical interpretation of our experimental results was provided by Feng and co-workers [8,57]. They generalized the dark photon theory by coupling the X17 particle to the quarks along with the electric charge and determined the coupling constants by considering all existing experimental data including also our new observations. They introduced their theory as "protophobic" since
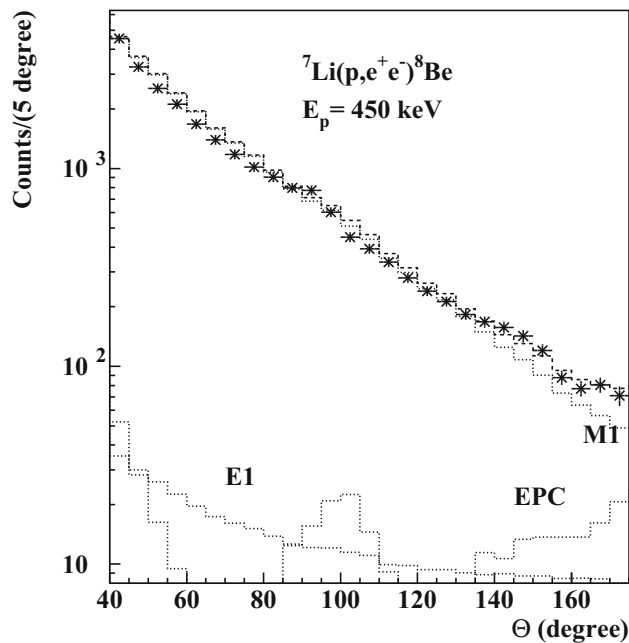
Fig. 4 e^+e^- angular correlations obtained for the 17.6 MeV transition of ^{8}Be by using a thin target (snow flakes). The results of the simulations performed for M1 and for E1 transitions as well as for the external pair creation (EPC) are indicated as dotted histograms and their sum (dashed histogram) fitted to the experimental data are also shown

Table 1 Internal Pair Creation Coefficients (IPCC), X17 Boson branching ratios (B_x), masses of the X17 particle, and confidences derived from the fits obtained in the experiment with tritium target. Errors are given in parenthesis

E_p (keV)	IPCC $\times 10^{-4}$	B_x $\times 10^{-6}$	Mass (MeV/c^2)	Confidence
510	2.5(3)	6.2(7)	17.01(12)	7.3σ
610	1.0(7)	4.1(6)	16.88(16)	6.6σ
900	1.1(11)	6.5(20)	16.68(30)	8.9σ
Averages		5.1(13)	16.94(12)	
^{8}Be values		6	16.70(35)	

the coupling of X17 to protons was found to be much weaker than to neutrons. In contrast to our published results [1], they predicted that the X17 particle should also be created in the 17.6 MeV transition of the ^{8}Be with a reduced boson to γ-decay branching ratio of $B_x(17.6) \approx 0.435 \times B_x(18.15)$ according to the phase-space suppression factor.

Ellwanger and Moretti formulated another possible explanation of our experimental results through a light, pseudoscalar particle [58]. Given the quantum-numbers of the initial and final states of ^{8}Be, the X17 boson could still be a $J^\pi = 0^-$ pseudoscalar particle, if it was emitted with L = 1 orbital momentum. A ten times smaller branching ratio was estimated for the 17.6-MeV transition compared to the 18.15 MeV one, which was in a good agreement with our experimental results.

Alves and Weiner [59], Alves [60] and Liu et al. [61] revisited the experimental constraints on the QCD axions in the $O(10$ MeV) mass window, and they found a variant axion model that remains compatible with the existing constraints. This reopened the possibility of solving the strong CP problem. Such axions or axion-like particles (ALPs) are expected to decay predominantly by the emission of e^+e^- pairs.

In 2017, we re-investigated the ^{8}Be anomaly in the 18.15-MeV transition with an improved and independent setup. We have confirmed the signal of the assumed X17 particle and constrained its mass [$m_X = 17.01(16)$ MeV] and branching ratio [$B_x = 6(1) \times 10^{-6}$] [62,63]. We repeated the experi-

ment also for the 17.6-MeV M1 transition in ^{8}Be to validate the different theoretical predictions, but different branching ratios [4,5,64] were found in a number of different measurements. We recognized a more pronounced anomaly for thicker targets which could be explained by the larger integrated energy range of the non-resonant, direct proton capture contribution to the excitation function.

Very recently, we also observed a similar anomaly in ^{4}He by employing the ^{3}H(p, γ)^{4}He reaction at different proton energies [53,63,65,66]. The values obtained for the mass and branching ratio of the X17 boson and for the IPC coefficients are summarized in Table 1.

Figure 5 presents the measured angular correlations of e^+e^- for $E_p = 510$, 610 and 900 keV together with the fit of the simulated background and the simulated contribution of the hypothetical X17 boson.

The particle mass extracted from the present dataset is [$m_X = 16.94 \pm 0.12$(stat.)± 0.21(syst.) MeV]. It agrees reasonably well with the mass of the previously proposed X17 boson. It was also shown that the branching ratios of X17 are identical within uncertainties for all three beam energies, proving that the X17 was most probably created in the direct proton capture having a dominant multipolarity of E1. Our present results obtained for ^{4}He at different beam energies is supported by the theoretical results of Viviani et al. [67], who calculated the e^+e^- pair production in the four nucleon system by using state-of-the-art approach to nuclear strong-interaction dynamics and nuclear electromagnetic currents.

Zhang and Miller [68] studied the protophobic vector boson explanation by deriving an isospin relation between the coupling of photon and X17 to nucleons. They concluded that the X17 production may be dominated by direct capture transitions and a smooth energy dependence is predicted for all proton beam energies above the 17.6 MeV $J^\pi = 1^+$ resonance [68], but not for the resonance for which the M1-induced X17 production was found to be very important.

In our very recent work [54], we report the results of the measurements of the angular correlations of the e^+e^- pairs created in the ^{7}Li(p, γ) reaction at proton energies of
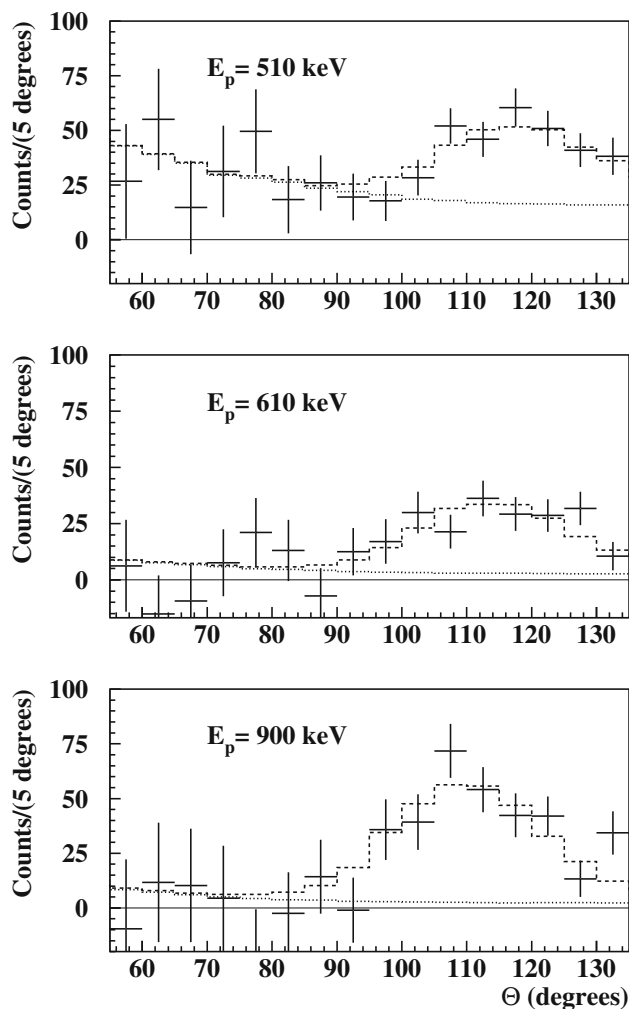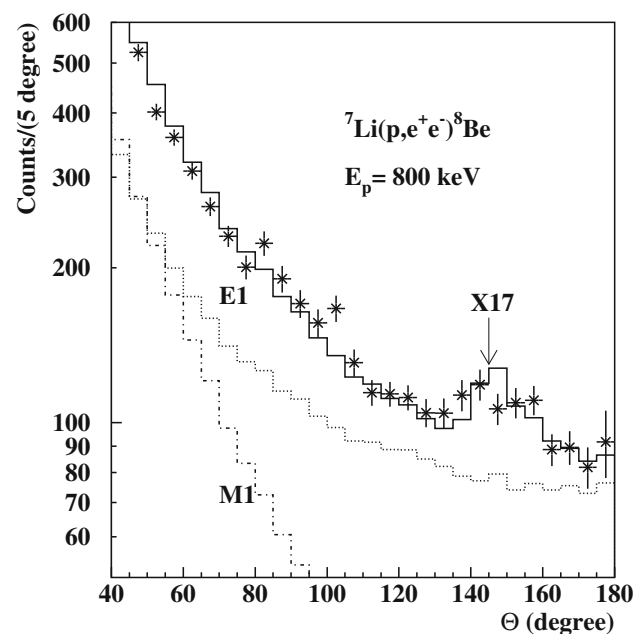
Fig. 5 Comparison of the experimental and the simulated angular correlations of the e^+e^- pairs obtained for ^{4}He at different proton bombarding energies as indicated in the figures. The best fit (dashed line) as the sum of the simulated background (dotted line) and the simulated contribution of the hypothetical X17 boson is compared with the experimental signal values (dots with error bars)

$E_p = 450$ keV, 650 keV, 800 keV and 1100 keV. As a typical example, Fig. 6 shows the angular correlation measured at $E_p = 800$ keV.

The resonance at 18.15 MeV is much wider ($\Gamma = 138$ keV) than the resonance at 17.6 MeV ($\Gamma = 10.7$ keV) in ^{7}Li$(p, \gamma)^8$Be and due to the distributed strength, the peak-to-background ratio at E = 18.15 MeV is two orders of magnitude smaller than at 17.6 MeV. In both cases, the background stems from the direct capture of protons, and its multipolarity is essentially E1.

The present data suggests that the X17 boson does not only form in the 18.15-MeV M1 transition, it appears to be generated also in the direct proton capture. Stable LiF targets could only be applied for the excitation of the 17.6-MeV resonance, but at higher proton energies (above $E_p = 441$ keV), the

Fig. 6 Comparison of the experimental and the simulated angular correlations of the e^+e^- pairs obtained from the ^{7}Li$(p, e^+e^-)^8$Be reaction at a proton bombarding energy of 800 keV. The best fitted sum (solid line) as sum of the simulated background for E1 (dotted line) and M1 (dashed line) transitions and the simulated contribution of the hypothetical X17 boson is compared with the experimental signal values (snow flakes with error bars)

6.05-MeV $0^+ \rightarrow 0^+$ transition is also excited by the nuclear reaction of ^{19}F$(p, \alpha)^{16}$O. The very intense e^+e^- yield created in the $0^+ \rightarrow 0^+$ transition would hinder the measurement of the much weaker transitions in focus. Therefore, in our previous experiments, metallic Li targets (on Al backings) were applied with LiF only appearing as a contaminant. Even though treated in Ar atmosphere, the targets were found to be very unstable: the Li was heated by the beam and diffused into the Al backing. The targets were quickly degraded and the diffusion increased the effective target (Li layer) thickness significantly. As a result, our target integrated undetermined regions of the background varying also with time. Thus, the previously measured excitation function of the anomaly cannot prove that the anomaly was created only in the 18.15 MeV M1 transition. In contrast, we used much more stable Li$_2$O targets in the present experiment to avoid the above uncertainty in the effective proton energy.

In conclusion, the major features of the spectra can be described convincingly by considering both the internal pair creations (IPC) in the M1 decay of the 1^+ states and the E1 following the direct proton capture of ^{7}Li. However, a peak-like, anomalous excess of the e^+e^- pairs in the angular correlation spectra around 140° was observed weakly at $E_p = 650$ and 800 keV as well.

Table 2 The fitted mass [m(X17)] and the integrated yields I(X17), I(E1) and I(M1) of the X17, the E1 and the M1 contributions. The ratio of I(X17)/(I(E1)+I(M1)) is also highlighted [B(X17)]

E_p (keV)	m(X17) (MeV/c^2)	I(X17)	I(E1)	I(M1)	B(X17)
450	16.6(3)	43(49)	30(25)	79(2)	0.39(44)
650	16.94(14)	24(16)	46(5)	32(4)	0.31(19)
800	16.81(9)	33(10)	62(4)	5.9(4)	0.49(13)
1100	17.11(12)	28(8)	66(2)	15(1)	0.35(11)

The fitted parameters for the E1 and M1 IPC distributions as well as the contribution of the X17 particle are summarized in Table 2.

The ratio of I(M1)/I(E1) determined for $E_p = 1100$ keV is about a factor of two larger than the ratio extracted for $E_p = 800$ keV as suggested also by Hayes and co-workers (Fig. 3 of Ref. [69]).

In summary, our recent result revealed that the particle is created both in the direct proton capture and in the M1 decay of the 18.15 MeV $J^\pi = 1^+$ state. The results obtained for ^{8}Be at different beam energies agree reasonably with the prediction of Zhang and Miller [68], except for the 17.6 MeV sharp resonance. They found the contribution of the M1-induced X17 creation more significant there, than the one we observed.

According to the experimental results, the protophobic X17 particle could be produced in the direct capture dominated resonance-free regime as well. At the same time, it strengthens the $J^\pi = 1^-$ vector boson interpretation of the data [8]. Given the X17 particle seems to be created in E1 transitions, we are now planning to observe it in the decay of Giant Dipole Resonance (GDR) excitations of different nuclei as well.

2.1.1 Acknowledgements

2.2 X17 search with the MEGII apparatus

Angela Papa for the MEGII collaboration

Abstract The MEGII experiment has successfully completed its upgrade and just recently started data taking. The astonishing expected performances of the new and upgraded detectors in MEGII, together with the availability of a Cockcroft–Walton (CW) accelerator normally used for MEGII calibration purposes, turn out to offer a great opportunity to search for a light neutral boson via nuclear reactions. The intense proton beam delivered by the MEGII CW accelerator, impinging on a thin Li-compound target can be used for this purpose. The conceptual design, the experimental method and feasibility studies in view of the search for the hypothetical X17 possibly observed at ATOMKI are described.

2.2.1 Introduction

The MEG experiment has set the most stringent upper limit on the $\mu^+ \to e^+\gamma$ decay, BR ($\mu^+ \to e^+\gamma < 4.2 \times 10^{-13}$ @90% CL) [70]. An upgrade of the experiment (MEGII) has been successfully completed to increase the sensitivity on the $\mu^+ \to e^+\gamma$ decay search down to $\mathcal{O}(6 \times 10^{-14})$.

The characteristics of the MEGII experiment allow for a precise measurement of the hypothetical X17 boson with an improved geometrical acceptance and invariant mass resolution with respect to ATOMKI and give an independent confirmation of this anomaly. Moreover, the larger angular acceptance allows to study the X17 production not only in the plane perpendicular to the beam, as was done at ATOMKI. An angular analysis could then provide information on the particle's quantum numbers, allowing to discriminate between the different scenarios proposed for the anomaly interpretation. In fact, the Cockcroft–Walton (CW) accelerator used to calibrate the MEGII calorimeter can generate a proton beam of sufficient energy to inspect both the 17.6 MeV and the 18.15 MeV ^{8}Be excited states on an appropriate Li-compound target. The drift chamber, used to track the positron in MEGII, can provide precise tracking and momentum measurement for the e^+e^- pair produced in the X17 decay, while the scintillation detector, which provides the positron time, can be used as an efficient trigger. The photon calorimeter can instead be used to continuously monitor the photon spectrum. The present experimental apparatus can be used without major modifications, the only exception being the CW target, its support structure and the area surrounding the interaction vertex. A redesign of this region is necessary because the present $Li_2B_4O_7$ target is too thick, and there is too much material in the surroundings, reducing the tracking capabilities because of the multiple scattering and the e^+e^- energy loss. Moreover, the magnetic field has to be reduced

a factor 0.15 (optimized with Monte Carlo simulations), to take into account the lower e^+e^- momentum with respect to the MEGII signal positrons.

2.2.2 The MEGII apparatus

A schematic view of the MEGII apparatus is shown in Fig. 7.

In MEGII, an intense beam of surface (positive) muons with a momentum of 29 MeV/c is stopped in a thin slanted polyethylene target (thickness 140 μm; angle 15 deg), located at the center of the detector system. Photons and positrons from the decay of the stopped muons are measured by the liquid xenon photon detector (LXe) and the positron spectrometer consisting of a superconducting magnet, a cylindrical drift chamber (CDCH), and two sets of pixelated timing counter (pTC), respectively. A detector identifying background photons is installed on the beam axis (RDC).

The LXe calorimeter is a "C-shaped" detector made of $\approx$ 900 L of liquid xenon where the photosensors, both photomultipliers and silicon-photomultipliers, are directly immersed. The photosensors have been developed in collaboration with Hamamatsu to work in the VUV region where the xenon scintillation light is emitted ($\approx 175 \pm 5$ nm) and at a temperature of 165 K. The upgrade of the LXe calorimeter involves a denser allocation of photo-detectors on the front face, replacing the current PMTs (Hamamatsu R9869) 2 inch diameter with smaller SiPM (MPPC Hamamatsu VUV sensitive) 12×12 mm^2.

The new spectrometer has been designed to maintain all the benefits of the former one and to overcome previous limitations. The main feature is the increased spectrometer granularity which allows to work at higher beam rate and provide better resolutions for all the positron kinematical variables. The positron trajectory is measured up to the point where the positron reaches the new pTC tiles, with minimum presence of passive material and an increased number of hits per track, both in the CDCH and in the pTC. These aspects immediately have an impact on the detector acceptance and efficiency, which is increased by more than a factor 2, on the positron momentum and angular resolutions and on the positron timing.

The new CDCH is a 1.91 m long cylinder with inner and outer radii of 17 cm and 29 cm respectively filled with an ultra-low gas mixture of helium and isobutane (C_4H_{10}) in the ratio 90:10. The wires will follow a stereo configuration. Each drift cell (with an approximately squared shape, with a variable side size from 6.6 mm to 9.0 mm moving from the inner towards the outermost layer) is made of a 20 μm diameter gold plated W sense wire surrounded by 40 μm diameter silver plated Al field wires in a ratio of 1:5. Two guard wires layers (50 μm diameter silver-plated Al) are added at proper radii and voltages for gain equalising of the innermost and outermost layers. The total number of wires

would be more than 13,000 for an equivalent radiation length per track turn of about 1.6×10^{-3} X_0.

The new pTC is made by a large number of small ultra-fast scintillator plates coupled with SiPM, with improved timing resolution and acceptance. The pTC is made by two sections (Upstream and Downstream) each one made of 256 plates of BC422 of different size ($120 \times 40(50) \times 5$ mm^3) readout by SiPM (AdvanSiD ASD-NUM3S-P-50-High-Gain). The high TC segmentation allows to reach a better timing resolution due to multi-hits events (typically one event would be characterised by about 10 hits), a reduced ambiguity in the positron path length and less scintillation light propagation effects. The use of SiPM overcomes the limited performances of the PMT in magnetic fields, together with a lower transit time spread and higher quantum efficiency.

New auxiliary detectors are added with respect to the MEG experiment. The RDC enables to increase the capability of rejecting the accidental background by tagging low energy positrons associated with the high energy photons in the signal region and sampling beam monitoring detectors (SciFi and MatriX), based on scintillating fibres and small plastic scintillators coupled to SiPM respectively, to measure both beam profile and rates when needed.

Finally, the MEG II Trigger and Data Acquisition system (TDAQ), called WaveDAQ, had to be completely redesigned to cope with the increased segmentation of the detectors and the higher muon rate. At its heart, it still uses the same DRS4 chip for full-waveform digitization with sampling frequencies above the GHz; in addition, the new WaveDREAM board also contains the amplification and biasing circuit needed to connect the SiPMs sensors used in the upgrade. The integrated FPGA-based Trigger allows the combination of the information from all the boards in the system to perform the high background rejection needed for the $\mu^+ \rightarrow e^+\gamma$ search.

A large number of calibration and monitoring methods have been introduced and commissioned for the MEG experiment and are inherited into MEGII with some modifications accordingly with the increased complexity of the upgraded experiment. They allow to know in depth the detector behaviour, crucial for building the probability density functions of the observables used to identify a signal event. Furthermore they ensure that the beam characteristics and the detector performances are reached and maintained over the time. Among these, a devoted 1 MeV CW accelerator which allows to calibrate the LXe with photons produced in nuclear reactions, that will be described in the following section and will be used for the X17 search.

The MEGII detector design and performances obtained in engineering runs are described in [9].

Fig. 7 MEGII experimental setup layout (3D view). An example of a $\mu^+ \to e^+ \gamma$ decay event is shown
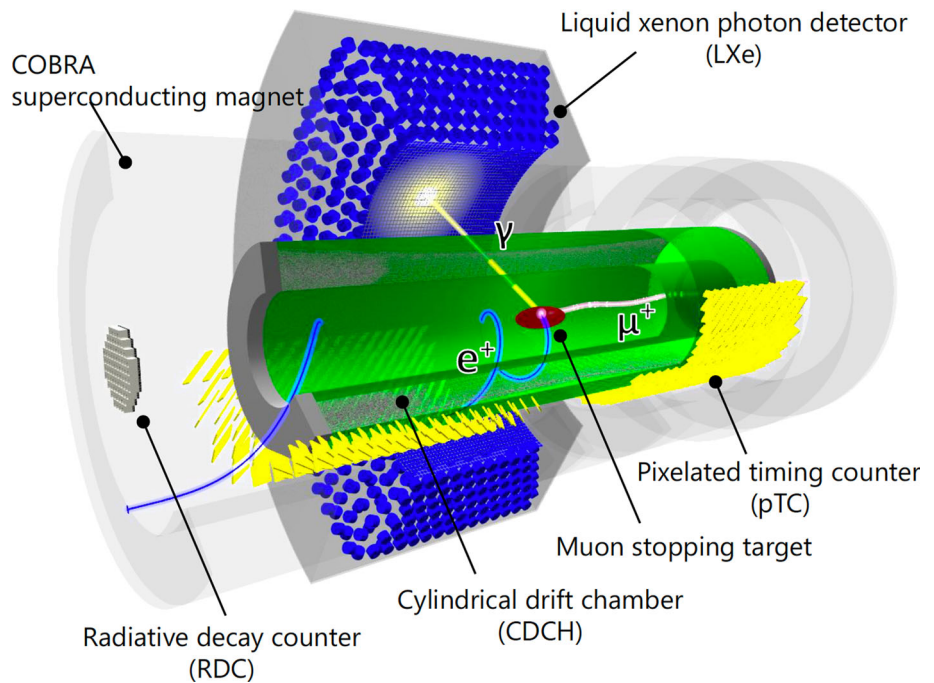
2.2.3 The CW accelerator

The CW accelerator [71] is used for the frequent MEGII calibrations needed to reach good detector resolutions on the photon observables. The proton beam can reach an energy up to $E_p = 1.1$ MeV and a current up to $100\,\mu$A, and is brought to the center of the experiment by a special bellows insertion system. The accelerator is placed in the DownStream (DS) side of the apparatus, thus the proton beam travels in an opposite direction with respect to the μ beam. The target used for LXe calibrations is made of $Li_2B_4O_7$, so that the impinging protons can produce two reactions: $^7Li(p, \gamma)^8Be$ or $^{11}B(p, \gamma\gamma)^{12}C^*$. The first reaction is used to produce one 17.6 MeV photon at $E_p = 441$ keV, needed for energy calibration, and the second reaction is used to produce two coincident 11.67 MeV and 4.4 MeV photons for energy and time calibration.

A controlled beam pipe insertion system is used to insert the target used to produce the calibration reactions. The system is automated, and brings the target at the center of the magnetic spectrometer.

An additional rubber bellows insertion system with a larger diameter is needed to allow the insertion of the beam pipe with the target. It is connected to the DS endcap of the apparatus and is coupled to the CW bellows system so that they can be simultaneously moved inside the CDCH volume. During the calibration both bellows are fully extended inside the detector, and they are retracted during MEGII muon beam data taking. The outermost bellows, though retracted, remains inside the detector, while the beam pipe goes completely outside the endcap. Albeit the accelerator is designed to reach 1 MeV proton energy, it has been successfully tested

up to a 1.1 MeV energy. It was also possible to reach high currents at the same time. It was in fact successfully tested to run at $50\,\mu$A at $E_p = 1.1$ MeV and $100\,\mu$A at $E_p = 1.05$ MeV. These specifications fulfill the requirements for the X17 measurement, most importantly the proton energy, that allows to populate the 18.15 MeV ^8Be excited state.

2.2.4 The target region

This setup used in MEGII is not directly suitable for the X17 search, because of the excessive quantity of material in the target region, which would deteriorate the measurement of the e^+e^- pair. The $Li_2B_4O_7$ target is too thick, and need to be substituted with a thinner target; LiO_2, LiPON, LiF targets are under test. The optimal thickness of the lithium compound layer is of the order of 5–10 μm. We studied different possibilities and found that the best option is to remove completely the bellow system and substitute it with a new vacuum chamber directly attached to the CW beamline, in order to keep the $e^+ e^-$ tracks in vacuum as much as possible. The target is supported by an arm connected to the CW beamline. The target substrate, the arm and the connections are built is copper in order to guarantee an optimal heat transport while keeping a reasonable material budget. The target and the supporting arm are placed inside the vacuum chamber, which should be as thin as possible. Several laboratory tests have been performed and a 400 μm carbon fiber (CF) chamber has been finally selected for the first test with the MEGII apparatus. Figure 8 shows a drawing of the vacuum chamber with the target support and arm inside.

The mechanical stability, heat dissipation, resolution and efficiency have been studied with ANSYS and GEANT4 [72]
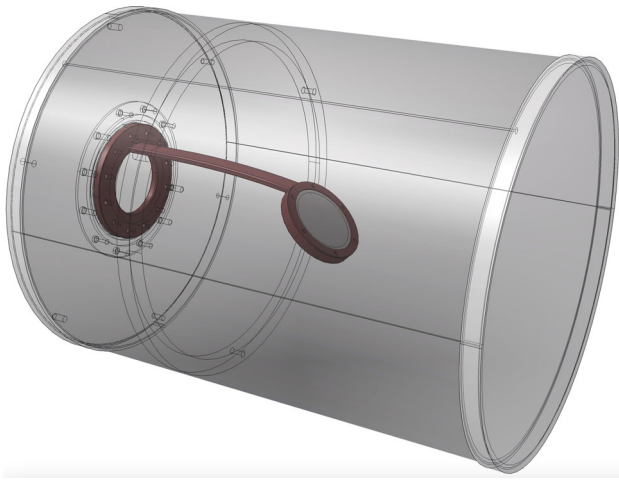
Fig. 8 Drawing of the vacuum chamber with the target support and arms

simulations that allowed to optimize thickness, material, target inclination, etc. The best material is epoxy fiber for the vacuum chamber, steel for the beam pipe and aluminum for the adapter. Copper (10 and 25 μm depending of the target) has been chosen as the final material to form the substrate, in comparison with aluminum. The optimal slant target angle is 45 deg.

2.2.5 Resolution and efficiency

Geant4 simulations have been used to evaluate the e^+e^- invariant mass resolution and efficiency in the final configuration of the target region. In the generation, the X17 is produced at a depth in the target taking into account the proton energy loss and the energy dependent cross section. The X17 decays into a e^+e^- isotropically. The MEGII detector with the modified target region is fully simulated while the events are reconstructed under the ideal assumption that a track finding algorithm will be able to associate all the reconstructed hits to the corresponding track, which is then fitted with a Kalman filter. With this procedure, although the track finding efficiency is assumed to be 100%, the hit reconstruction efficiency, fit efficiency and single hit resolutions are correctly taken into account. An event selection is applied to the analysis to exclude events that are not related to the X17 decay. First of all, the accepted events have to include both a positron and an electron; then, a χ^2 cut is applied to the momentum and angle distributions, so that only the reconstructed particles with characteristics similar to the MC truth are considered; finally, a vertex constraint is applied, so that the two tracks are forced to cross the target plane in the same point. The combined application of these energy and vertex cuts reduces the tail of the invariant mass distribution, that can be well fitted by a double Gaussian. The resolution

quoted here is the core width of the distribution. The resolution σ and efficiency ε obtained for the final configuration are $\sigma \approx 504$ keV and ε of few %, including the request of a pTC hit, which is needed for triggering purposes.

2.2.6 Background estimate

A deep understanding of all the background sources is crucial in this measurement. A comprehensive and reliable theoretical model, in fact, can validate the hypothesis that the anomaly is generated by a new physics signal and not by the combination of the background sources. The dominant background will come from the IPC process. The BR for the production of a real photon, BR(^{8}Be* $\to^8$ Beγ), is about 1.5×10^{-5}, and a further factor of about 3.19×10^{-3} is paid for the IPC production. It means that the IPC rate is at least a factor ~ 500 above the X17 $\to e^+e^-$ production rate extrapolated by the ATOMKI result. The e^+e^- conversion of a real photon in the target or in the surrounding material (external pair conversion, EPC) has found to be negligible using simulations in the X17 invariant mass region, while background from cosmic rays is strongly suppressed by using an optimized trigger configuration including both pTC and CDCH.

The IPC background is calculated generating photons in the target with an energy distributed according to the Zhang–Miller model [27], taking into account the energy loss of the proton in the target. This model provides a description both for the photon production and the e^+e^- pair cross sections. In this way it is possible to predict the rate of the IPC background.

2.2.7 Significance and DAQ time

Knowing the reaction rates, the resolution and the efficiency of the X17 measurement, it is possible to estimate the significance and thus the DAQ time needed to achieve a satisfactory result.

Figure 9 shows the invariant mass distribution for both signal and IPC background in a range around the expected signal region. Here the signal region is considered as $\mu \pm 3\sigma$ with μ and σ parameters of the core of the double Gaussian fit to the invariant mass distribution of signal events. Based on the branching ratio of the different reactions and the detection efficiency it is possible to extrapolate the expected number of signal and background events. The distribution shown in the figure corresponds to an excess that has a significance of $s = 5$ where the significance is defined as $s = \frac{N_{sig}}{\sqrt{N_{sig}+N_{IPC}}}$. Combining this information with the real experimental conditions, defined also by the CW beam intensity, the selected target, the TDAQ operational conditions is possible to estimate a data taking of several weeks for addressing such a significance.
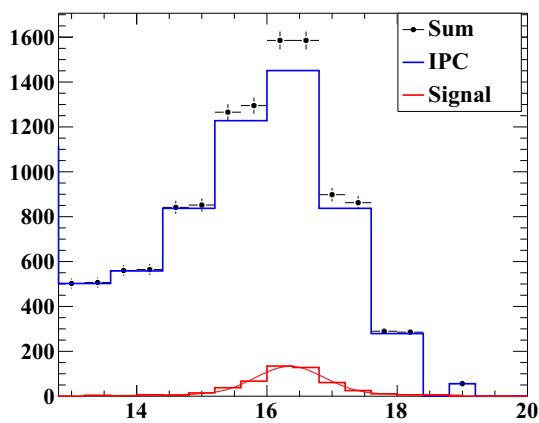
Fig. 9 Invariant mass distribution of signal and IPC background from simulations. The "sum" distribution is also reported

2.2.8 Conclusion

The MEGII experiment has a unique opportunity to confirm or disprove the anomaly observed by ATOMKI in the $^7\mathrm{Li}(p, e^+e^-)^8\mathrm{Be}$ reactions exploiting the CW accelerator used routinely in the calorimeter calibrations. Feasibility studies, performed with a complete detector simulation and including realistic background models, suggest that 5σ sensitivity can be addressed. First tests performed during 2021 showed promising results. The measurement is foreseen at the end of 2022.

2.3 Measurements of internal pair creation with a time projection chamber-based setup

Hugo Natal da Luz

Institute of Experimental and Applied Physics-Czech Technical University in Prague, Husova 5, Prague 1, Czech Republic

Abstract Theoretical prediction for distribution of the angle between electrons and positrons originating in internal pair creation is a monotonic featureless decrease with the opening angle. Studies on excited states of $^8\mathrm{Be}$ and $^4\mathrm{He}$ nuclei made in ATOMKI, Hungary, however, revealed deviations from this expectation. If confirmed by an independent laboratory, such a result may have a fundamental impact: the anomaly could be explained by introducing a new short-lived neutral boson still fitting in known experimental and theoretical constraints. We describe an experimental setup – based on a time projection chamber (TPC) equipped with magnetic field to measure energy, supplemented by multiwire proportional counters (MWPC) and Timepix3 (TPX3) pixel detectors to improve angular resolution – intended to redo the original nuclear experiment.

2.3.1 Introduction

In 2016 Krasznahorkay et al. observed an anomaly in the angular distribution of the e^+e^--pair members originating in the decay of the 18.15-MeV 1^+ $^8\mathrm{Be}$ nuclear level [1]. Signal enhancement at folding angles close to $140°$ was measured and interpreted as a signature of an additional decay channel via a new neutral boson X with mass of around $m_X = 17$ MeV that is emitted on-shell from the excited nucleus and subsequently decays to the registered e^+e^- pair. The same group later reported a similar effect also in the decay of the 17.64-MeV 1^+ excited $^8\mathrm{Be}$ state [64] (at present, however, this result is questioned by the original authors themselves, and is thought not to hold after all), and more recently in the decay of the 21.01-MeV 0^- state of $^4\mathrm{He}$ [6].

The anomaly and its possible interpretation triggered interest in the scientific community. While many theoretical aspects have been discussed, an independent experimental confirmation of the effect is missing, no sign of the X17 particle has been observed in other studies (which generally probed elementary-particle rather than nuclear physics).

In an attempt to contribute to the understanding of the anomaly, the Institute of Experimental and Applied Physics at the Czech Technical University in Prague is building a spectrometer with the aim to essentially repeat the original ATOMKI experiment, ie, to check the existence of the effect within the nuclear reaction induced by protons impinging on either $^7\mathrm{Li}$ or $^3\mathrm{H}$ target. Our spectrometer is based on three layers of detectors. The innermost (closest to the target) layer is composed of Timepix3 (TPX3) silicon pixel detectors, the middle layer consists of multiwire proportional counters (MWPC), and finally time projection chambers (TPC) equipped with magnetic field follow in the outermost layer. The first two layers are to provide necessary angular resolution, the TPCs then to measure particle energies. Below we consider various aspects of the intended measurements, show preliminary tests of the detectors as well as include some discussion about their advantages and limitations.

2.3.2 General concept

Our intention is to measure the e^+e^- pairs emerging from resonances of the same nuclear reactions as used in the ATOMKI experiments [1,6,64]. Namely, these are the $^7\mathrm{Li}(p, e^+e^-)^8\mathrm{Be}$ and $^3\mathrm{H}(p, e^+e^-)^4\mathrm{He}$ reactions. In the former case, the two excited states of $^8\mathrm{Be}$, at 17.64 MeV (Be'*) and at 18.15 MeV (Be*), are produced by protons accelerated to kinetic energy of 441 keV and 1.03 MeV, respectively. In the latter case, the low-energy tail of the broad ($\Gamma \approx 0.84$ MeV) 21.01-MeV second excited level of $^4\mathrm{He}$ is to be excited with about 900-keV protons (these excite the nucleus to about 20.5 MeV; the tail is used to stay below the neutron-production threshold at 1.02 MeV of kinetic energy of protons). While these

reactions are shared with the ATOMKI measurements, the detection methods differ.

In our experiment a target is positioned in an evacuated beamline where it is hit by protons from an accelerator. The electrons (positrons) emerge with energies E_- (E_+) ranging from the rest mass (zero kinetic energy) up to the available energy in the reaction E_r, while always summing to the latter, $E_+ + E_- = E_r$.

The anomaly essentially arises from pairs with not much different energies of their members [1] and the 'disparity' cut $-0.5 \leq y \equiv (E_- - E_+)/E_r \leq 0.5$ was imposed. Equivalently, the interesting events should rarely have a particle with energy less than $E_r/4$, roughly 4 MeV, and the detector should be capable of following particles at least down to such an energy. However, as follows from analytic estimates (see [73], sec. 3.8, and Fig. 3.33 therein in particular) as well as from our simulations, even a thin layer of fairly light material scatters electrons of thus low energies considerably: a silicon layer of $500\,\mu$m (i.e., 0.12 g/cm^2) leads to about $10°$ scattering[3] of (perpendicularly impinging) 4-MeV electrons. Consequently, between the target and the detector measuring the direction of created particles there should be as little material as possible, and, if unavoidable, be as close to the direction-detector as possible and as far as possible from the target. Requiring reasonable solid-angle coverage (while keeping the number and size of detectors limited) on the other hand generally favours compactness, and a compromise must be made.

Timepix3 [74] detectors have a granularity and size compatible with the experiment's requirements. Six of these devices will form the first detector layer surrounding the target, still within the vacuum beamline, and provide the needed information about particles direction, see Fig. 10.

After the TPX3-detector ring, particles leave the beamline. The ATOMKI group used a 1 mm-thick carbon (to reduce scattering) beamline segment [2]. We contemplate doing the same, using a thinned aluminium segment, or a segment with (possibly reinforced) Kapton™ windows introducing particles to further detector parts.

Just outside the beamline there is a second layer of detectors composed of MWPCs to record one more point in the trajectory of the particles, helping to estimate the magnitude of the scattering in the TPX3 ring and yielding updated directional information. The MWPCs also provide signal useful for triggering purposes and coincidence considerations.

Finally, particles enter gaseous TPCs constituting the third, outermost, layer of detectors. The TPCs are equipped with magnetic field and allow determination of particle momentum (energy) and charge sign from the trajectory bending radius inferred from the ionization track. At the same

---

[3] Root-mean-square-angle.
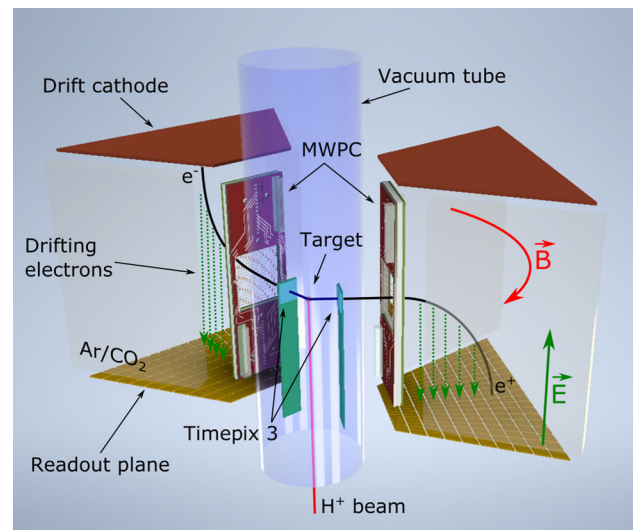
Fig. 10 A schematic view of the planned experiment where two out of six sectors are shown and the three layers of detectors are visible. See the text for details

time, some degree of particle identification is possible from particle energy loss per unit distance.

Combining the information provided by the three layers of detectors, running synchronously, should lead to necessary background suppression as well as sufficient energy and angular resolution. We expect to reach energy resolution of 7% and angular resolution of about $3°$.

2.3.3 The Timepix3 (TPX3) detectors

TPX3 is a pixel-detector ASIC read-out chip developed within the Medipix collaboration, CERN [74]. The chip bump-bonded to a suitable sensor may be viewed as a square matrix of 256×256 independent detectors (i.e., pixels), each of $55\,\mu$m $\times\ 55\,\mu$m size, hence with a total active area of 14×14 mm^2. In the so-called data-driven mode each pixel measures both the time-of-arrival (ToA) and the time-over-threshold (ToT) of each detected signal, where ToA has a 1.6-ns precision and ToT reflects the energy deposited in the pixel.

The TPX3 performance for our experiment has been studied at the Van de Graaff facility of IEAP using a simple triangular TPX3 setup surrounding a lithium fluoride (LiF) or cerium trifluoride (CeF$_3$) target inside a vacuum chamber; see Fig. 11, where a photo of the setup and the CAD schematics are shown on the top. Targets evaporated onto 12-μm aluminium foils with thicknesses of tens of nanometers have been used. The fluorine inside the compounds serves as an e$^+$e$^-$ 'factory' through the resonant ^{19}F(p, e$^+$e$^-\ \alpha)^{16}$O reaction at proton energy of 843 keV, providing numerous electron and positron tracks in a short amount of time (the total energy of a particle pair is 6.05 MeV here). The hit-maps
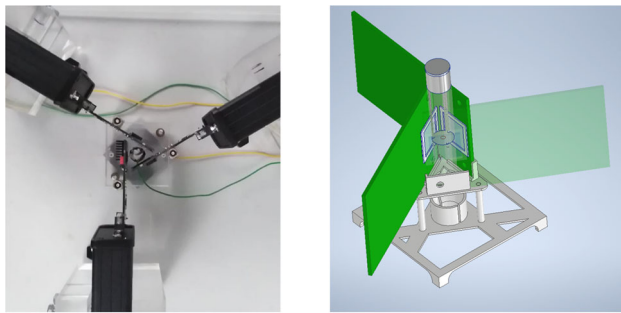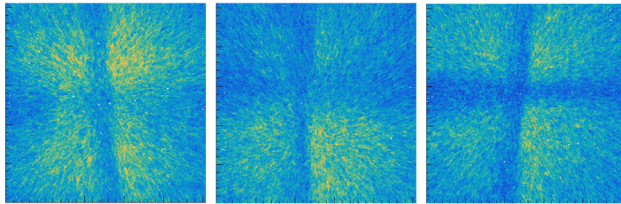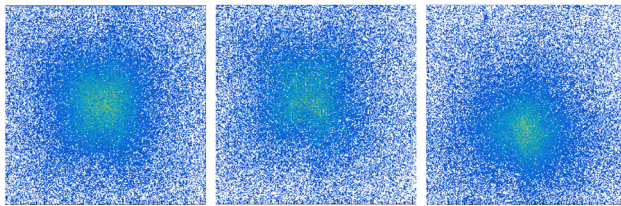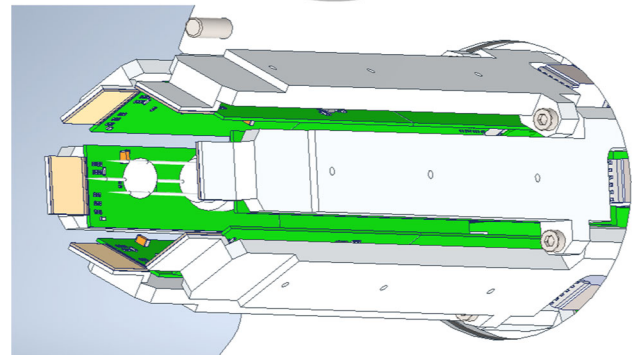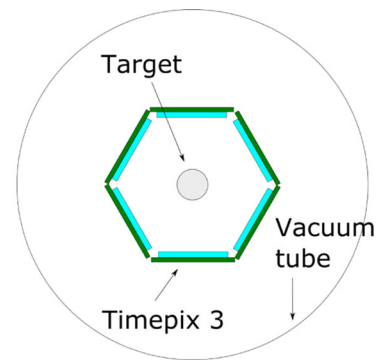
Tracks

Vertices

Fig. 11 Top: A triangle of TPX3 detectors surrounding a target, used to test performance of the detectors. Middle: Tracks detected in each of the three TPX3 detectors. Bottom: Reconstruction of the reaction vertex

Fig. 12 Top: A hexagonal array of TPX3 detectors surrounding a target. Bottom: CAD of the planned assembly to be inserted in a beam pipe with an outer diameter of 60 mm

in the middle row of Fig. 11 show accumulated electron and positron tracks recorded by three silicon TPX3 detectors with thickness of $500\,\mu m$. The vertical and horizontal shadows in the figure are shadows of the aluminium foil and of the stainless steel needles holding it, respectively. By considering coincidence tracks, the reaction vertex can be determined, as the bottom row in Fig. 11 shows. The position of the target can be (statistically) estimated with accuracy better than 1 mm. We note that there is a 60-μm-thick aluminium foil inserted between the target and the TPX3 detectors to shield off elastically scattered protons and alpha particles that get created in the reaction.

In the full experimental setup of Fig. 10, an array of six (instead of three) TPX3 detectors surrounds the target inside the beam pipe, see Fig. 12, top. In order to accommodate all the six detectors in such a small volume, the chipboards have been redesigned to become longer and narrower, Fig. 12, bottom. A new data-acquisition motherboard provides common clock to all six detectors. The TPX3 detectors are farther from the target than in the triangle pilot setup, improving the resolution of the vertex reconstruction at the cost of diminishing the solid-angle coverage (an ideal triangle covers 81%, an ideal hexagon 48% of the full sphere).

The optimal thickness of the TPX3 sensor is still debated. A thicker sensor can potentially allow 3D tracking within its volume [75,76], but at the same time introduces more scattering and leads to creation of more Compton electrons. Our preliminary attempts to do the 3D tracking with 500-μmSi sensors have not been too successful so far (due to excessive scattering resulting in too-curly tracks). But as we only used fairly low-energy pairs from deexcitation of the first excited oxygen level (individual particles have kinetic energy of about 2.5 MeV), the situation in the real experiment should be significantly more favourable.

We note that the default thickness of the ASIC, 0.8 mm, can be reduced to 0.2 mm in order to cut down the background. If we ever find out that the 3D tracking is not a viable option, a Si sensor of comparable thickness to the ASIC then seems optimal. The removal of the usual PCB from behind the sensor/ASIC assembly will reduce the background further.

2.3.4 The multiwire proportional counters (MWPC)

Six multiwire proportional counters (MWPC) [77] will be placed outside the beam pipe, each with an active area of 40×38 mm^2. These detectors will provide one more point in the trajectory of the produced particles. Together with the information coming form the TPX3 detectors, this second
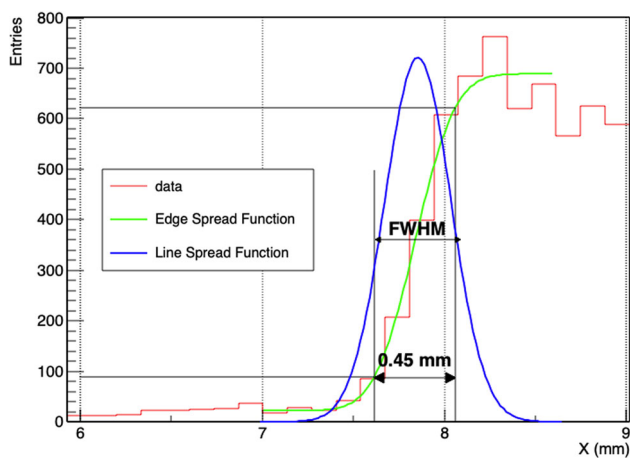
Fig. 13 The edge spread function as was obtained from X-rays striking a MWPC

point can help better estimate the reaction vertex and the particle entry point to the TPC. The MWPC consists of three wire planes separated by 2 mm: one central plane with anode wires and two cathode planes rotated by 90° with respect to each other. There are 19 25-μm wires in each plane, with a pitch of 2 mm. The 2D position of the interaction point is encoded in the time difference between the signals at each end of a delay line interconnecting the cathode wires. Only 4 electronic channels per detector are used, simplifying the data acquisition.

The edge spread function of the detector obtained by imaging a sharp edge with an X-ray source is depicted in Fig. 13, showing that the resolution of these detectors is about 500 μm.

2.3.5 The time projection chambers (TPC)

Time projection chambers [78] provide 3D track reconstruction and subsequent momentum and particle identification from ionization tracks left in the gas under magnetic field. TPC fits most of the requirements of this experiment: measurement of particle's energy with minimal interaction (avoiding radiative losses), background suppression (from the topology of the events) and particle identification.

Six TPCs form the outermost detector layer of our setup. The field cage has 150 mm depth, matching the expected bending radius of 8-MeV electrons in the field of 0.3 T. The readout plane is composed of triple gas electron multiplier (GEM) stacks [79], a type of micropattern gaseous detector (MPGD) [80] with good energy and position resolution [81,82], a good dynamic range and stability against discharges [83,84] and the possibility of building very large area detectors, such as ALICE and CMS [85,86], at the CERN LHC.

The data-acquisition (DAQ) requirements demand a system with a number of channels of the order of 1000, that can operate continuously without significant dead time. CERN's
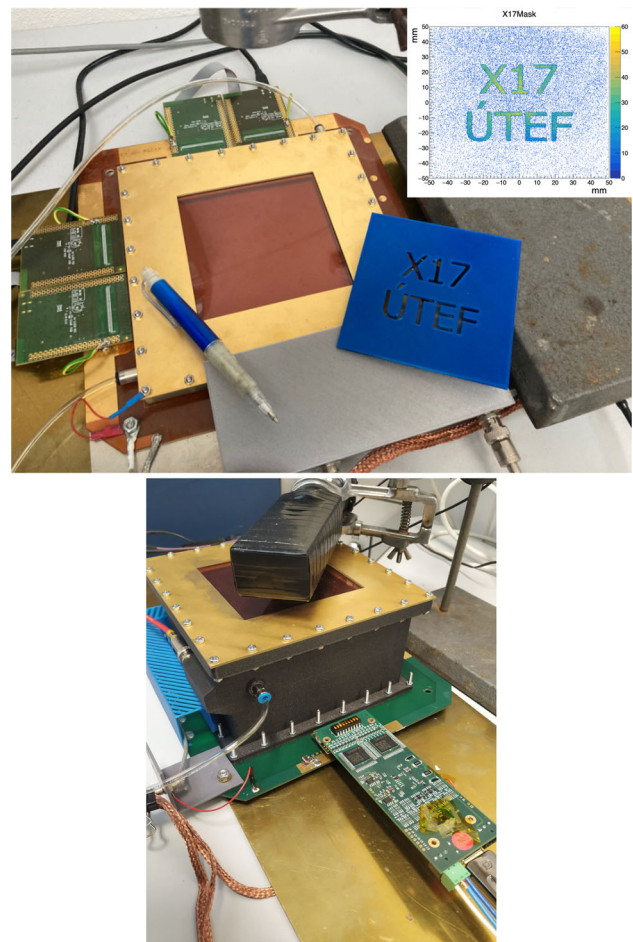
Fig. 14 Top: The 2D, 10×10 cm^2 triple GEM prototype with a simple imaging mask. Bottom: The TPC prototype with a SAMPA frontend

scaleable readout system (SRS) [87] has been implemented in a 10×10 cm^2 2D GEM detector prototype, using the APV25 ASIC, developed for the CMS tracker. We achieved position resolution of 350 μm, similar to those reported by other groups [88,89].

Among the most recent developments of the SRS is its integration with the SAMPA ASIC, originally designed for CERN's ALICE experiment [90]. This chip is suited for the operation with TPCs, providing waveforms up to 100 μs long at a sampling rate of 10 MS/s. Our group collaborates with the University of São Paulo on the task. Figure 14 shows our 2D prototype on the left, the inset depicting an X-ray transmission image of a simple mask, and its upgrade to a TPC on the right, where the board with four SAMPA chips can be seen attached to the readout.

Simulations of the TPC performance under different magnetic field configurations are ongoing to estimate the limitations of this detector in the particles' energy determination.

2.3.6 Conclusion

A spectrometric system integrating TPX3, MWPC and TPC detectors is under construction for measurement of angular correlations in internal pair creation in the excited states of ^{8}Be and ^{4}He nuclei.

An array of TPX3 detectors inside a vacuum tube, will provide six different projections of the target's position in addition to e^+e^- tracks originated from that target or from the reported X17 neutral boson. These detectors, operating together with the MWPC, will provide enough information to improve the angular resolution and to estimate the scattering that the particles experience, allowing for small corrections in energy. The TPC detectors, which will be used to measure the energy by means of a magnetic field, provide a good energy resolution due to the smaller radiative energy loss, compared to the solid state calorimeters. We are also participating on the final integration of a new frontend ASIC, designed for operation with TPC (SAMPA). The first set of measurements using our TPC-based spectrometer setup with a ^{7}Li target is foreseen to take place during the year 2023.

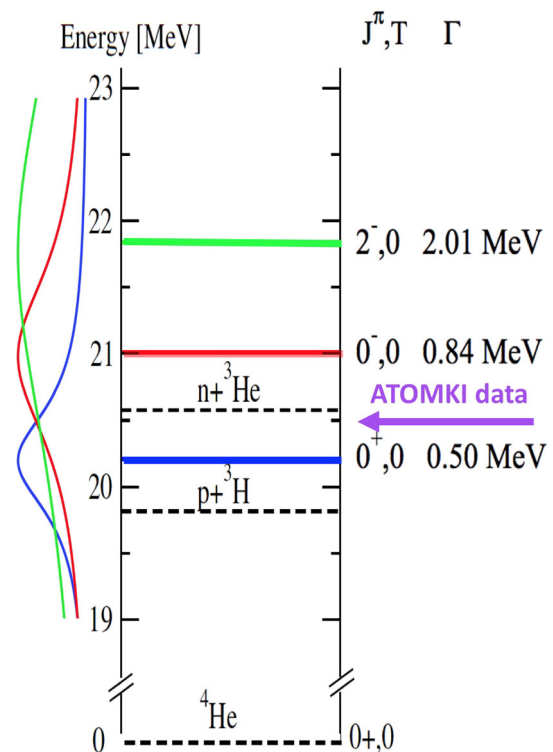*Acknowledgments*

Fig. 15 The low-energy spectrum of ^{4}He. The dashed lines indicate the thresholds for the opening of the $1 + 3$ channels, while the solid lines indicate the energy levels of the first resonances with corresponding widths, J^π, and isospin assignments to the right. Also indicated is the highest energy of the ATOMKI measurements, performed just below the threshold for the $^3He(n, p)^3H$ reaction opening. See [67] for more details

## 2.4 The search for ^{4}He anomaly at n_TOF experiment

Carlo Gustavino
INFN-Rome

Abstract A new approach to clarify the present X17 scenario is discussed, by searching for the X17 boson in the decay of excited A = 3, 4 (Tritium, helium-3, helium-4) nuclei. The study of the ^{3}He(n, e^+e^-)^{4}He and ^{3}H(p, e^+e^-)^{4}He reaction in a wide energy window would probe the X17 existence. If the anomaly is confirmed, these reaction can provide the determination of the relevant characteristics of the X17 boson such as its mass and quantum numbers, as suggested by a recent ab-initio calculations in which the existence of a 17 MeV boson is considered. If the existence of the X17 boson is confirmed, the analysis of the $^2H(n, e^+e^-)^3H$ and $^2H(p, e^+e^-)^3He$ cross section ratio offers a unique opportunity to study the purported protophobic nature of the fifth force mediated by the X17 particle. In this paper is also discussed the performance of an experimental setup, that should have a large acceptance and an adequate capability of measuring the four-momenta of ejectiles as well the capability to reject beam induced backgrounds.

2.4.1 Introduction

Two significant anomalies have been observed in the emission of electron-positron pairs in the ^{7}Li(p, e^+e^-)^{8}Be and ^{3}H(p, e^+e^-)^{4}He reactions [1,53]. These anomalies have been interpreted as the signature of the existence of a boson (hereafter referred to as X17) of mass $M_{X17} = 16.8$ MeV that could be a mediator of a fifth force, characterized by a strong suppression of the coupling to protons compared to neutrons (protophobic force) [8]. Beyond the importance of such a discovery – if confirmed – this scenario could explain, at least partially, the long-standing (recent) anomaly on the muon (electron) magnetic moment (see [91] and reference therein). More in general, the possible existence of a new particle is of paramount importance in particle physics and in cosmology (dark matter). Therefore, the ATOMKI claim clearly calls for new experimental studies. Our proposal is to carry on a new study of the ^{3}H(p, e^+e^-)^{4}He process already studied at ATOMKI, accomplished with the study of the conjugated ^{3}He(n, e^+e^-)^{4}He process exploiting the neutron beam of the n_TOF facility at CERN [12]. This approach has relevant advantages:
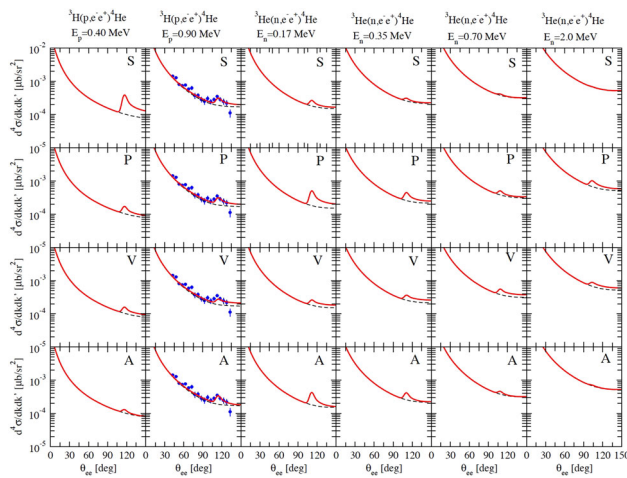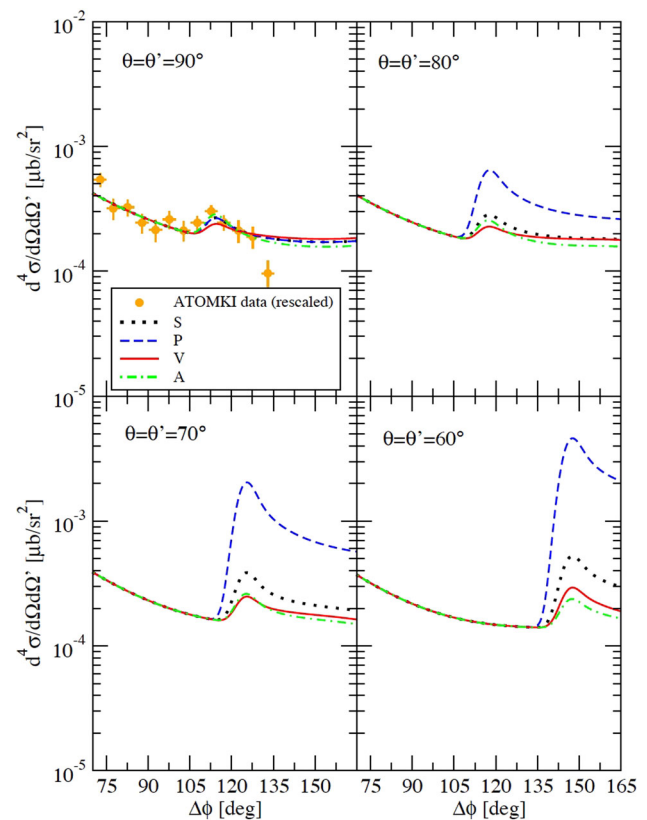
Fig. 16 Cross section for the ^{3}He(n, e^+e^-)^{4}He and ^{3}H(p, e^+e^-)^{4}He processes at six different incident nucleon energies as function of the angle $\theta_{e^+e^-}$ between them. It is considered a configuration similar to the ATOMKI experiment one, in which the e^+ and e^- momenta are in the plane orthogonal to the beam axis. The panels labeled S, P, V, and A show the results obtained by including the exchange of a scalar, pseudoscalar, vector, and axial X17, respectively. In all cases, it is assumed $M_{X17} = 17$ MeV/c^2. The dashed (black) and solid (red) curves show the results obtained by including the electromagnetic only or both the electromagnetic and X17 amplitudes. The coupling constants have been adjusted so as to reproduce the ATOMKI ^{3}H(p, e^+e^-)^{4}He cross section data at the incident proton energy of 0.90 MeV. See [67] for more details

(i) the X17 existence is investigated for the first time by a neutron induced reactions;

(ii) The X17 boson study will be carried out in a wide energy range to extract the X17 quantum numbers [92];

(iii) the ^{4}He de-excitation data can be compared with recent ab-initio calculations, both for the standard internal pair conversion (IPC) of virtual photons and for the X17 channel [67].

In case of a clear appearance of X17 boson, it looks rather promising the experimental study of the ^{2}H(p, e^+e^-)^{3}He and ^{2}H(n, e^+e^-)^{3}H processes. In fact, the isospin-specular ^{3}He and ^{3}H nuclei would have a very different probability to produce the X17 boson, provided that it is confirmed to be the mediator of a protophobic fifth force, as suggested in [8].

2.4.2 The ^{3}He(n, e^+e^-)^{4}He and ^{3}H(p, e^+e^-)^{4}He reactions

As already mentioned above, the experimental study of the ^{3}H(p, e^+e^-)^{4}He reaction performed by the ATOMKI group seems to indicate the existence of a boson with a mass of 17 MeV/c^2. However, the reported data are limited to few proton-beam energies and only leptons emitted in the plane orthogonal to the beam line were detected. As suggested in [67] (see also Figs. 16 and 17) a measurement covering a wide energy range of the ^{4}He excited nucleus would enable

Fig. 17 The cross section for the ^{3}H(p,e^+e^-)^{4}He process at 0.90 MeV incident proton energy for several configurations in which the e^+ and e^- momenta are emitted at angles $\theta = \theta'$ with respect to the incident proton momentum, and as function of the difference $\Delta\phi = \phi' - \phi$. The curves labeled S, P, V, and A show the results obtained by including the exchange of a scalar, pseudoscalar, vector, and axial X17, respectively. In all cases, it is assumed $M_{X17} = 17$ MeV. The coupling constants have been adjusted so as to reproduce the ATOMKI ^{3}H(p, e^+e^-)^{4}He cross section data at the incident proton energy of 0.90 MeV and in which $\theta = \theta' = 90^o$. See [67] for more details

the study the 0^+, 0^-, 2^-, 1^- levels (see Fig. 15). In this way it is possible to either confirm or exclude the existence of the X17 and ultimately study its properties. Concerning the ^{3}H(p, e^+e^-)^{4}He reaction, a promising facility is the LUNA-MV accelerator that will soon be operative at the underground Gran Sasso Laboratory (LNGS). At LNGS the cosmic ray induced background is many orders of magnitude lower than at overground facilities, and the proton beam intensity is a hundred time higher than the one used at the ATOMKI facility. Thus, LUNA-MV is well suited to perform accurate measurements in a relatively short time by using protons with energy up to 1.02 MeV, i.e. before the onset of the ^{3}H(p,n)^{4}He channel (see Fig. 15). The study at higher excitation energy of ^{4}He can be performed at the CERN n_TOF facility, through the ^{3}He(n, e^+e^-)^{4}He reaction. This facility provides a pulsed neutron beam in a wide energy range ($E_n = 1 - 10^8$ eV) in which the energy of each interacting neutrons can be accurately derived with the

Time-of-Flight (TOF) technique [12]. Although the excess of pair-production events as a function of the energy depends on the X17 quantum numbers (i.e., on the nature of its coupling to electrons and nucleons), an experimental setup similar to the ATOMKI one, in which only particles orthogonal to the beam axis are detected, might be hindering our ability to discriminate among different quantum numbers, and hence uniquely identify the X17 properties. This limitation can be appreciated by inspecting Fig. 16, where the predicted trend of the excess is found to be similar for the pseudoscalar and axial cases. However, as shown in Fig. 17, the use of a detector with a large angular acceptance would make it possible to discriminate among different options since the angular distribution of the emitted pair depends appreciably on the X17 quantum numbers.

2.4.3 Conceptual detector setup

As stated above, the main requirements for the detector are the following:

(i) large acceptance, i.e. the detector should have almost a 4π coverage around the target. Besides statistics, this condition is highly desirable to measure the J^π of the X17 boson.

(ii) good tracking capability, in order to identify direction and vertex of e^+e^- pairs due to IPC (irreducible background) and by the X17 decay (signal);

(iii) good energy resolution to measure the energy of ejectiles;

(iv) good particle identification, to reject beam induced backgrounds and to establish the nature of X17 ejectiles (in the ATOMKI experiment the ejectiles are only deduced to be electron positron pairs).

Figure 18 shows the conceptual setup for the study of the ^{3}He(n, e^+e^-)^{4}He and the ^{3}H(p, e^+e^-)^{4}He reactions. It consists of two large radial TPC with the electric field orthogonal to the beam axis. the external read out planes are based on the use of Micro Pattern Gas Detector and equipped with orthogonal readout strips. Consequently, the two TPC provide the 3D reconstruction of crossing particles and contribute to the particle identification by measuring the energy loss in the gas. Two prototype detectors equipped with μRwell, with an area of 30×30 cm^2 and with a 2 cm drift gap have been realized. The energy of particle is provided by external scintillating planes properly segmented and readout by SiPM. Presently is under study the use of planes 10 cm thick and with an area of 40×40 cm^2 based on the use of EJ-200 plastic scintillator bars. A test to evaluate the beam induced background in the described sub-detector is foreseen in June 2022 at the EAR2 area of n_TOF [92]. The test also foresees targets of ^3He at high pressure (~ 300 bar) encapsulated in a carbon fibre envelope 600 μm thick. A preliminary study of a Ring
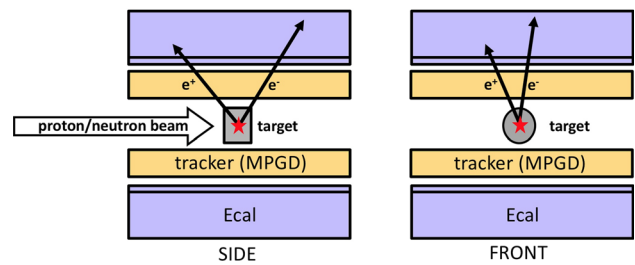

Fig. 18 Sketch of the experimental setup

Imaging Cherenkov detector surrounding the target is also scheduled. the possible use of this detector is finalised to flag the ejectile pairs.

2.4.4 Conclusion

In this contribution the activity of a working group aimed at exploiting the n_TOF facility to probe the existence and possibly the properties of the X17 boson is briefly reported. Presently the study is focused in "few nucleons" reactions, namely ^{3}He(n, e^+e^-)^{4}He, ^{3}H(p, e^+e^-)^{4}He and successively ^{2}H(n, e^+e^-)^{3}H and ^{2}H(p, e^+e^-)^{3}He. However, the X17 activity can be extended also to other reactions by using the same dedicated detector, such as the ^{7}Li(p, e^+e^-)^{8}Be, already studied by the ATOMKI group, and the ^{7}Be(n, e^+e^-)^{8}Be. The last one take advantage of the existing know-how to realize ^{7}Be targets [93].

2.5 Experiments on ^{8}Be* internal pair creation at INFN Legnaro Laboratories

R. Bolzonella[1,2] , D. Tagnani[3], S. Barlini[4,5], G. Casini[4], A. Celentano[4], M. Cicerchia[1], M. Cinausero[1], G. Collazuol[2,7], L. Domenichetti[1,2], D. Fabris[7], C. Frosin[4], B. Gongora-Servin[1,8], F. Gramegna[1], I. Lombardo[9], A. Mengarelli[1], G. Pasquali[4,5], A. Passeri[3], S. Piantelli[4], M. Vigilante[10], T. Marchi[1]

[1]INFN-Laboratori Nazionali di Legnaro, Legnaro (PD), Italy. [2]Università degli Studi di Padova, Dipartimento di Fisica e Astronomia, Padova, Italy. [3]INFN-Sezione di Roma Tre, Roma, Italy. [4]INFN-Sezione di Firenze, Sesto Fiorentino (FI), Italy. [5]Università degli studi di Firenze, Dipartimento

di Fisica e Astronomia, Sesto Fiorentino (FI), Italy. [6]INFN-Sezione di Genova, Genova, Italy. [7]INFN-Sezione di Padova, Padova, Italy. [8]Università degli Studi di Ferrara, Ferrara, Italy. [9]INFN-Sezione di Catania, Catania, Italy. [10]INFN-Sezione di Napoli and Uniersità di Napoli Federico II, Napoli, Italy.

Abstract The ATOMKI results and the related interpretations triggered a renewed interest in the spectroscopy of light ions by Internal Pair Creation. To this purpose, and to better characterize the X17 anomaly, a new experimental setup is being developed. The first goal is to provide an independent replica of the Hungarian experiment exploiting the low energy proton beams available at the INFN Legnaro National Laboratories.

We present the current design for the construction of a new dedicated device, meant to improve the angular resolution and to reduce the material budget. The spectrometer should be able to detect electron–positron pairs sharing up to 20 MeV kinetic energy, with an angular resolution smaller than 1 degree. The detectors will be hosted in the same vacuum chamber where the nuclear reaction takes place.

The simulations done to optimize the design of the setup and estimate the expected performances are summarized, together with the first experimental tests on the detector prototypes.

2.5.1 Introduction

The recent ATOMKI results on the Internal Pair Creation (IPC) anomalies from low energy nuclear transitions [1,65,94] call for an independent confirmation of the experimental observations, together with the development of dedicated models for the signal interpretation. Experimentally, the observed signature of the X17 particle is a very characteristic angular correlation of the e^+e^- pairs emitted from the decay of excited ^{8}Be and ^{4}He states. The angular correlation between the e^+ and e^- emitted by internal pair creation depends on the multipolarity of the transition and is expected to drop rapidly with the separation angle $\theta_{e^+e^-}$ for the considered cases [2]. In striking contrast, the measured angular correlations show peaks at large angles that are compatible with the emission of a short-lived ($\tau \leq 10^{-13}$ s) neutral particle decaying into the e^+e^- pair. This contribution focuses on the ^{8}Be case [1,65], where the p+^{7}Li reaction at the $E_p = 0.441$, and 1.03 MeV resonances have been used to selectively populate the 17.6, and 18.15 MeV 1^+ states. In the Hungarian facility, the pairs are detected by five plastic ΔE-E detector telescopes similar to those built by Stiebing and co-workers [52]. In particular, large telescope detectors in combination with position sensitive detectors were used to match position resolution and coincidence detection efficiency [2]. Plastic ΔE scintillators of $38 \times 45 \times 1$ mm^3 and the E detectors

of $78 \times 60 \times 70$ mm^3 were placed perpendicularly to the beam direction at azimuthal angles of $0°$, $60°$, $120°$, $180°$, and $270°$. The positions of the hits were initially determined by using multi-wire proportional counters (MWPC) placed in front of the plastic telescopes [2]. In a second optimized version of the experimental setup, these were replaced by segmented strip detectors [65].

In this contribution we discuss the design and prototyping of a new setup for IPC spectroscopy at LNL, specifically optimized to detect electron-positron pairs sharing up to 20 MeV kinetic energy, matching the X17 case. The experiments will be performed at the INFN Legnaro National Laboratories (LNL), exploiting the low-energy proton beams provided by the AN2000 and CN facilities.

### 2.5.2 New experimental setup at LNL

The building block of the setup is the plastic scintillator ΔE-E telescope shown in Fig. 19 composed by three detector layers. The E stage is constituted by a 5 cm $\times$ 5 cm $\times$ 10 cm EJ200 scintillator [95] read by a Silicon PhotoMultiplier (SiPM). The ΔE stage is formed by two sub-layers: each one is composed by 10 EJ200 bars of dimensions 0.5 cm$\times$0.2 cm$\times$5 cm, read by an array of 2 mm $\times$ 2 mm SiPMs. The SiPM signals are read at the two extremes of the array through a resistive partition chain exploiting the LG technology developed by FBK [96]. This allows to limit the number of readout channels to 2 for each layer: the sum of the signals amplitudes at the two extremes of the line gives the total energy deposited, while the ratio between their difference and their sum makes it possible to know which bar has been hit, thus allowing to determine one coordinate of the entry position of the electrons in the telescope. By placing the bars of the second layer orthogonally with respect to the first one, a grid is obtained, as shown in Fig. 20, allowing to know both coordinates of the particle entry positions in the telescope.

The telescopes are organized in groups of 4 forming a *clover* held by a plastic cage. As shown in Fig. 19, there are no plastic interfaces between the calorimeters of the same clover, making it equivalent to a unique 10 cm^3 calorimeter.

The clovers will be placed at 15 cm from the center of the target, with the ΔE layer facing it. The target-detector distance has been chosen to optimize the compromise between angular resolution and solid angle coverage given the fixed pitch of the tracking layer bars (5 mm). The project plans to produce and use a minimum set of five clovers, placed at different angular positions in the plane containing the target center and orthogonal to the beam direction z, as represented in Fig. 21.
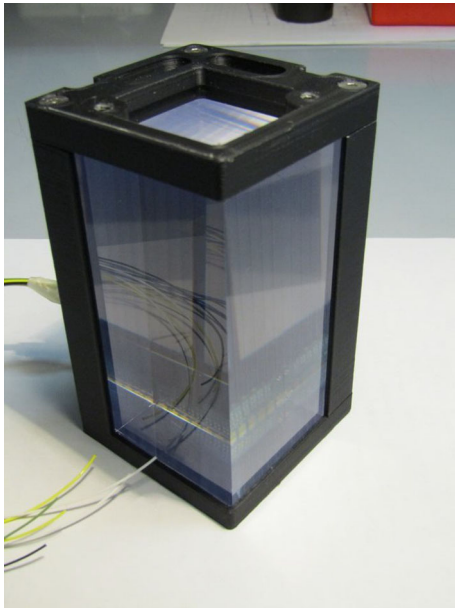
Fig. 19 ΔE-E telescope prototype
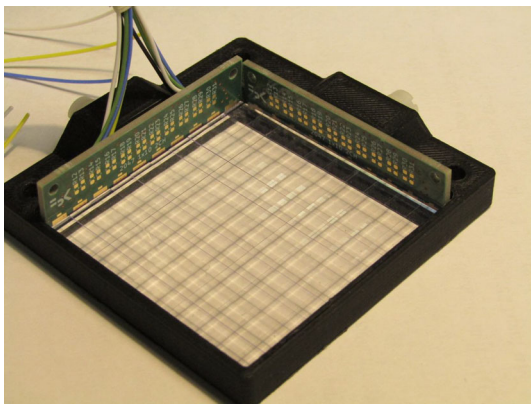
Fig. 20 Complete ΔE of the telescope, composed by two layers of orthogonal bars, read by 2 arrays of SiPMs

2.5.3 Spectrometer simulation

A Monte Carlo simulation of the overall setup has been performed using the GEANT4 [97] simulation software, in order to define the expected response to the pairs emitted by the isovector magnetic dipole 17.6 MeV ($J^\pi = 1^+$, T = 1) state $\rightarrow$ ground state ($J^\pi = 0^+$, T = 0) and the isoscalar magnetic dipole 18.15 MeV ($J^\pi = 1^+$, T = 0) state $\rightarrow$ ground state transitions in ^{8}Be. The simulation aimed at estimating the response to the γ-ray background, the deposited energy spectrum and resolution, and the detection efficiency. The presence of an experiment-like target is taken into account by using a particle source of finite dimensions ($\sim$ 1 mm $\times$ 1 mm $\times$ 0.0035 mm) placed at the expected target-detector distance (Fig. 21).
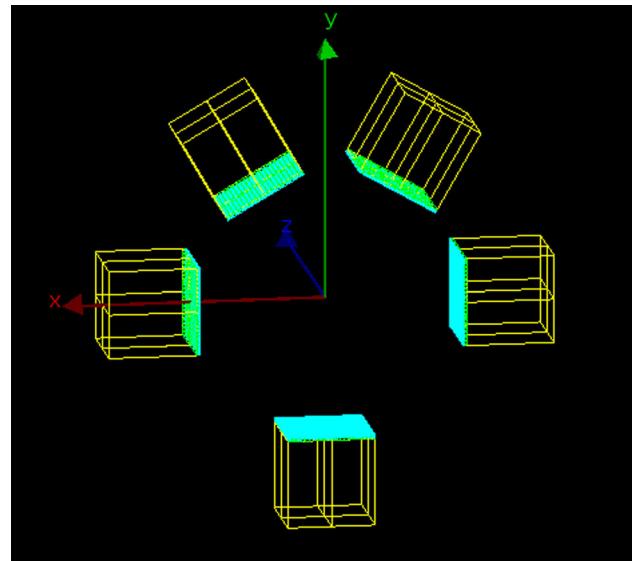
Fig. 21 Simulated spectrometer with relative angular disposition $0°-60°-120°-180°-270°$, similar to the setup used in the ATOMKI experiment

2.5.4 Background suppression

The dominant background source is due to the γ-rays emission from the populated resonances. Requiring a triple coincidence in the three layers of the telescopes reduces this kind of background. Indeed, few MeV γ-rays interact with the detectors mostly through Compton scattering and the simulation shows that given the EJ200 stopping power, the γ detection efficiency in a single clover is $\epsilon_\gamma \sim 6 \cdot 10^{-6}$. This probability further reduces requiring the detection of two particles (pair) in two separate clovers.

Taking into account the estimated efficiencies and the branching ratio between γ and IPC emission, the expected signal-over-noise ratio results to be of the order of 10.

2.5.5 Detection efficiency and resolution

In order to study the detection efficiency and resolution of the detectors, electrons and positrons have been simulated separately, emitting them in three different configurations: pointing to the center of the front face of a telescope; pointing to the center of the front face of a clover; with an isotropic distribution on the solid angle covered by a clover. The number of photons collected has been estimated starting from the known light-yield of the EJ200 material (10k photons/MeV), properly scaled down to consider light absorption effects and quantum efficiency of the photosensors. Therefore, the simulations were run using three different light yield values (30 phe/MeV, 60 phe/MeV and 100 phe/MeV). Moreover, a Poisson distribution of the number of photons was used to take into account the light collection statistics. The
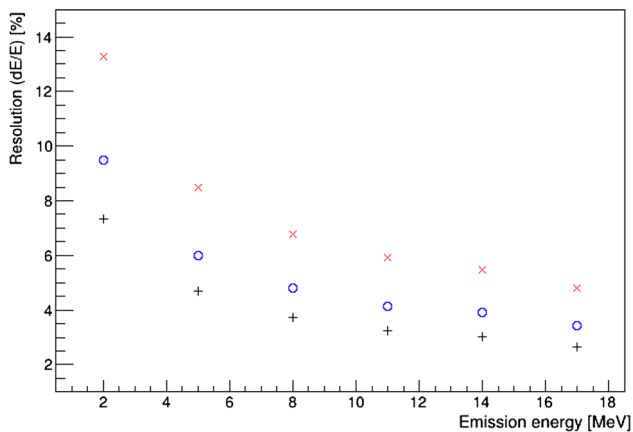
Fig. 22 Energy resolution of a single clover measuring electrons entering perpendicular to the center of its front face, as a function of the emission energy of the particles. The three data sets account for different light-yields: 30 phe/MeV (red stars), 60 phe/MeV (blue circles), 100 phe/MeV (black crosses)
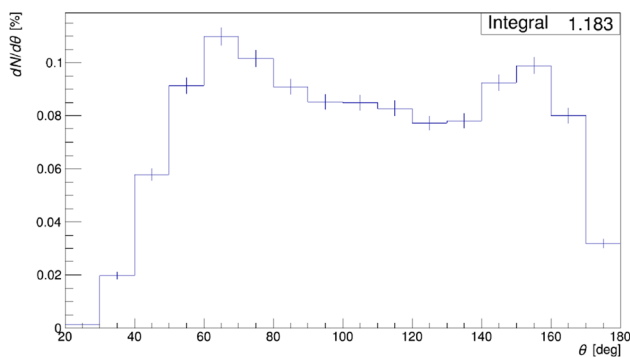

Fig. 23 Detection efficiency distribution as a function of the correlation angle between e^+ and e^- for detector placed at angles 0°, 60°, 120°, 180° and 270°

efficiency distributions have been obtained integrating the measured energy peak within 3σ. Figure 22 shows the resolutions obtained simulating electrons emitted orthogonally with respect to the clover face center varying the light-output yield.

2.5.6 Efficiency as a function of the correlation angle

The efficiency distribution as a function of the correlation angle between the leptons belonging to the same pair has been estimated considering uncorrelated and isotropic electron and positron emissions. Considering a detector arrangement similar to the one reported in reference [2] (0°, 60°, 120°, 180° and 270°), the integrated detection efficiency results to be $\epsilon_{\text{pairs}} \sim 1.18\%$, which is consistent with the purely geometrical acceptance of the setup that is $\epsilon_{\text{max}}^{\text{pair}} \sim 2.5\%$. The shape of the angular distribution obtained in this configuration (Fig. 23) is also compatible with the one obtained by ATOMKI's group with the same disposition [2].
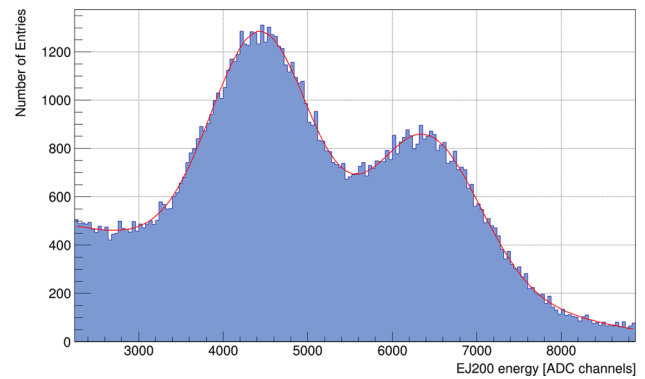
Fig. 24 Pseudo-peaks generated in the EJ200 spectrum by the projections, at fixed energies measured in the NaI(Tl) detector, of the Compton scattering events of 1173 MeV and the 1332 MeV γ-rays

### 2.5.7 Detector prototype characterization

A characterization of the first detector prototypes and a comparison between the calculated and the experimental performances are necessary to validate the simulation work and use it for a detailed analysis of the systematic errors.

2.5.8 Calorimeter characterization

The first component of the setup that has been characterized is the E layer calorimeter. The energy resolution has been analyzed as a function of the area covered by the SiPM used to read the calorimeter. The lack of mono-energetic electron sources in the few MeV region requires the use of indirect calibration methods. One possibility is to exploit low energy electrons emitted by Compton scattering reactions induced by low energy γ-rays. Indeed, one can determine the electron energy on an event by event basis by measuring the Compton scattered γ-ray energy in an external detector and applying energy conservation laws. To this purpose, a ^{60}Co source has been used, coupling the EJ200 calorimeter with an NaI detector, kept at a fixed relative angle. Intervals of electron energies can be selected by gating on the ancillary γ-ray detector spectrum. Figure 24 shows the output of such procedure, where two pseudo-photopeaks are present, due to the two major transition channels of ^{60}Co (1173 MeV and 1332 MeV). Several measurements using different SiPM dimensions have been performed, with a reading area of 36 mm^2, 72 mm^2 and 1 cm^2, showing a clear improvement of resolution as a function of the covered area.

As shown in Fig. 25, gating on different electron energies we observe a linear trend between the inverse of the square resolution and the deposited energy. The measurement performed using the SiPM with 1 cm^2 returns a light yield value of $L_y = 237 \pm 5$ phe/MeV.
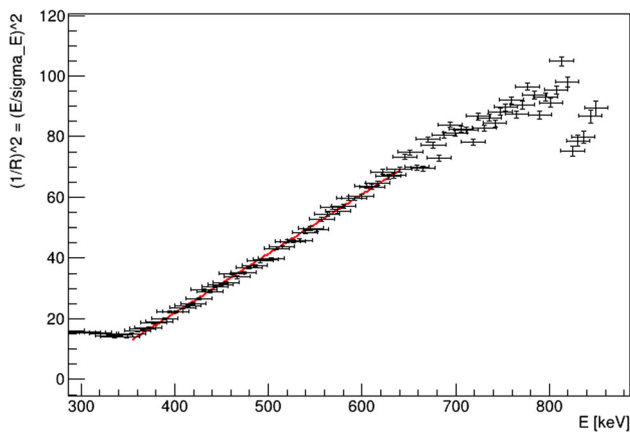
Fig. 25 Trend of the inverse of the square resolution obtained for several pseudo-photopeaks in the EJ200 calorimeter as a function of the electron energy. In this case, the EJ200 calorimeter is read out by a 1 cm × 1 cm SiPMs
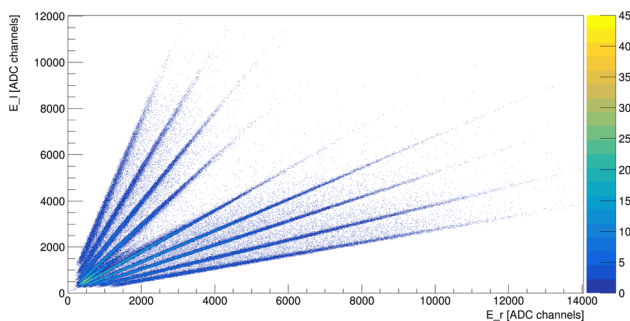

Fig. 26 Correlation spectrum obtained by the signals E_r and E_l measured using 9 scintillator bars coupled to 9 SiPMs

2.5.9 Tracking layer characterization

A characterization of the ΔE layer is also needed, especially in view of the novel readout scheme implemented. As previously mentioned, the tracking stage is made of two orthogonal segmented layers. Each layer is composed of an array of 10 bars, and is read from the two ends of a voltage divider. Such chain distributes the signals produced by the single SiPMs, attached to each bar, to the two ends of the array, where the signal is amplified and read out. A coincidence spectrum between the two sides signals is shown in Fig. 26.

In order to estimate the resolving power two quantities have been computed: the total energy of a measured event $E_{tot} = E_l + E_r$ and its energy asymmetry $y = \frac{E_r - E_l}{E_r + E_l}$. The correlation spectrum between the asymmetry and the total energy, presented in Fig. 27, shows that the setup is able to reach a good resolving power. Further work is needed to precisely determine the position identification thresholds.
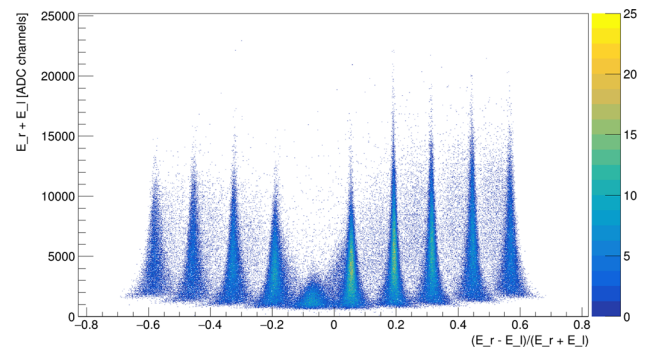
Fig. 27 Correlation of the total energy $E_l + E_r$ against the energy asymmetry $(E_r - E_l) / (E_r + E_l)$

2.5.10 Resolution on the reconstructed invariant mass

The presence of the X17 boson would lead to a structure in the invariant mass distribution of the detected pairs, as well as in the distribution of the correlation angle between the leptons [1,6].

Being the invariant mass dependent on the energies of the two leptons of a pair, and on their correlation angle, its associated error depends on this two quantities and their resolutions. The electron and positron energies are correlated because of the energy conservation of the boson decay, and the energy resolution is related to the light yield. Thus, the invariant mass resolution can be computed as a function of E_{e^-}, L_y, $\theta_{e^+e^-}$ and σ_θ. Marginalizing the electron energy and the correlation angle, which are not fixed in the experiment, the invariant mass resolution depends only on the angular resolution and the light yield: with the results obtained for these two parameters it has been proved that it will be possible to reach a final resolution of $\frac{\sigma_{M_{+-}}}{M_{+-}} \sim 1\%$.

2.5.11 Conclusions

The construction of a new pair spectrometer for the measurement of electron-positron pairs sharing up to 20 MeV kinetic energy is ongoing. The aim is to build a device capable of repeating the ATOMKI experiment [1] on ^{8}Be decays exploiting the low energy proton beams provided by the AN2000 and CN facilities at LNL. The proposed design of the detector tries to optimize material budget and angular resolution by keeping a simple and cost-effective layout. This is done by exploiting a specific arrangement of EJ200 plastic scintillator bars read-out by SiPMs arrays. The device can be operated in vacuum, allowing to minimize the amount of matter seen by the particles before reaching the first detection layer. This turns out to be quite important both to constrain the detection thresholds and to improve the angular resolution by minimizing multiple scattering effects. The work done so far shows that the proposed design is compatible with the exper-

imental specifications and is expected to achieve an invariant mass resolution of about 1%. It is also worth noticing that this device could be operated in a magnetic field, allowing for future coupling to charge sensitive e^+e^- spectrometers.

3 Theoretical interpretations

3.1 Theoretical introduction to new physics explanations of the ATOMKI ^{8}Be and ^{4}He anomalies

Jonathan L. Feng

Department of Physics and Astronomy, University of California, CA 92697, USA

Abstract The ATOMKI ^{8}Be and ^{4}He results are among the most interesting anomalies to appear in many years. In this talk, I briefly review why these results are particularly tantalizing from a new physics perspective and the essential features that must be explained by any new physics interpretation. I then give examples of new physics explanations that don't work and proposed solutions that do work, and I conclude with thoughts about what must be done to reach a compelling resolution.

3.1.1 Could this be new physics?

The ATOMKI ^{8}Be results [1] shown in Fig. 28 and similar results for ^{4}He [53] are among the most interesting anomalies to appear in many years. There are many reasons these results are particularly tantalizing from a new physics perspective:

1. The anomalies are statistically significant. They are both roughly 7σ excesses and are unlikely to disappear with more data. Irrespective of whether they will ultimately be explained by new physics, we are likely to learn something interesting.
2. The excesses are bumps. They are localized in opening angle $\theta_{e^+e^-}$ and invariant mass $m_{e^+e^-}$. Diffuse excesses or excesses that appear at an experiment's kinematic limit are much more likely to have mundane explanations. (Of course, higher resolution and sharper bumps would be even better.)
3. The excess reported in Ref. [1] rises and falls as one scans through the resonance by varying the proton beam energy. (For recent results indicating continuum production, consistent with the analysis of Refs. [8,68], see other contributions to these proceedings [98].)
4. There are no compelling SM explanations. After 7 years, possible SM explanations have been studied [27,67], and no SM resolution has been found.
5. There are no experimental explanations. After 7 years, there are also no simple experimental resolutions.
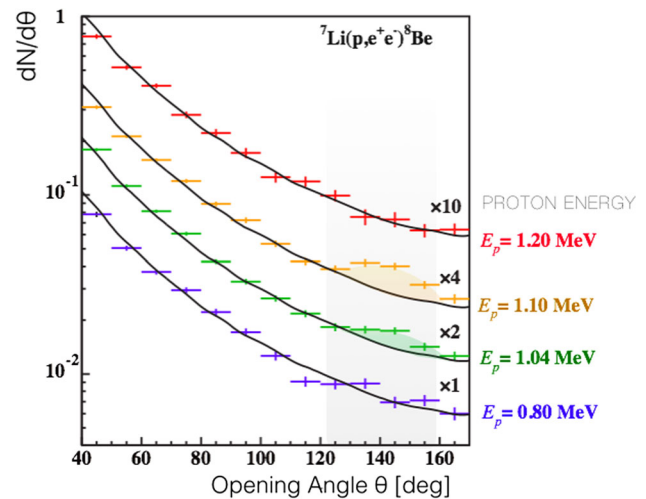
Fig. 28 The ATOMKI excess at opening angle $\theta_{e^+e^-} \approx 140°$ observed in the reaction $p\,^7\text{Li} \to\,^8\text{Be}\,e^+e^-$ [1]. The different colors show the spectrum as one scans through resonance by varying the proton beam energy, as indicated. From Ref. [99]

6. The fit improves drastically with the introduction of a single new particle [1,94]. *A priori* the excess need not have a shape consistent with the simplest new physics explanations.
7. The ^{8}Be and ^{4}He results support each other. In particular, the excess shifts from $\theta_{e^+e^-} \approx 140°$ for ^{8}Be [1] to 115° for ^{4}He [94]. Such a shift excludes many experimental systematic error explanations, but it is exactly what is expected for all of the simplest new particle explanations [8,57]. Additionally, the size of the ^{4}He excess is consistent with the *prediction* of the protophobic gauge boson explanation of the ^{8}Be anomaly [39].
8. And last, very generally, the observations fit beautifully with current ideas in physics and cosmology that motivate weakly-interacting, light particles; see Fig. 29.

3.1.2 Essential features of the signal

If the ATOMKI anomalies are evidence for the production of a new particle X, one can quickly identify a few essential features that constrain any viable new physics explanation:

1. X is produced through its nuclear (quark) couplings and decays through its electron coupling.
2. The bumps at $\theta_{e^+e^-} \approx 140°$ for ^{8}Be and 115° for ^{4}He imply that the X has a two-decay $X \to e^+e^-$ and $m_X \approx 17$ MeV.
3. X is therefore a neutral boson, and the discovery of X implies the discovery of a fifth force with a characteristic range of 12 fm.
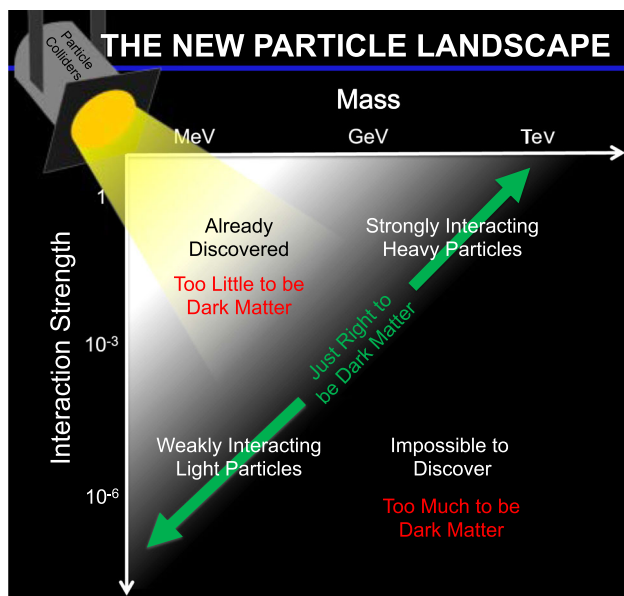
Fig. 29 The new particle landscape. New particles are classified in the (mass, interaction strength) plane. Strongly-interacting, light particles have already been discovered, and weakly-interacting, heavy particles are impossible to discover at particle and nuclear accelerator experiments. The current frontier therefore lies on the diagonal that contains strongly-interacting, heavy particles and weakly-interacting, light particles. Remarkably, this diagonal is also motivated by thermal relic dark matter and the WIMPless miracle [100,101], and the X17 anomalies are naturally explained by weakly-interacting, light particles that lie in this same diagonal swath of parameter space

4. The signal rate is determined by $\sigma(^8\text{Be}^* \to {}^8\text{Be}\, X) \times \text{BR}(X \to e^+e^-)$.

5. Other decay modes are possible ($X \to \nu\bar{\nu}$, DM, . . .), but to maintain the signal rate, these would require larger nuclear couplings, which are more prone to exclusion. Without much loss of generality, then, one can assume $\text{BR}(X \to e^+e^-) = 1$.

6. With this assumption, X's nuclear couplings are completely determined by the signal rate.

7. X's electron coupling cannot be too small, since the X cannot travel too far before decaying.

8. The quantum numbers of the reactions and symmetries of the physics models impose theoretical constraints on possible explanations.

9. All experiments that have probed the 10 MeV-scale since the early days of nuclear and particle physics impose additional experimental constraints on possible explanations.

3.1.3 Explanations that don't work

Scalars Can the X particle be a spin-0 boson with quantum numbers $J^P = 0^+$? The decay $^8\text{Be}^* \to {}^8\text{Be}\, X$ would then be a $1^+ \to 0^+0^+$ decay. Angular momentum conservation then

implies that the final state has $L = 1$, but parity conservation implies $P = (-1)^L = 1$, leading to a contradiction. A scalar X is therefore not a viable explanation of the ^8Be results, at least in parity-conserving theories [8,57].

The Dark Photon One may instead consider a spin-1 boson. In general, one may parameterize this boson's couplings to fermions f as $\epsilon_f e$, where e is the SM electromagnetic coupling. Drawing on the similarities to the photon to determine the necessary nuclear matrix elements, one finds that the ^8Be signal rate implies $|\epsilon_u + \epsilon_d| \approx 3.7 \times 10^{-3}$ [8,57].

The dark photon A' is the specific example of a spin-1 boson that has couplings that are identical to the photon's, but suppressed by a small, universal parameter ϵ; that is $\epsilon_f = \epsilon Q_f$, where Q_f is the fermion's SM electric charge. To get the right signal rate, then, one needs $\epsilon \approx 0.01$, which is excluded by experiments. The dark photon is therefore not a viable explanation of the ATOMKI results [8,57].

3.1.4 Possible solutions

Vectors, Axial Vectors, Pseudoscalars To find a possible solution, then, one must consider other neutral bosons. Viable explanations of the original ^8Be signal include candidates in all of the possible categories: vectors that are not dark photons [8,57,102–106], axial vectors [41,107], and pseudoscalars [58,59]. For a review of the early works, see Ref. [108], and for other, more recent proposals, see the other talks at this workshop.

The Protophobic Gauge Boson The protophobic gauge boson was the first new physics proposal to resolve the ^8Be anomaly. It is still viable and remains interesting, in part because, unlike other proposed explanations of the ^8Be results, it also explains the observed ^4He excess.

As noted in Sect. 3.1.3, the dark photon is excluded by other experimental constraints. The most stringent of these constraints are from searches for exotic pion decays to 17 MeV X particles $\pi^0 \to \gamma X$, followed by $X \to e^+e^-$. The X particle is produced by the SM pion decay triangle diagram, with one photon replaced by X. Its amplitude is therefore proportional to $\epsilon_u Q_u - \epsilon_d Q_d$, and so this production is suppressed if $2\epsilon_u + \epsilon_d = \epsilon_p \approx 0$, that is, if the spin-1 gauge boson is protophobic. A spin-1 gauge boson that couples to neutrons but not protons, may therefore explain the ^8Be results without violating other constraints. Examples of protophobic bosons include $B - Q$ and $B - L - Q$ gauge bosons, where B, L, and Q are the SM baryon number, lepton number, and electric charge.

A detailed analysis [8,57] of all existing constraints found that the viable hadronic couplings of the protophobic gauge boson are $\epsilon_u, \epsilon_d \sim 10^{-3}$, with $2\epsilon_u + \epsilon_d \lesssim 0.1\epsilon_u$, which is sufficiently protophobic to satisfy the pion constraints. For the
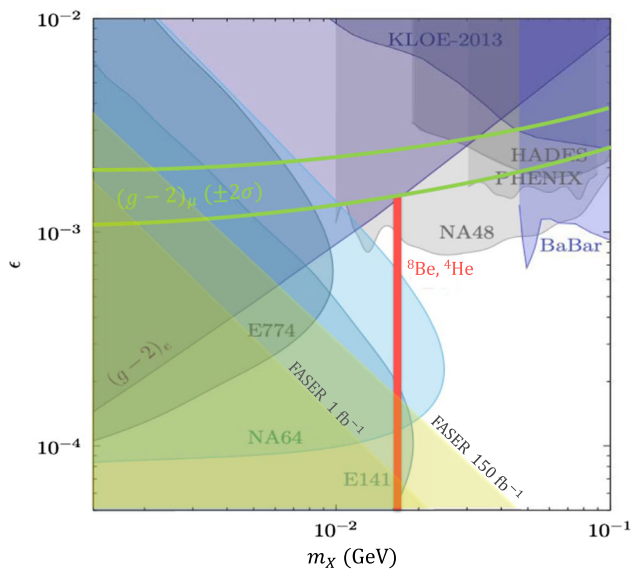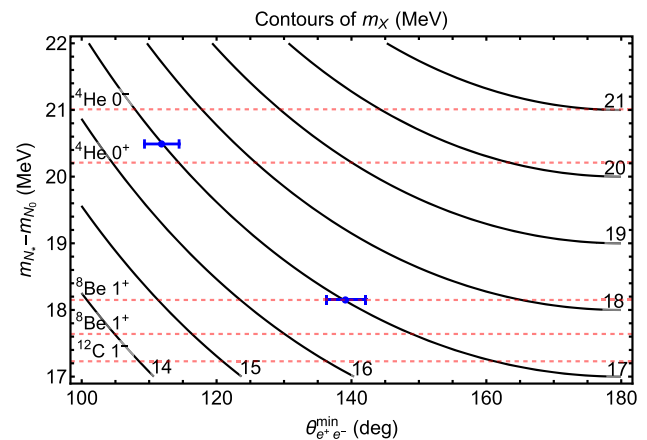
Fig. 30 Protophobic gauge boson parameter space, where m_X is the mass of the X boson, and ϵ is its electron coupling. The figure is adapted from Ref. [15] with a few supplementary contours. The ^{8}Be and ^{4}He anomalies may be resolved in the red region [8,57]. Between the green contours, assuming $\epsilon_\mu = \epsilon_e$, the X boson also reduces the current 4.2σ discrepancy in $(g-2)_\mu$ to 2σ. The blue and purple regions are excluded by the indicated experiments; the gray NA48 region is not applicable to protophobic gauge bosons. FASER will be sensitive to the yellow regions with the LHC Run 3 integrated luminosities indicated [110]

Fig. 31 Contours (black solid lines) of the X boson mass m_X in the plane of the minimum opening angle $\theta_{e^+e^-}^{\min}$ and the nuclear state mass splitting $m_{N_*} - m_{N_0}$. Particularly relevant mass splittings are indicated by red dashed lines. The blue points and error bars indicate the parameters where 7σ excesses have been found in ^{8}Be and ^{4}He nuclear decays. As can be seen, the excesses are at different opening angles $\theta_{e^+e^-}^{\min}$, but both are consistent with the production of a 17 MeV X boson. From Ref. [39]

3.1.5 Paths toward a resolution

When the protophobic explanation was announced in April 2016, it and the ATOMKI anomaly itself elicited a large range of reactions. The most interesting to me was from James Bjorken, who noted that all new physics interpretations may be considered longshots, and they need not be demoted further by theoretical arguments. Instead, he asked: How can these ideas be tested? What are their other experimental implications?

electron coupling, the allowed values are shown in Fig. 30. The originally allowed range was $5 \times 10^{-5} \lesssim \epsilon_e \lesssim 2 \times 10^{-3}$, where the lower and upper limits are set by constraints from beam dump experiments and $(g-2)_e$, respectively. Assuming $\epsilon_\mu = \epsilon_e$, the current 4.2σ discrepancy in $(g-2)_\mu$ [109] may be reduced to 2σ at the upper end of the allowed range of ϵ_e. The range $5 \times 10^{-5} \lesssim \epsilon_e \lesssim 2 \times 10^{-4}$ is disfavored by E141, but, as can be seen in Fig. 30, $m_X = 17$ MeV is at the kinematic limit of this constraint and, given this caveat, this range should probably not be considered definitively excluded. Later null results from NA64 have excluded the range $1 \times 10^{-4} < \epsilon_e < 7 \times 10^{-4}$ [15]. Anomaly-free models supporting the viable parameter ranges have been constructed in Ref. [57].

Clearly, it would be good to have additional measurements of the nuclear decays. We are now in the bizarre situation that after 7 years, the revolutionary and specific claims of the ATOMKI group have not yet been checked by others. This status quo should not be allowed to persist for much longer. For the reasons given in Sect. 3.1.2, essentially all new physics interpretations postulate a new 17 MeV particle, and so all nuclear decays with sufficient mass splittings to produce a 17 MeV particle are suitable targets. Obviously, it would be good for other collaborations to study the ^{8}Be (18.15) decay. But other systems can also be valuable. As noted, the ATOMKI group has already provided further evidence for a new physics interpretation of the ^{8}Be anomaly by discovering a similar effect in ^{4}He decays. As illustrated in Fig. 31, the excesses peak at different opening angles, but both are consistent with the production of a new 17 MeV particle, providing a spectacular kinematic cross check. Additional decays of interest are those of the excited ^{8}Be (17.64) nucleus, which is very similar to the ^{8}Be (18.15) state and so has a similar, but phase space-suppressed, decay in most models, and the decays of the $J^P = 1^-$ state ^{12}C (17.23), which has different quantum numbers (and is, unfortunately, also quite phase-space suppressed).

The signal rates are also important, as the couplings required to explain the ^{8}Be anomaly imply definite branching ratios for other decays. For example, in the protophobic gauge boson model, the required couplings imply a ^{4}He decay width of $\Gamma(^4\text{He}(20.21) \rightarrow {}^4\text{He}\, X) = (0.3-3.6) \times 10^{-5}$ eV [57]. This is in remarkable agreement with the observed value of $(2.8-5.2) \times 10^{-5}$ eV and is highly non-trivial. For other new physics models, an effective field theory analysis shows that

the predicted and observed ^{4}He signal may differ by two or more orders of magnitude [57].

Other experiments may also confirm or exclude the proposed new physics interpretations by testing either the hadronic or electronic couplings. For example, many experiments will be sensitive to the required electron couplings in the near future. These include NA64, which has already excluded relevant ranges for ϵ_e [15], and will be sensitive to values in the remaining "high-ϵ_e" window, $7 \times 10^{-4} < \epsilon_e < 2 \times 10^{-3}$ in the next few years. Starting with the first fb^{-1} of data at LHC Run 3 in a few months, FASER will provide a complementary probe of the "low-ϵ_e" window, $5 \times 10^{-5} < \epsilon_e < 1 \times 10^{-4}$, and will completely cover this window with the full LHC Run 3 integrated luminosity of 150 fb^{-1} [20,110,111]. Another direct probe is provided by PADME [18], a fixed target experiment with a mono-energetic e^+ beam that can search for X resonances in the process $e^+e^- \to X \to e^+e^-$.

In summary, the ATOMKI ^{8}Be results have been tantalizing for 7 years, and their interest has been supplemented now by the ^{4}He results. New physics explanations require a new weakly-interacting particle with a mass of 17 MeV, with connections to beautiful ideas in particle physics and cosmology. There are by now many interesting explanations, and these strongly motivate a diverse set of nuclear and particle experiments to confirm or exclude this potentially revolutionary discovery of new physics.

3.2 Explanation of the Atomki anomaly in $U(1)'$-extensions of the Standard Model

Luigi Delle Rose

Institut de Fisica d'Altes Energies (IFAE), The Barcelona Institute of Science and Technology, Campus UAB, 08193 Bellaterra (Barcelona), Spain
Dipartimento di Fisica, Università della Calabria, I-87036 Arcavacata di Rende, Cosenza, Italy
Shaaban Khalil
Center for Fundamental Physics, Zewail City of Science and Technology, 6 October City, Giza 12588, Egypt
Stefano Moretti
School of Physics and Astronomy, University of Southampton, Southampton, SO17 1BJ, United Kingdom
Department of Physics and Astronomy, Uppsala University, Box 516, SE-751 20 Uppsala, Sweden

Abstract Motivated by the anomalies observed by the Atomki collaboration, we study some extensions of the Standard Model with a gauged $U(1)'$ symmetry. We focus on the role of an extended scalar sector and of the origin of the new mass scale suggested by the anomaly.

3.2.1 Introduction

The quest for New Physics has always been characterised by a twofold approach, the high energy frontier, typically pursued through multi-purpose experiments at hadron colliders, and the high precision frontier, typically exploited at lepton collider experiments. However, surprises may also arise in other contexts such as from lower energy experiments. In this respect, an interesting result has recently been reported in [1] (see also [4,5,64,66]) by the Atomki experiment [2]. In the data collected by the pair spectrometer a 6.8σ anomaly was observed in the decay of an exited state of the ^{8}Be. Upon analysis of the electron-positron properties, the spectra of both their opening angle and invariant mass presented the characteristics of an excess consistent with an intermediate boson X being produced on-shell in the decay of the ^{8}Be* state, with the X object subsequently decaying into e^+e^- pairs. As further investigations, the collaboration has also considered the decays of other excited beryllium and carbon nuclei and recently it has reported the observation of a 7.2σ excess in one of the ^{4}He transitions [6,65].

In this contribution we discuss the theoretical aspects of possible solutions to these results, assuming that the neutral boson could be a spin-1 object, and we comment on the embedding of such solutions in beyond Standard Model (SM) scenarios.

3.2.2 The $U(1)'$ extension of the SM and its scalar sector

An attempt to explain the nature and the properties of the X boson was carried out in [8,57], in which a new spin-1 boson, Z', was considered, with vector-like couplings to the SM quarks and leptons and a mass $M_{Z'} \simeq 17$ MeV. Further studies of such, or other, scenarios have been performed in [36,39,58,67,102–105,112–115]. The interactions of such a light state are strongly constrained by the $\pi^0 \to Z' + \gamma$ searches at the NA48/2 experiment [116] which require the Z' to be 'protophobic', namely, that its couplings $e\epsilon_u$ and $e\epsilon_d$ of up and down quarks, defined as multiple of the electric charge, satisfy the condition $2\epsilon_u + \epsilon_d \lesssim 10^{-3}$ [8,57].

Here we will consider, in full generality, one of the simplest extensions of the SM, described by an extra $U(1)'$ group, that is able to accommodate for a light spin-1 gauge boson [117–122]. This scenario potentially provides a the-

oretically consistent framework that is able to address the physics involved in the Atomki anomaly [123]. In this contribution we will focus on model-building.

A key property of this class of models, arising from the presence of two abelian symmetries, $U(1)_Y \times U(1)'$, is that the kinetic Lagrangian of the corresponding gauge fields, $\hat{B}_\mu$ and $\hat{B}'_\mu$, allows for a gauge invariant mixing of the corresponding field-strengths, namely

$$\mathscr{L}_{\text{kin}} = -\frac{1}{4}F_{\mu\nu}F^{\mu\nu} - \frac{1}{4}F'_{\mu\nu}F'^{\mu\nu} - \frac{\kappa}{2}F'_{\mu\nu}F^{\mu\nu}, \qquad (1)$$

with κ being the kinetic mixing parameter between $U(1)_Y$ and $U(1)'$. The Lagrangian can be recast into a diagonal form by a suitable transformation of the gauge fields. In the diagonal basis, the gauge covariant derivative becomes

$$\mathscr{D}_\mu = \partial_\mu + \cdots + ig_1 Y B_\mu + i(\tilde{g}Y + g'z)B'_\mu, \qquad (2)$$

where Y and z are the SM hypercharge and the $U(1)'$ charge, respectively, and g' and $\tilde{g}$ are the two gauge coupling constants of the $U(1)'$, with $\tilde{g}$ playing the role of the kinetic mixing κ introduced above.

Due to the mixing coupling $\tilde{g}$ in the covariant derivative given above, after spontaneous symmetry breaking, the EW vev v affects the $U(1)'$ mass term (even if the Higgs sector is neutral under the new abelian symmetry). As an example, if we consider only Higgs doublet charged under $SU(2)$, the Lagrangian providing the neutral gauge boson mass matrix reads as

$$-\mathscr{L}_{\text{Higgs}} = \frac{v^2}{8}(g_2 W^3_\mu - g_1 B_\mu - g_\Phi B'_\mu)^2 + \frac{m^2_{B'}}{2}B'^2_\mu + \cdots, \qquad (3)$$

where we have defined $g_\Phi = \tilde{g} + 2z_\Phi g'$ with z_Φ being the $U(1)'$ charge of the SM Higgs. The mass term $m^2_{B'}$, instead, represents a possible source for the Z' mass from a sector neutral under the SM gauge group. In its simplest instance, this can be achieved by the vev v' of a SM-singlet scalar χ that has a z_χ charge under $U(1)'$ and in this case $m_{B'} = g'z_\chi v'$. The mixing in the neutral gauge sector is only triggered by the g_Φ coupling and, as such, is unaffected by the details of the sector generating the mass term $m_{B'}$. As one can infer from the equations above, a non-vanishing g_Φ can be achieved either by the non-zero $U(1)'$ charge of the Higgs field, $z_\Phi \neq 0$, or by the presence of a non-zero kinetic mixing $\tilde{g} \neq 0$. Both of them equally contribute to a $Z - Z'$ mass mixing. For a weakly interacting and light Z', namely $g', \tilde{g} \ll g_Z$ and $m^2_{B'} \ll v^2$, the masses and the mixing angle of the neutral gauge bosons are

$$M^2_Z \simeq \frac{1}{4}g^2_Z v^2, \quad M^2_{Z'} \simeq m^2_{B'}, \quad \tan 2\theta' \simeq -2\frac{g_\Phi}{g_Z}. \qquad (4)$$

As expected, the Z' mass is controlled by the $m_{B'}$ parameter or, equivalently, by the vev v' of a putative SM-singlet χ. The

Z' massless limit for $m_{B'} = 0$ is naively reproduced. Indeed, if spontaneous symmetry breaking is turned off in the SM-singlet scalar sector, no new scalar degrees of freedom are available to describe the longitudinal component of a massive Z'. For a 17 MeV Z' with $g' \sim 10^{-3}$, as required to reproduce the Atomki anomaly in these scenarios, we get $v' \sim 10$ GeV. A new mass scale, unrelated to the EW one, is necessarily introduced.

The expansions in Eq. (4) are obtained in scenarios with only one $SU(2)$ Higgs doublet, as in the SM. This assumption can be obviously relaxed and more Higgs doublets can be envisaged. We show, indeed, that this possibility leads to an interesting phenomenology in the Z' sector and provides alternative solutions to the ^{8}Be anomaly.

Among several possibilities, we focus on a 2-Higgs Doublet Model (2HDM) scenario, with the two scalar doublets Φ_1 and Φ_2 having the same hypercharge $Y = 1/2$ but two different charges z_{Φ_1} and z_{Φ_2} under the extra $U(1)'$. As we will comment below, this scalar sector has the advantage to provide a simple explanation of the new mass scale, pointed out by the Atomki anomaly, naturally binding it to the EW one.

For the sake of generality, we also consider, alongside spontaneous symmetry breaking in the EW sector, a contribution to $U(1)'$ symmetry breaking through the VEV $\langle\chi\rangle = v'$ of an extra SM-singlet scalar χ, indeed connected to the mass term $m_{B'} = g'z_\chi v'$. In the limit of small $g', \tilde{g}$ couplings, the mass of the Z' is

$$M^2_{Z'} \simeq m^2_{B'} + \frac{v^2}{4}g'^2(z_{\Phi_1} - z_{\Phi_2})^2 \sin^2(2\beta), \qquad (5)$$

where $\tan \beta = v_2/v_1$. The mass is non-vanishing even when $m_{B'} \to 0$ if the two scalar doublets have different charges, z_{Φ_1} and z_{Φ_2}, under the $U(1)'$ group. In this case, an extra sector is not strictly required to generate a mass for the Z'. In particular, in the $m_{B'} \simeq 0$ limit (which is equivalent to $v' \simeq 0$) there is no contribution from the dark sector and one finds, for $M_{Z'} \simeq 17$ MeV and $v \simeq 246$ GeV, that $g' \sim 10^{-4}$. Interestingly, the same order of magnitude of the gauge coupling is required to explain the Atomki anomaly if the Z' gauge boson interacts with the SM fermions with both vector and axial-vector couplings.

To summarise: (1) in case of one Higgs doublet, the limit $m_{B'} \ll v$ leads to $M'_Z \simeq m_{B'}$ and the SM Higgs sector does not play any role in the generation of the Z' mass; (2) in an extended scalar sector instead, such as the 2HDM case with $z_{\Phi_1} \neq z_{\Phi_2}$, the symmetry breaking of the $U(1)'$ can actually be realised without the extra SM-singlet χ, namely with $v' = 0$. The typical CP-odd state of the 2HDM extensions here plays the role of the longitudinal degree of freedom of the Z' and, as such, differently from standard constructions, the particle spectrum is characterised by a missing pseudoscalar state.

Table 3 Flavour universal charge assignment in the $U(1)'$ extension of the SM

	$SU(3)$	$SU(2)$	$U(1)_Y$	$U(1)'$
Q_L	3	2	1/6	z_Q
u_R	3	1	2/3	z_u
d_R	3	1	$-1/3$	$2z_Q - z_u$
L	1	2	$-1/2$	$-3z_Q$
e_R	1	1	-1	$-2z_Q - z_u$
s_i	1	1	0	z_{s_i}

3.2.3 The fermion sector

Having discussed the spontaneous symmetry breaking of the $U(1)'$, we can now comment on the fermion sector and the constraints imposed by the new gauge symmetry.

Firstly, as common in 2HDM extensions, one has to deal with the presence of large tree-level flavour changing neutral currents. In this class of models, this is automatically taken into account by the new abelian gauge symmetry which replaces the ad-hoc discrete Z_2 symmetry [124,125]. Secondly, the cancellations of gauge and gravitational anomalies strongly constrain the charge assignment of the SM spectrum under the extra $U(1)'$ gauge symmetry. These typically imply the introduction of SM-singlet fermions, s_i, which could also be exploited, in some scenarios, for implementing a seesaw mechanism generating light neutrino masses. The actual charges and masses of these new states, if present, strongly depend on the specific realisation of the fermion sector. Nevertheless, these SM-singlet states are irrelevant for the explanation of the anomaly. Much more complicated fermion sectors are obviously possible. Here we choose to explore a scenario that is minimal in that respect. Indeed, while an extended scalar sector (either dark or visible) is necessarily required to provide a mass for the Z', the SM light fermions are enough to describe the physics of the Atomki anomaly.

The general charge assignments of the spectrum in our extension of the SM, in a flavour universal scenario, are given in Table 3, where the z_{s_i}'s are chosen to cancel the anomaly in the $U(1)'U(1)'U(1)'$ and $U(1)'GG$ triangle diagrams, G being the gravitational current.

The interactions between the SM fermions and the Z' gauge boson are described by the Lagrangian $\mathscr{L}_{\text{int}} = -J_{Z'}^\mu Z'_\mu$, where the gauge current is given by

$$J_{Z'}^\mu = \sum_f \bar{\psi}_f \gamma^\mu \left(C_{f,L} P_L + C_{f,R} P_R \right) \psi_f \qquad (6)$$

with left- and right-handed couplings

$$C_{f,L} = -g_Z s' \left(T_f^3 - s_W^2 Q_f \right) + (\tilde{g} Y_{f,L} + g' z_{f,L}) c',$$

$$C_{f,R} = g_Z s_W^2 s' Q_f + (\tilde{g} Y_{f,R} + g' z_{f,R}) c'. \qquad (7)$$

In these equations we have used the notation $s_W \equiv \sin\theta_W$, $c_W \equiv \cos\theta_W$, $s' \equiv \sin\theta'$ and $c' \equiv \cos\theta'$. We have also introduced Y_f the hypercharge, z_f the $U(1)'$ charge, T_f^3 the third component of the weak isospin and Q_f the electric charge of a generic fermion f. These equations can considerably be simplified by exploiting the fact that the product $g_Z s'$ is of the same order of $\tilde{g}$ for g', $\tilde{g} \ll 1$. In terms of the vector and axial-vector components of the Z' interactions one finds

$$C_{f,V} \simeq \tilde{g} c_W^2 Q_f + g' \left[z_\Phi (T_f^3 - 2s_W^2 Q_f) + z_{f,V} \right],$$

$$C_{f,A} \simeq g' \left[-z_\Phi T_f^3 + z_{f,A} \right], \qquad (8)$$

where we have also introduced the vector and axial-vector $U(1)'$ charges $z_{f,V/A} = 1/2(z_{f,R} \pm z_{f,A})$.

Notice that z_Φ can be either z_H for a single Higgs doublet (H) model or a combination of z_{Φ_1} and z_{Φ_2}, namely $z_\Phi = z_{\Phi_1} \cos^2\beta + z_{\Phi_2} \sin^2\beta$, for a 2HDM. The z_Φ charge arises from the small gauge coupling expansion of the $Z - Z'$ mixing angle θ' which implies $c' \simeq 1$ and $s' \simeq -g_\Phi/g_Z = -\tilde{g} - 2g' z_\Phi$.

The structure of the Z' couplings is characterised by the sum of three different contributions.

- The kinetic mixing $\tilde{g}$ induces a vector-like term proportional to the electromagnetic current. This is the only source of interactions with the Z' when all the SM fields are neutral under $U(1)'$. In this case the Z' is commonly dubbed **dark photon**.
- The second term is induced by z_Φ, the $U(1)'$ charge in the Higgs sector, and leads to a **dark Z**, namely a gauge vector that mixes with the SM Z boson. The SM fermions are not required to be charged under $U(1)'$ in this case.
- Finally, there are the usual gauge interactions proportional to the fermionic $U(1)'$ charges $z_{f,V/A}$. There are the typical interactions of the most general $U(1)'$ extensions of the SM.

We can further delineate different physical scenarios depending on the structure of the axial-vector couplings of the Z' boson.

Indeed, the $C_{f,A}$ coefficients can be suppressed with respect to the vector-like counterparts (see also [107]). This emerges, for instance, by enforcing the gauge invariance of the Yukawa Lagrangian under the new abelian symmetry, in the scenarios where only one $SU(2)$ scalar doublet is considered. Indeed, the gauge invariance requires the $U(1)'$ charge of the Higgs field to satisfy the conditions

$$z_\Phi = z_Q - z_d = -z_Q + z_u = z_L - z_e. \qquad (9)$$

Inserting the previous relations into Eq. (8), one finds $C_{f,A} \simeq 0$ that describes a Z' with only vector interactions with

charged leptons and quarks. We stress again that the suppression of the axial-vector coupling mentioned above is only due to the structure of the scalar sector (with only one $SU(2)$ Higgs doublet) and the gauge invariance of the SM Yukawa Lagrangian. This feature is completely unrelated to the $U(1)'$ charge assignment of the fermions, to the requirement of anomaly cancellation and to the matter content potentially needed to account for it.

In contrast, in the scenario characterised by two Higgs doublets, the axial-vector couplings of the Z' are, in general, of the same order of magnitude of the vector ones and the cancellation between the two terms of $C_{f,A}$ in Eq. (8) is not achieved regardless of the details of the Yukawa Lagrangian (such as which type 2HDM). The same result can be achieved if a single Higgs doublet is considered but the conditions in Eq. (9) are not satisfied as in scenarios in which the fermion masses are generated radiatively or through horizontal symmetries.

To summarise, we can identify three different situations that can provide a light Z' with interactions potentially explaining the Atomki anomaly. Below we provide some references to the literature where these scenarios have been worked out. In all of them, the SM is extended by an additional abelian gauge group.

1. The SM scalar sector is unchanged, being characterised by only one Higgs doublet. In this case the mass of the Z' is entirely generated in the dark sector. The Yukawa Lagrangian preserves the SM structure and its gauge invariance under the $U(1)'$ necessary implies that the Z' has only vector interactions with the SM fermions at leading order in the couplings $\tilde{g}, g'$ [8,57].

2. The SM scalar sector is extended by an additional Higgs doublet. Even though the Yukawa Lagrangian is invariant under the local $U(1)'$ symmetry, the cancellation between the two terms in $C_{f,A}$ in Eq. (8) does not occur and both the vector and axial-vector couplings of the Z' are non-vanishing. The mass of the Z' acquires contribution from both the dark and the EW sectors [41,106,107].

3. The SM scalar sector is characterised by a single Higgs doublet but the constraints in Eq. (9) are avoided by relying on more complicated Yukawa structures. As such, the cancellation providing $C_{f,A} \simeq 0$ is not realised and the vector and axial-vector interactions of the Z' are of the same order of magnitude [44].

3.2.4 Conclusions

While the possibility that the Atomki anomaly can be explained as a statistical fluctuation combined with yet unknown nuclear physics properties and/or unforeseen experimental conditions is still open, the fact that such an effect in the beryllium decay has been determined with a 6.8σ significance and that it has been supported by the recent observation of a compatible anomaly in the helium system, clearly calls for a thorough investigation of plausible theoretical explanations. With this in mind, here, we have presented and discussed particle physics scenarios that extend the SM with the inclusion of a spin-1 boson.

3.3 The nuclear physics aspects of the ATOMKI anomaly

Xilin Zhang
Facility for Rare Isotope Beams, Michigan State University, MI 48824, USA
Gerald A. Miller
Department of Physics, University of Washington, Seattle, WA 98195, USA

Abstract During this workshop, the original experimental group that announced the Atomki anomaly presented more results. In several talks, different experiments, which we consider to be timely and important, were proposed or presented for checking the original observation. Multiple talks discussed interesting theoretical explanations for the anomaly. In this contribution, we provide a few comments on the nuclear physics aspects of the anomaly and summarize our previous two papers on this subject, which hopefully can be useful for others working on this topic.

The so-called Atomki anomalies, first seen in $^7\text{Li}(p, e^+ + e^-)^8\text{Be}$ [1] and then in $^3\text{H}(p, e^+ + e^-)^4\text{He}$ [53], have generated considerable interest in particle and nuclear physics communities. This workshop sampled a range of theoretical studies from the two fields (see those contributions in this workshop report).

In our latest work [68], we specifically focused on a beyond-the-Standard-Model (BSM) physics explanation [8,39,57] that conjectures that protophobic vector bosons were produced in the $^7\text{Li} - p$ interactions and then decayed into e^+-e^- pairs. Based on the existing $^7\text{Li}(p, e^+ + e^-)^8\text{Be}$ data, we predicted the production cross section for such bosons (X) up to an overall factor in a wide range of $^7\text{Li} - p$ scattering energies. The result clearly shows that the anomaly should have been seen at all beam energies of the origi-

nal $^7\text{Li}(p, e^+ + e^-)^8\text{Be}$ measurements [1]. However, the anomaly was only seen at the ^8Be 1^+ resonance located at 18.15 MeV above its ground state [1]. [The resonance is mostly isoscalar (MIS), while the other one at 17.64 MeV is mostly isovector (MIV).] This contradiction led us to conclude that the X explanation was not viable.

During our preparation of this contribution, we were informed by the experimental collaboration that its latest measurement observed similar anomalies at various beam energies (see Krasznahorkay et al.'s contribution in this report). Considering this interesting development, we (as theorists) put forward the following wish list, which could be helpful for resolving questions about these anomalies.

– We need independent measurements on these reactions (preferably using a blind data analysis approach [126]), besides other indirect search of various BSM particles that were proposed to explain the anomaly (see related contributions in this report).

– Theorists compute cross sections, but only event counts are available right now. In the future, experimental cross sections results will be needed so that theorists (and even different experiments) can make quantitative comparisons. Another way to facilitate such comparison is to provide necessary information about detector responses and the beam flux integrated over time, which will enable theorists to produce event counts in both the anomalous region and other regions where the Standard Model (SM) can explain the data according to the original experiment.

– In the original paper [1], the event counts were binned against either e^+-e^- invariant mass or their correlation angle, but not both. As discussed in Ref. [27], the differential information on the joint distribution of these two kinematic quantities could provide more information.

Now, we discuss our (unsuccessful) nuclear physics explanations [27] as well as other relevant nuclear physics studies [7,69] not covered in the workshop. Then we will explain our latest work [68] on the X boson.

In Ref. [27], we expanded the theoretical formalism [3] that was used by the experimental group [1] for describing $e^+ - e^-$ production in nuclear transitions by including the direct capture component in the full $^7\text{Li}(p, e^+ + e^-)^8\text{Be}$ reaction. The interference terms between different electromagnetic (EM) multipoles are also included and studied, considering that the experiment's detector doesn't have full angular coverage [1]. Even though the interference effect is significant (and sensitive to ^7Li-p scattering energy), it is not able to explain the anomaly in the e^+-e^- correlation angle distribution and their invariant mass distribution. We further studied the strength of the resonance's EM decay on the virtual photon's momentum (with the photon energy fixed by the Q value of the reaction). I.e., the strength could be accompanied

by a transition form factor. However, the form factor would need to have a dramatic dependence on the virtual photon's momentum in order to explain the signal. This dependence is unlikely because the photon wave length is much bigger than any length scale in the dynamics.

Both efforts to explain the anomaly in terms of nuclear physics turned to be unsuccessful, but we found that at the MIS 1^+ (^8Be) resonance, the E1 contribution to the $e^+ - e^-$ production is about 40% of the total cross section (the sum of the E1 and M1 contributions). In contrast, the original experimental analysis fixed it at 20%. In another recent theoretical study [69], this number is 30% at the MIS resonance. Therefore, there is still disagreement in our understanding of the Standard Model background for the experiment. Moreover, as emphasized in that study, the E1 to M1 ratio is highly sensitive to the energy, because the M1 contribution drop rapidly as energies vary from the resonance energy. However, in the original experimental analysis, the ratio is assumed to be constant around the resonance.

These studies are based on the one photon-exchange approximation for describing the EM transition. How about the two-photon contribution? A recent paper [7] studied this in a phenomenological approach and pointed out such contributions together with the experimental detector response could potentially explain the anomaly. If this explanation turns out to be correct, $e^+ - e^-$ production could be an interesting way to study the two-photon contribution in nuclear reactions. This approach would be valuable for nuclear physics in its own right. In recent years, there are growing interests in studying this type of contributions involving one $W^\pm$ (or Z) and one γ (as radiative corrections) in nuclear weak decay, as well as the two-boson contribution (involving $W^+ - W^-$) in neutrinoless double beta decay. In principle, these two-boson contributions should be described in a unified hadronic physics framework. Therefore, any experimental information on the two-γ contribution in nuclear reactions could help calibrate such framework.

Our study of the X-production explanation [68] is mainly based on a nuclear physics fact that the E1 and M1 multipoles are dominated by the isovector component of the EM current. The same is true for production of an X boson. As a result, its production amplitude is directly related to that of the $^7\text{Li}(p, \gamma)^8\text{Be}$ reaction up to an overall coupling strength. Taking into account the X's finite mass and three polarizations, we predicted the cross section for the X production up to an overall factor. Strikingly, the beam-energy dependence of the total X-production cross section is very smooth in the region around the MIS 1^+ resonance, because the direct capture reaction component without going through any nuclear resonance dominates over the resonance-induced (M1X) production. (At the MIV resonance region, the production is dominated by the resonance-induced component, if the kinematic threshold determined by the X's mass is

low enough.) This clearly contradicts the original experimental observation [1], where the anomaly was only seen at the MIS resonance and absent away from that resonance. However, as shown in the experimental collaboration's contribution in this report, the anomalies were observed in a wide window of beam energies in their recent re-measurements of $^7\text{Li}(p, e^+ + e^-)^8\text{Be}$, lending support for the X-production explanation. This new development makes it clear that independent experimental checks are necessary and urgently needed!

3.4 The QCD axion interpretation of the X17 anomalies

Daniele S. M. Alves

Theoretical Division, Los Alamos National Laboratory, Los Alamos, NM 87544, USA

Abstract I provide a brief overview of the QCD axion interpretation of the e^+e^- excesses reported in transitions of the ^8Be and ^4He nuclei. I also comment on the implications of recent preliminary results, and highlight independent measurements that could be performed to test the hypothesis that the '$X17$' boson is the QCD axion.

3.4.1 Introduction

The origin of the ^8Be and ^4He anomalies as the nuclear emission of a new, beyond the Standard Model particle remains highly speculative and subject to debate. Nonetheless, several candidates for the "$X17$" boson have been considered in the recent literature, including vectors, axial-vectors, and pseudoscalars. The vector boson interpretation (*a.k.a* the "protophobic" $X17$ boson [8,57]), while being the most popular, faces significant challenges. For instance, its emission rate cannot be easily suppressed in the transition $^8\text{Be}^*(17.64) \rightarrow {}^8\text{Be} + X17$ (which is predominantly isovector), nor in the "continuum" E1 component of non-resonant proton capture on ^7Li [68]. The pseudoscalar $X17$ interpretation, on the other hand, can easily account for the absence of anomalous excesses in reactions with electric multipole emission, and, if such pseudoscalar has suppressed isovector couplings, its emission is also naturally suppressed in isovector transitions.

If the existence of the $X17$ boson were established and its spin-parity were confirmed to be pseudoscalar, then one would be faced with the task of uncovering the more fundamental origin of such a particle, here on dubbed "$a(17)$". Emission of the $a(17)$ pseudoscalar in nuclear de-excitations

would *necessarily* imply that $a(17)$ couples to quarks and/or gluons in the UV through the following generic operators:

$$a \frac{m_q}{f_a} \bar{q} \, i \gamma_5 q \quad \text{and/or} \quad a \frac{\alpha_s}{f_a} G\tilde{G}. \tag{10}$$

Any such couplings, if generic, would contribute to the CP-violating phase in the strong sector, θ_{CP}, which is stringently bound from neutron EDM searches to be $\theta_{\text{CP}} \lesssim \mathcal{O}(10^{-10})$. Therefore, either a mechanism would have to be invoked to cancel the $a(17)$ contributions to θ_{CP} with $\mathcal{O}(10^{-10})$ precision, or the vacuum expectation value of $a(17)$ itself would have to be dynamically driven to cancel the overall strong CP phase. The latter scenario, which is significantly more compelling theoretically and experimentally, would imply that $a(17)$ is *the* QCD axion originally proposed by Peccei, Quinn, Weinberg, and Wilczek to solve the strong CP problem [45–48].

Most variants of QCD axion with mass of $m_a \sim 17$ MeV, however, are severely excluded by a variety of constraints from rare meson decays, beam dumps, and fixed target experiments. Alves and Weiner have shown in [59] that a *piophobic* variant of the QCD axion remains experimentally viable and could potentially explain the KTeV anomaly [127], i.e., the $(2 - 3)\sigma$ excess above the SM expectation in the rate for $\pi^0 \rightarrow e^+e^-$. Intriguingly, Alves has shown in [60] that such a piophobic QCD axion could also *simultaneously* account for the anomalous emission rates reported by the ATOMKI collaboration in $^8\text{Be}^*(18.15) \rightarrow {}^8\text{Be} + e^+e^-$ [1] and in $^4\text{He}^*(21.01) \rightarrow {}^4\text{He} + e^+e^-$ [6].

The required properties of the piophobic QCD axion have been discussed in detail in [59]. Here, we mention them briefly for completeness. First, the level of piophobia necessary to explain the KTeV anomaly and remain compatible with the SINDRUM bounds on $\pi^+ \rightarrow e^+\nu(a \rightarrow e^+e^-)$ [128] requires $\pi^0 - a$ mixing at the level of $\theta_{a\pi} \lesssim \mathcal{O}(10^{-4})$. Second, the piophobic axion must have suppressed couplings to the 2nd and 3rd generations of SM fermions in order to avoid large contributions to the muon's $(g - 2)_\mu$, and to axionic meson decay rates from, e.g., quarkonia, B and D mesons, and charged Kaons. Finally, the piophobic QCD axion must have unsuppressed couplings to electrons, $\mathcal{O}(m_e/f_a)$, so that it has a short $a \rightarrow e^+e^-$ decay lifetime of $\tau_a \lesssim 10^{-13}$ s and is therefore compatible with beam dump and fixed target constraints.

3.4.2 The a(17) hypothesis for the ATOMKI anomalies

The linear couplings of the QCD axion can be *uniquely* and *unambiguously* specified by a generalized Bardeen-Tye current [129]. In the specific case of the piophobic axion with mass $m_a \simeq 16.7$ MeV and decay constant $f_a \simeq 1030$ MeV,

the Bardeen-Tye current takes the form:

$$
\begin{aligned}
J_\mu^{a_{\text{phys}}} &\equiv f_a \, \partial_\mu a_{\text{phys}} \\
&\equiv \frac{f_a}{f_\pi} \Big(f_\pi \, \partial_\mu a + \theta_{a\pi} \, J_{5\,\mu}^{(3)} + \theta_{a\eta_{ud}} \, J_{5\,\mu}^{(ud)} + \theta_{a\eta_s} \, J_{5\,\mu}^{(s)} \Big),
\end{aligned}
\tag{11}
$$

where $J_{5\,\mu}^{(3)}$ is the isovector quark axial current, and $J_{5\,\mu}^{(ud)}$ and $J_{5\,\mu}^{(s)}$ are the two isoscalar quark axial currents in the heavy-light basis (see [59] for concrete expressions). Heuristically, the parameters $\theta_{a\pi}$, $\theta_{a\eta_{ud}}$, and $\theta_{a\eta_s}$ in (11) can be understood as the axion mixing angles with the pseudoscalar states π^3, η_{ud}, and η_s, respectively [130]. It is safe to make the approximation $\pi^3 \approx \pi^0$, where π^0 is the physical neutral pion state. The states η_{ud} and η_s, on the other hand, are not mass eigenstates, but instead linear combinations of the physical states η and η'.

The usefulness of the Bardeen-Tye parametrization, specially in comparison with convoluted LO approaches such as in [131], is that it offers a simple parametrization of the axion's hadronic couplings that is straightforward to map into χPT, and automatically accommodates the higher order χPT contributions to the QCD axion couplings. In particular, the uncertainties from χPT at NLO are significant for the piophobic axion, and one cannot calculate the mixing angles $\theta_{a\pi}$, $\theta_{a\eta_{ud}}$, and $\theta_{a\eta_s}$ with better than order-of-magnitude precision. Still, these uncertainties can be taken into account by considering the following ranges for these mixing angles:

$$
|\theta_{a\pi}| \sim \mathcal{O}(10^{-5} - 10^{-4}),
\tag{12a}
$$

$$
|\theta_{a\eta_{ud}}|, \; |\theta_{a\eta_s}| \sim \mathcal{O}(10^{-4} - 10^{-3}).
\tag{12b}
$$

The axion's hadronic couplings in (11) can then be easily recast in terms of effective isovector and isoscalar nuclear couplings through:

$$
\mathcal{L}_{aNN} = a \, \overline{N} \, i\gamma^5 \Big(g_{aNN}^{(1)} \tau^3 + g_{aNN}^{(0)} \Big) N, \text{ with}
\tag{13a}
$$

$$
g_{aNN}^{(1)} = \theta_{a\pi} \, g_{\pi NN} = \theta_{a\pi} \, (\Delta u - \Delta d) \frac{m_N}{f_\pi},
\tag{13b}
$$

$$
g_{aNN}^{(0)} = \Big(\theta_{a\eta_{ud}} (\Delta u + \Delta d) + \sqrt{2} \, \theta_{a\eta_s} \Delta s \Big) \frac{m_N}{f_\pi}.
\tag{13c}
$$

Above, Δu, Δd, and Δs quantify the matrix elements of quark axial currents in the nucleon.

With (13b) and (13c), it is straightforward to obtain the axion emission rate in the magnetic dipole nuclear transitions $^8\text{Be}^* \to {}^8\text{Be} + a$ [49,130,132,133],

$$
\frac{\Gamma_a}{\Gamma_\gamma} \bigg|_{^8\text{Be}^*} = \frac{1}{2\pi\alpha} \frac{|\vec{p}_a|^3}{|\vec{p}_\gamma|^3} \left| \frac{\sum_{I=0,1} g_{aNN}^{(I)} \langle I \, | \, ^8\text{Be}^* \rangle}{\sum_{I=0,1} (\mu^{(I)} - \eta^{(I)}) \langle I \, | \, ^8\text{Be}^* \rangle} \right|^2,
\tag{14}
$$

and in the isoscalar magnetic monopole nuclear transition $^4\text{He}^*(21.01) \to {}^4\text{He} + a$ [49,132]

$$
\Gamma_a \big|_{^4\text{He}^*} \approx |a_{\text{M0}}^{(0)}|^2 \frac{2 \, |\vec{p}_a|^5}{m_N^2 \, Q_N^2} |g_{aNN}^{(0)}|^2.
\tag{15}
$$

The range for the nuclear matrix elements $|a_{\text{M0}}^{(0)}|^2$, $\mu^{(I)}$ and $\eta^{(I)}$ in (14) and (15), as well as the isospin composition of $|^8\text{Be}^*\rangle$ in (14), are discussed in [60]. The uncertainties in these quantities can be folded in the overall rate calculation to obtain the range of axion isoscalar couplings that fit the anomalous rates in ^8Be and ^4He reported by the ATOMKI collaboration. Assuming, conservatively, the following range for the de-excitation rate $^8\text{Be}^*(18.15) \to {}^8\text{Be} + a(17)$,

$$
\frac{\Gamma_a}{\Gamma_\gamma} \bigg|_{^8\text{Be}^*(18.15)} \approx (6 \pm 1) \times 10^{-6},
\tag{16}
$$

we obtain the following fitted range for the piophobic axion's isoscalar couplings:

$$
\begin{aligned}
&-\Big(\theta_{a\eta_{ud}} (\Delta u + \Delta d) + \sqrt{2} \, \theta_{a\eta_s} \Delta s \Big) \Big|_{^8\text{Be}^*(18.15)} \\
&\approx (1.1 - 6.3) \times 10^{-4}.
\end{aligned}
\tag{17}
$$

As for the width of the transition $^4\text{He}^*(21.01) \to {}^4\text{He} + a(17)$, the ATOMKI collaboration initially estimated it to be [6]:

$$
\Gamma_a \big|_{^4\text{He}^*(21.01),\text{1st estimate}} \approx 3.9 \times 10^{-5} \text{ eV},
\tag{18}
$$

based on the assumption that the primary SM contribution to the rate of $^3\text{H}(p, e^+e^-)^4\text{He}$ would come from de-excitations of the lowest 0^+ state, $^4\text{He}^*(20.21)$. This would imply the following range for the axion isoscalar couplings:

$$
\begin{aligned}
&-\Big(\theta_{a\eta_{ud}} (\Delta u + \Delta d) + \sqrt{2} \, \theta_{a\eta_s} \Delta s \Big) \Big|_{^4\text{He}^*(21.01),\text{1st estimate}} \\
&\approx (0.58 - 5.3) \times 10^{-4}.
\end{aligned}
\tag{19}
$$

However, this assumption may have to be revised based on calculations by Viviani et al. [67], who claim that the dominant SM contribution to $^3\text{H}(p, e^+e^-)^4\text{He}$ at $E_p = 900$ keV come from farther 1^- resonances and E1 emission from direct (non-resonant) capture. While estimates for this rate in [67] have not been confirmed with preliminary data [53], if true they could shift the initial estimated rate for $^4\text{He}^*(21.01) \to {}^4\text{He} + a(17)$ by an order of magnitude,

$$
\begin{aligned}
&\Gamma_a \big|_{^4\text{He}^*(21.01),\text{2nd estimate}} \\
&\approx \mathcal{O}(10) \times \Gamma_a \big|_{^4\text{He}^*(21.01),\text{1st estimate}}
\end{aligned}
\tag{20}
$$

with a corresponding shift in the favored isoscalar coupling range of

$$
-\Big(\theta_{a\eta_{ud}} (\Delta u + \Delta d) + \sqrt{2} \, \theta_{a\eta_s} \Delta s \Big) \Big|_{^4\text{He}^*(21.01),\text{2nd estimate}}
$$

$$\approx (1.7 - 16) \times 10^{-4}. \tag{21}$$

Regardless of these uncertainties in the determination of the axionic de-excitation of $^4\mathrm{He}^*$, there are two remarkable things about (17) and (19)/(21). First, they are compatible with the natural range for the QCD axion's isoscalar couplings in (12b). Second, they are compatible with each other, which is nontrivial since the $^8\mathrm{Be}$ and $^4\mathrm{He}$ nuclei are significantly distinct many-body systems.

We can also use (14) and the axion isovector and isoscalar couplings in (12a) and (17) to obtain the expected range of axionic emission in the predominantly isovector transition $^8\mathrm{Be}^*(17.64) \to {}^8\mathrm{Be} + a(17)$,

$$\left. \frac{\Gamma_a}{\Gamma_\gamma} \right|_{^8\mathrm{Be}^*(17.64)} \approx (0.08 - 10) \times 10^{-7}. \tag{22}$$

We infer from (22) that the $a(17)$ hypothesis provides a natural explanation for the absence of a statistically significant excess in this transition (at least with the integrated proton beam luminosity of public results to date).

Finally, we re-iterate that because the axion is a pseudoscalar, it can only be produced in magnetic multipole emissions. Hence, unlike the protophobic $X17$ vector boson case, the rate for the *non-resonant* capture reaction $p + {}^7\mathrm{Li} \to {}^8\mathrm{Be} + a(17)$ is expected to be zero (or negligible) due to absent (or extremely suppressed) magnetic multipole contributions.

3.4.3 Independent channels to test the a(17) hypothesis

We now briefly discuss other, independent experimental measurements that could either confirm or falsify the $a(17)$ explanation of the ATOMKI anomalies.

Other nuclear transition measurements If the backgrounds and experimental systematics in the measurements of the reaction $^3\mathrm{H}(p, e^+e^-)^4\mathrm{He}$ can be controlled, it would be very useful to probe which $^4\mathrm{He}$ transitions are contributing to the anomalous e^+e^- emission. This could in principle distinguish between the various $X17$ hypotheses: scalar, vector, and pseudoscalar/axial-vector. In fact, the ATOMKI collaboration has recently released preliminary results for the scaling of the e^+e^- anomalous excess in $^3\mathrm{H}(p, e^+e^-)^4\mathrm{He}$ with three proton energies, $E_p = [510, 610, 900]$ keV [53] (this test was originally suggested in [39]). These preliminary results seem to favor the pseudoscalar or axial-vector hypothesis for $X17$, since the strength of the excess at different energies appears to be compatible with the Breit–Wigner scaling of the cross-section for the excitation of the 0^- state, $^4\mathrm{He}^*(21.01)$:

$$\sigma_{0^-}(E^*) \propto \frac{1}{(E^* - E_{0^-})^2 + \Gamma_{0^-}^2/4}, \tag{23}$$

where, above, E^* is the excitation energy, and $E_{0^-} \simeq 21.01$ MeV, $\Gamma_{0^-} \simeq 0.84$ MeV are the 0^- resonance energy and total width, respectively. The three proton energies tested in [94] roughly correspond to $^4\mathrm{He}$ excitation energies of $E^* = [20.21, 20.29, 20.49]$ MeV (although this correspondence is a crude approximation that does not take into account the proton energy loss in the thick target). Plugging these energies in (23), the expectation from the $a(17)$ hypothesis would be that the rate would scale as 0.56:0.65:1 for $E_p = [510, 610, 900]$ keV, respectively, which is compatible with the scaling reported in [94] of $(0.4 \pm 0.1){:}(0.7 \pm 0.1){:}1$. Viviani et al. [67], who additionally took into account the contribution from the higher 2^- excite state, also appears to support this preliminary conclusion (see fig. 17 of [67]).

Another possibility, if feasible, would be to measure the dependence of the excess in $^3\mathrm{H}(p, e^+e^-)^4\mathrm{He}$ away from the transverse plane (i.e., at different angles of the $e^\pm$ emission relative to the beam direction; see, e.g., fig. 6 of Viviani et al. [67]). This could in principle discriminate between the pseudoscalar and axial-vector [41] hypotheses, which is otherwise not possible by simply scanning the proton beam energy while fixing the detectors in the transverse plane.

Finally, searching for the $X17$ particle in other nuclear transitions could also help corroborate its existence and/or rule out spin-parity possibilities. For instance, [39] suggested searching for an $X17$ 'bump' in the e^+e^- spectrum of $^{12}\mathrm{C}^*(17.23) \to {}^{12}\mathrm{C} + e^+e^-$. Since this is a predominantly E1 transition, no significant $a(17)$ emission is expected in this case, and any confirmation of an $X17$ 'bump' in this reaction would rule out the $a(17)$ hypothesis.

Rare and exotic meson decays Another classical prediction of visible QCD axion models are rare meson decays via axion emission. Table 4 lists the most promising axionic meson decays for upcoming experimental searches. The expected rates from the $a(17)$ model, in particular, should be well within sensitivity of upcoming Kaon and η/η' factories [134, 135].

Besides the well-known axionic meson decays containing only one axion in the final state [60], Table 4 also includes more exotic meson decays with two or three axions in the final state, which were recently pointed out in [136]. Because the $a(17)$ decay constant is so low, $f_a \approx 1$ GeV, these multi-axion decays are relatively unsuppressed, leading to surprisingly large branching ratios that could be easily probed with dedicated pion and Kaon decay searches. Of note is the exotic pion decay final state $\pi^0 \to aaa \to 3(e^+e^-)$ with a branching ratio ~ 30 times larger that the SM double-Dalitz decay $\pi^0 \to \gamma^*\gamma^* \to 2(e^+e^-)$ [137]. Despite its significant branching ratio, this exotic decay has not been definitively excluded, and dedicated searches for this 6-pronged final state could be performed by experiments with large π^0 samples.

Table 4 The most promising rare meson decay channels with one or more axions in the final state, and the expected range of branching ratios in the $a(17)$ piophobic axion model

Decay channel	Expected rate
$\mathrm{Br}(\eta \to \pi\pi a)$	$\mathcal{O}(10^{-3} - 10^{-4})$
$\mathrm{Br}(\eta' \to \pi\pi a)$	$\mathcal{O}(10^{-3} - 10^{-4})$
$\mathrm{Br}(K^+ \to \pi^+ a)$	$\mathcal{O}(10^{-6} - 10^{-8})$
$\mathrm{Br}(K^+ \to \mu^+ \nu a)$	$\mathcal{O}(10^{-7} - 10^{-8})$
$\mathrm{Br}(K_L^0 \to \pi\pi a)$	$\mathcal{O}(10^{-6} - 10^{-8})$
$\mathrm{Br}(K_S^0 \to a a)$	$\mathcal{O}(10^{-7})$
$\mathrm{Br}(K_L^0 \to a a)$	$\mathcal{O}(10^{-9})$
$\mathrm{Br}(K_L^0 \to \pi^0 a a)$	$\mathcal{O}(10^{-4})$
$\mathrm{Br}(K^+ \to \pi^+ a a)$	$\mathcal{O}(10^{-5})$
$\mathrm{Br}(\pi^0 \to a a a)$	$\approx 10^{-3}$

Probes of the a(17) coupling to electrons Finally, another promising way to probe not only the $a(17)$ hypothesis, but also other $X17$ candidates, is through its coupling to electrons. Recent results from the NA64 experiment [138] have chipped away part of the available range of couplings of the piophobic axion to electrons,

$$\mathscr{L}_{aee} = \frac{q_{\mathrm{PQ}}^e m_e}{f_a} \, a \, \bar{e} \, i \gamma_5 e. \tag{24}$$

In the specific case of the $a(17)$ model, the NA64 limits translate into a lifetime bound of $\tau_a \lesssim 10^{-13}$ s, or $q_{\mathrm{PQ}}^e \gtrsim 1/5$, which is a weak constraint.

Nonetheless, planned fixed target and e^+e^- collider experiments will be able to probe, and possibly fully exclude, the remaining $a(17)$ parameter space. These experiments include PADME and Belle II, which will search for $e^+e^- \to \gamma \, (a \to e^+e^-)$, and fixed target experiments, such as NA64, DarkLight, HPS, and MAGIX, which will search for axion-bremsstrahlung from a high energy electron beam impinging on a high Z target, $e^-N \to e^-N \, (a \to e^+e^-)$ (see, e.g., other contributions to this *review*).

Finally, improved measurements of the electron anomalous magnetic dipole moment, $(g-2)_e$, could also significantly narrow down the available $a(17)$ parameter space [59,139]. The current experimental situation regarding $(g-2)_e$ is ambiguous, with the two most recent and precise determinations of the fine-structure constant, α, by Parker et al. [140] and Morel et al. [91], favoring different ranges for $(g-2)_e$ that are discrepant by $\sim 3\sigma$. Further investigations from these experimental groups are needed to re-evaluate possible systematic effects and reconcile both measurements [141].

3.5 QED meson descriptio of the X17 and other anomalous particles

Cheuk-Yin Wong
Physics Division, Oak Ridge National Laboratory

Abstract The X17 particle, the E38 particle, and the anomalous soft photons are anomalous particles because they do not appear to belong to any known Standard Model families. We propose a QED meson description of the anomalous particles as composite systems of a light quark and a light antiquark bound and confined by the compact QED interaction, by combining Polyakov's transverse confinement of opposite electric charges in compact QED in $(2+1)$D and Schwinger's longitudinal confinement for massless opposite electric charges in QED in $(1+1)$D. With predicted QED meson masses close to the observed X17 and E38 masses, QED mesons may be good candidates for the description of the anomalous particles.

3.5.1 Introduction

The observed X17 particle [1,94], the E38 particle [142,143], and the anomalous soft photons [144–148] are anomalous particles because their masses of many tens of MeV do not lie in the mass region of any known family of particles of the Standard Model. Many different interpretations have been presented and their theoretical implications discussed [98]. We focus our attention on the description of the X17 particle and other anomalous particles as composite particles of a light quark and a light antiquark bound and confined by their mutual QED interaction [149–153]. We shall call such a composite particle a QED meson (compactly written as a "qedmeson"), in analogy with the QCD meson.

Previously, in many exclusive experiments in high-energy hadron-hadron collisions and e^+e^- annihilations, it has been consistently observed that whenever hadrons are produced, anomalous soft photons in the form of e^+e^- pairs about 4 to 8 times in excess of the bremsstrahlung expectations are produced, and when hadrons are not produced, these anomalous soft photons are also not produced [144–148]. The transverse momenta of the excess e^+e^- pairs lie in the range of a few MeV/c to many tens of MeV/c, corresponding to masses from a few MeV to many tens of MeV. Owing to its correlated and simultaneous production alongside with hadrons, a parent

particle of an anomalous soft photon is likely to contain elements of the hadrons, such as a pair of light quark and light antiquark. According to the Schwinger's $m^2 = g^2/\pi$ relationship between the coupling constant g and the boson mass m of the composite fermion–antifermion pair interacting in a gauge interaction in $(1 + 1)$D [154,155], the QED gauge interaction will bring the quantized mass m of a $q\bar{q}$ pair to the mass range of the anomalous soft photons, when we consider the QCD and QED coupling constants and the mass scale of a QCD meson. It was therefore proposed in [149,150] that a quark and an antiquark in a $q\bar{q}$ system interacting in the QED gauge interaction may lead to new open-string bound and confined QED mesons with a mass of many tens of MeV. These QED mesons may be produced simultaneously along with mesons in high-energy collisions [144–148], and the excess e^+e^- pairs may arise from the decays of the QED mesons [149,150]. The predicted masses of the isoscalar $I(J^\pi) = 0(0^-)$ and $I(J^\pi) = 1(0^-)$ QED mesons are about 13–17 and 36–38 MeV respectively [149,150], which agree approximately with the masses of the X17 [1,94] and the E38 particles [142,143] subsequent observed. The tentative agreement lends support to the possible QED mesons interpretation of the anomalous particles of the X17, the E38, and anomalous soft photons.

3.5.2 Can a q interact with a $\bar{q}$ in QED alone?

A serious question arises whether a light quark and a light antiquark can ever be produced and interact in the QED interaction alone, without the QCD interaction. Actually, there are circumstances in the decays from highly excited nuclear states with the possible production of a light $q\bar{q}$ pair as in Fig. 32a, the hadron+hadron → hadrons+$(q\bar{q})^n$ reaction as in Fig. 32b, and the $e^+ + e^- → \gamma^* → q + \bar{q} → (q\bar{q})^n$ reaction as in Fig. 32c, when the CM energy, $\sqrt{s}(q\bar{q})$, of the produced $q\bar{q}$ pair lies in the range $(m_q + m_{\bar{q}}) < \sqrt{s}(q\bar{q}) < m_\pi$. In order to bring the produced $q\bar{q}$ pair in this CM energy range to a possible stable state, the produced q and $\bar{q}$ can only interact with the QED interaction alone, because the QCD interaction will otherwise endow the $q\bar{q}$ pair with a CM energy beyond the range, in a contradictory manner.

For the production of X17 in ^{4}He* and ^{8}Be* decays at ATOMKI [1,53], we envisage the scenario that the excited states of ^{4}He(0^- 20.02 MeV) and ^{8}Be(1^+ 18.15 MeV) are formed by pulling a proton out of one of n alpha-particles of the $(\alpha)^n$-nucleus and by placing the proton on an orbital that is considerably outside the corresponding tritium core as shown in Fig. 32a. The stretched string-like strong interaction between the proton and the tritium core polarizes the vacuum so much that the strong interaction may lead to the production of a $q\bar{q}$ pair. At the appropriate $\sqrt{s}(q\bar{q})$ eigenenergy, the QED interaction between the q and the $\bar{q}$ may result in the formation of the $q\bar{q}$ bound state X17 [149,150], which is
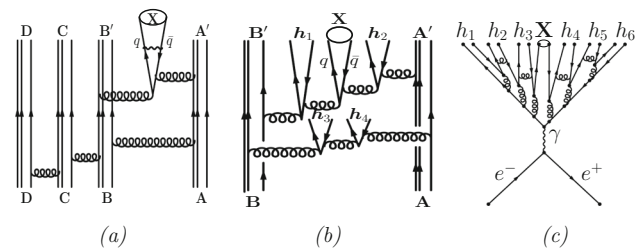
Fig. 32 Feynman diagrams for the production of a QED mesons X and hadrons h_i in **a** low-energy ^{4}He* and ^{8}Be* decays, **b** a high-energy hadron-hadron collision, and **c** a high-energy e^+e^- annihilation

subsequently emitted as the proton drops down to fill the hole in the tritium core to reach the $(\alpha)^n$-nucleus ground state. Such a production mechanism strong suggests that X17 may also be produced from the excited states of other $(\alpha)^n$-nuclei in which a proton is pulled out from one of its alpha particles. In this respect, the ^{12}C($(1+)$ 18.16 MeV) state with a width of $\Gamma = 240$ keV may be an interesting analog of the ^{8}Be*(1^+ 18.15 MeV) state with a width of $\Gamma = 138$ keV and may likewise decay with the emission of an X17 particle.

In other processes as illustrated in Fig. 32b, c, many $q\bar{q}$ pairs may also be produced in high-energy nuclear collisions at Dubna [142,143], in high-energy hadron collisions in anomalous soft photon production experiments [144–147], and in high-energy e^+-e^- annihilations in DELPHI experiments [147,148]. The $q\bar{q}$ pairs may also be produced in high-energy heavy-ion collisions at RHIC and LHC in two ways: either through the production of $q\bar{q}$ pairs in the multiple collision process similar to Fig. 32b, or through the coalescence of quarks in the deconfinement-to-confinement phase transition of the quark gluon plasma. While most produced $q\bar{q}$ pairs will lead to hadron production, there may be $q\bar{q}$ pairs with $(m_q + m_{\bar{q}}) < \sqrt{s}(q\bar{q}) < m_\pi$ for which the QED interaction between the quark and the antiquark may lead to the production of the X17 and E38 particles at the appropriate energies. The observation of the E38 particle at Dubna suggests that along with E38, the X17 particle with a mass of 17 MeV may also be produced in the same reaction at Dubna with an even greater probability because of its lower mass.

3.5.3 How can $q\bar{q}$ be produced and confined in QED?

To answer the question how a $q\bar{q}$ pair can be produced and confined in a QED meson, we note first of all that there are two different types of QED U(1) gauge interactions possessing different confinement properties [156–158]. There is the compact QED U(1) gauge theory in which the gauge fields A^ν are angular variables with a periodic gauge field action that allows transverse photons to self-interact among themselves. Defined on a lattice, the compact QED U(1) gauge

theory has the gauge field action [156–158]

$$S = \frac{1}{2g^2} \sum_{x,\alpha\beta} (1 - \cos F_{x,\alpha\beta}), \tag{25}$$

where g is the coupling constant and the gauge fields are

$$F_{x,\alpha\beta} = A_{x,\alpha} + A_{x+\alpha,\beta} - A_{x+\beta,\alpha} - A_{x,\beta},$$
$$\text{with} -\pi \leq A_{x,\alpha} \leq \pi. \tag{26}$$

There is also the non-compact QED U(1) gauge theory with the gauge field action [156–158]

$$S = \frac{1}{4g^2} \sum_{x,\alpha\beta} F_{x,\alpha\beta}^2, \quad \text{with} -\infty \leq A_{x,\alpha} \leq +\infty. \tag{27}$$

In non-compact QED gauge theories, the transverse photons do not interact with other transverse photons. Even though the compact and the non-compact QED gauge theories have the same continuum limit, they have different confinement properties. A pair of opposite electric charges are confined in compact QED in (2 + 1)D and strong coupling (3+1)D, but they are unconfined in weak coupling (3 + 1)D [156–158]. They are unconfined in non-compact QED in (3 + 1)D [156–158].

Which type of the QED U(1) gauge interaction does a quark interact with an antiquark? As pointed out by Yang [159], the quantization and the commensurate properties of the electric charges of the interacting particles imply the compact property of the underlying QED gauge theory. Because (i) quark and antiquark electric charges are quantized and commensurate, (ii) quarks and antiquarks are confined, and (iii) there are experimental evidences for possible occurrence of confined $q\bar{q}$ QED mesons states as we mentioned in the Introduction, it is therefore reasonable to propose that quarks and antiquarks interact with the compact QED U(1) interaction.

In compact QED, Polyakov [156,157] showed previously that a pair of opposite electric charges in $(2 + 1)D_{\{x^1,x^2,x^0\}}$ space-time are confined, and that the confinement persists for all non-vanishing coupling constants, no matter how weak. As explained by Drell and collaborators [158], such a confinement in $(2+1)D_{\{x^1,x^2,x^0\}}$ arises from the angular-variable property of A_ϕ and the periodicity of the gauge field action as indicated in Eq. (25). Such gauge periodicity in the neighborhood of the produced opposite electric charges leads to self-interacting transverse gauge photons. These transverse gauge photons interact among themselves, they do not radiate away, and they join the two opposite electric charges by a confining linear interaction.

We can use the above Polyakov's result in compact QED in (2 + 1)D as the starting point to construct a model of a quark and an antiquark produced and confined in a QED meson. We envisage the production of the $q\bar{q}$ pair at the eigenenergy $\sqrt{s}(q\bar{q})$ of the QED meson and take the quark
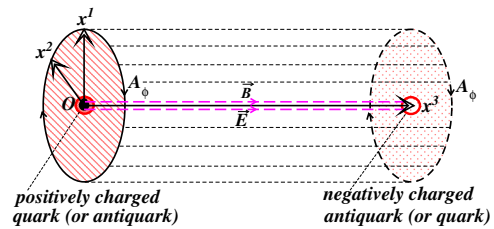
(*a*) Electric and magnetic lines of force of a QED meson
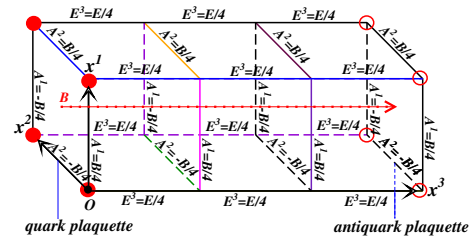
(*b*) Lattice description of the above QED meson

Fig. 33 a The 3D yo-yo motion for the bound state, reaching a momentary snapshot of the flux tube in the stretch (2 + 1)D configuration. **b** The upper figure transcribed in terms of the lattice link and plaquette variables

charge to be positive, which can be easily generalized to other cases. We consider the production of the $q\bar{q}$ charge pair at $(x^1, x^2, x^3) = 0$ with the antiquark separated initially from the antiquark along a direction chosen to be the longitudinal x^3 direction at an incipient separation Δx^3. The creation of the $q\bar{q}$ charge pair is accompanied by the creation of the gauge fields A, E, and $B(= \nabla \times A)$. We can apply Polyakov's result to infer that the produced charges and the QED gauge fields are confined in $(2 + 1)D_{\{x^1,x^2,x^0\}}$ transversely at the $x^3 \sim 0$ plane. We can now stretch the antiquark longitudinally along x^3 away from the quark at $x^3 = 0$ to execute the 3D yo-yo motion for the bound state, reaching a momentary snapshot of the flux tube in the stretch (2 + 1)D configuration shown in Fig. 33a. We can transcribe Fig. 33a in terms of the lattice link and plaquette variables in Fig. 33b, by following the Hamiltonian formulation and the notations of Drell et al. [158]. Specifically, in the $A^0 = 0$ gauge we specify the canonical conjugate gauge fields A and E at the links in Fig. 33b, where we display only the A^1, A^2 and E^3 values of the conjugate gauge fields. The magnetic field B associated with the plaquettes can be determined as the curl of A and is directed along x^3 in Fig. 33a, b. The magnetic field B sends the quark and antiquark charges into the appropriate Landau orbitals to execute transverse zero-mode harmonic oscillator zero-point motions on their $\{x^1, x^2\}$ planes. At the QED mesons eigenenergy, the electric field E and the magnetic field B along the longitudinal x^3 direction send the quark and the antiquark in longitudinal 3D yo-yo motion. The pos-

itive electric quark charge fractions (solid circles in Fig. 33b) reside at the $x^3 = 0$ plaquette vertices and the negative electric antiquark charge fractions (open circles in Fig. 33b) at the antiquark plaquette vertices at the x^3 plane. The transverse gauge fields A on the transverse links are copies of those on the quark and the antiquark plaquettes, and they are unchanged in the stretching, while the longitudinal links are all $E^3 = |E|/4$. Consequently, the self-interactions of the transverse gauge fields that initially confine the charges and the gauge field transversely will be retained and the cloud of gauge fields will continue to interact with each other to maintain the transverse confinement.

With transverse confinement and E and B aligned along the x^3 direction, it remains necessary to study longitudinal confinement, dynamical quark effects, and spontaneous chiral symmetry breaking. Therefore, we idealize the flux tube in stretch $(2 + 1)$D as a longitudinal string in $(1 + 1)D_{\{x^3, x^0\}}$ and approximate the quarks to be massless. With massless quarks in QED in $(1 + 1)D_{\{x^3, x^0\}}$, there is a gauge-invariant relation between the quark current j^μ and the gauge field A^μ as given by [154,155,160]

$$j^\mu = -\frac{g}{\pi}(A^\mu - \partial^\mu \frac{1}{\partial_\lambda \partial^\lambda} \partial_\nu A^\nu), \quad \mu, \lambda, \nu = 0, 3. \quad (28)$$

On the other hand, the gauge field A^ν depends on the quark current j^ν through the Maxwell equation,

$$\partial_\nu(\partial^\mu A^\nu - \partial^\nu A^\mu) = -g j^\mu, \quad \mu, \nu = 0, 3. \quad (29)$$

Equations (28) and (29) lead to $-\Box A^\mu = (g^2/\pi)A^\mu$ and $-\Box j^\mu = (g^2/\pi)j^\mu$, with j^ν and A^ν self-interacting among themselves and building a longitudinal confining interaction between the quark and the antiquark in $(1 + 1)$D. As a consequence, in accordance with Schwinger's exact solution for massless fermions in QED in $(1 + 1)$D [154,155], the light quark and the light antiquark interacting in QED will be longitudinally confined just as well and will form a stable QED quark-antiquark system. Possessing both transverse and longitudinal confinements as in an open-string, such a stable QED state may be experimentally observed as a QED mesons. By using the method of bosonization, we obtain the masses of the lowest-energy states of the open-string QED mesons which adequately match those of X17 and E38 [149,150] to support its approximate validity.

3.5.4 How can QED mesons be detected?

The QED mesons can be detected by the invariant masses of their decay products. In a QED mesons the quark and the antiquark can annihilate, leading to the emission of two real photons ($\gamma_1 \gamma_2$) as in Fig. 34a, two virtual photons ($\gamma_1^* \gamma_2^*$) or two dilepton ($e^+ e^-$) pairs as in Fig. 34b, or a single ($e^+ e^-$) pair as in Fig. 34c. We can make an order of magnitude esti-
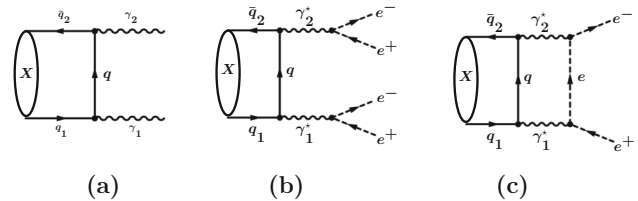
Fig. 34 Feynman diagrams of a QED meson decaying into a photon pair

mate on the decay width of X17 into two photons as depicted in Fig. 34a. From Eq. (89.3) of [161], we have for X17 $\to \gamma\gamma$,

$$\Gamma(X17 \to \gamma\gamma) = \left\{\frac{1}{2}\left[\left(\frac{1}{3}\right)^2 + \left(\frac{2}{3}\right)^2\right]\right\}^2 \frac{4\pi \alpha_{QED}^2}{M^2}|\psi(0)|^2, \quad (30)$$

where $\psi(0)$ is the wave function at the origin. The wave function at the origin can be estimated from the size of the QED mesons $|\psi(0)|^2 \sim 1/\pi R_T^2 L_z$, where $R_T \sim 0.4$ fm [150] and the longitudinal length $L_z \sim 7.15$ fm as estimated from Table 2 for the lowest QED mesons state in Ref. [151]. For the X17 with a mass of 17 MeV, $\Gamma(X17 \to \gamma\gamma) \sim 0.4$ MeV.

From the total width and the branching ratio into $e^+ e^-$ in ATOMKI measurements [1,53], the X17 width $\Gamma(X17 \to e^+ e^-)$ can be estimated to be 4.2 eV from ^{4}He decay and 0.828 eV from ^{8}Be decay. The knowledge of the approximate widths may facilitate future searches for the QED mesons.

In high-energy heavy-ion collisions at RHIC and LHC, one expect copious production of $q\bar{q}$ pairs either from the multiple collision process or from the coalescence of quarks and antiquarks in the confinement-to-deconfinement phase transitions. Among the produced $q\bar{q}$ pairs, there will be some pairs whose invariant masses match the QED mesons eigenenergies to lead to the production of QED mesons. For these produced QED mesons, the decay into two virtual photons via Fig. 34b offers an interesting tool for the search of the anomalous particles. Specifically, a decay into two virtual photons involves the measurement of the momenta of four final leptons which requires a high degree of correlation. As a consequence, the experimental noises of chance coincidences may be significantly reduced. One can construct the sum and the difference of the invariant momenta square of the virtual photon 4-momenta, $P = \sqrt{(p_{\gamma_1^*} + p_{\gamma_2^*})^2}$, and $Q = \sqrt{-(p_{\gamma_1^*} - p_{\gamma_2^*})^2}$. The virtual diphoton pair distribution $dN(P, Q)/dP\, dQ$ at RHIC and LHC will provides useful information to search for the QED mesons.

3.5.5 Conclusions and discussions

The observations of the X17 particle, the E38 particle, and the anomalous soft photons raise many interesting questions on the nature of these anomalous particles. While most theoretical discussions center on the elementary particle possibilities [98], we examine here the description of these anomalous particles as composite states of a quark and an antiquark interacting in compact QED. We propose a model of the production and the confinement of a quark and an antiquark in a QED meson by combining Polyakov's transverse confinement of opposite electric charges in compact QED in $(2+1)$D and Schwinger's longitudinal confinement in QED in $(1+1)$D. The important ingredients are (i) the self-interactions of the transverse photons in compact QED that confine the gauge fields and the opposite electric charges transversely in $(2+1)$D [156,157], (ii) the stretching of the $(2+1)$D with incipient longitudinal separation to come to the longitudinal flux tube configuration in a 3D yo-yo motion, (iii) the idealization of the longitudinal flux tube of the stretch $(2+1)$D configuration as a string in $(1+1)$D and the light quarks as massless, and finally (iv) Schwinger's solution of longitudinal confinement of massless quarks in QED $(1+1)$D [154,155], resulting in a bound and confined $q\bar{q}$ as a composite QED mesons state. The quark and the antiquark in a QED mesons are essentially electric charge monopoles and Polyakov's magnetic monopoles in dynamical motion. If this picture of a q and a $\bar{q}$ interacting in compact QED interactions is correct, it will imply that a quark and an antiquark obey QED laws that differ from those for an electron and a positron.

It will be of great interest to study in future lattice gauge calculations the problem of quark confinement and $q\bar{q}$ bound states in compact QED for quarks with different color and flavors in the stretch $(2+1)$D configuration, with the proper quantization and dynamical light quarks.

4 Beyond the Standard Model experimental searches for X17

4.1 X17 production mechanisms at accelerators

Luc Darmé[1], Mauro Raggi [2], Enrico Nardi[3]
Institut de Physique des 2 Infinis de Lyon (IP2I), UMR5822, CNRS/IN2P3, F-69622 Villeurbanne Cedex, France
Dipartimento di Fisica, Università di Roma La Sapienza and INFN, Sezione di Roma, I-00185 Rome, Italy
Istituto Nazionale di Fisica Nucleare, Laboratori Nazionali di Frascati, C.P. 13, 00044 Frascati, Italy

Abstract The signal observed in the ATOMKI experiment can be interpreted in terms of a new particle of 17 MeV, light enough to be produced in a broad range of accelerator-based experiments. We review and briefly discuss various production mechanisms and their relevance depending on the nature of the putative X_{17} boson. A particular focus is given on its resonant production in a positron beam dump facility.

4.1.1 Introduction

The anomaly observed by the ATOMKI experiment in the e^+e^- angular correlation spectra in ^{8}Be and ^{4}He nuclear transitions [1,53], can be interpreted in terms of a new boson X_{17} produced on shell and promptly decaying into an electron-positron pair. Nuclear decays of both isotopes point with remarkable precision to the same mass window:

$$M_X = \begin{cases} 16.70 \pm 0.35 \text{ (stat)} \pm 0.5 \text{ (syst) MeV} \\ \qquad\qquad\qquad\qquad (^8\text{Be [1]}) \\ 16.95 \pm 0.10 \text{ (stat)} \pm 0.21 \text{ (syst) MeV} \\ \qquad\qquad\qquad\qquad (^4\text{He [53]}). \end{cases} \quad (31)$$

Such a small mass implies that this hypothetical particle is potentially accessible in accelerator experiments with low center-of-mass (CoM) energy such as e^+ and e^- beam dump experiments, as well as in the decays of light mesons.

In order to fix notations, when presenting explicit formulae, we will assume that X_{17} is a vector particle, whose interaction with the lightest leptons and quarks is given by the following Lagrangian:

$$\mathscr{L} \subset g_e V_\mu \, \bar{e}\gamma^\mu e + \sum_{q \subset u,d} g_q V_\mu \, \bar{q}\gamma^\mu q. \quad (32)$$

However, we stress that the nuclear data are currently not sufficient to fully determine the spin/parity quantum numbers of X_{17} beyond its bosonic nature (see [39,67,68] for recent works in this direction). We will thus discuss also the possibility of a pseudo-scalar X_{17}, and briefly touch on the axial-vector cases.

The signal consists of electron-positron pairs originating from the decay of the excited nuclei, whose correlation angle is precisely measured in the ATOMKI spectrometer. This implies that the X_{17} must couple at the fundamental level to electrons as well as to quarks in order to be produced, whence the Lagrangian in Eq. (32).

In fitting the ATOMKI hint, the couplings to quarks appear dominantly in the combination $g_u + g_d$, and with relatively large values, at the few 10^{-3} level. The X_{17} interaction with electrons must also be at the per-mil level to allow for X_{17} leptonic decays within the ATOMKI apparatus. Altogether, the decay width must be dominated by e^+e^- final states and

is rather small:

$$\Gamma_X \simeq \frac{g_e^2}{12\pi} M_X \sim 0.5 \text{ eV} \times \left(\frac{g_e}{0.001}\right)^2. \tag{33}$$

The experimental facilities at accelerators with the potential to probe such particle can be broadly classified as follow: first, proton-based beam dump, which include all the currently running beam neutrino experiments, as well as Kaon factories. While they typically have access to very large intensity, these experiments suffer from large backgrounds. The study of mesons decay has proved nonetheless successful, with the dominant constraints on the X_{17} arising from π^0 decays [116]. Second, electron-positron colliders can produce efficiently the X_{17}, but generally suffer from poor background rejection since the small X_{17} mass implies that its decay products have little p_T compared to the CoM energy. Finally, $e^\pm$ beam dumps feature good production rates and a relatively clean background environment. Some of the most competitive limits currently come from the NA64 [15,138] e^- beam dump experiment.

We will describe in more detail the features of these experimental strategies in Sect. 4.1.2. Then, in Sect. 4.1.3 we will provide a first estimate of an alternative approach which relies on the resonant production of X_{17} in positrons beam dump experiments.

4.1.2 Review of productions mechanisms

The experimental approaches to search for the X_{17} can be divided into two broad classes: in the first one the X_{17} is produced via its coupling to the quarks, in the second one via its coupling to $e^\pm$.

Production via X_{17}-quark couplings The X_{17} is expected to interact rather strongly with the nucleons given the amplitude of the signal seen in the ATOMKI experiment. Thanks to its small mass, the X_{17} could thus be produced in several different rare mesons decay. However these processes have a strong dependence on the nature of the particle, and on the details of its interaction with quarks.

If the X_{17} is a spin-1 vector state, the main channels are:

– $\pi^0 \to \gamma X_{17}$ (followed by $X_{17} \to e^+ e^-$). This channel has been thoroughly explored by the NA48 collaborations [116], who has set rather strong limits. The corresponding bounds can however be evaded by assuming that the X_{17} exhibits a certain amount of piophobia, which in turn implies that the X_{17} is also protophobic [8,39,57].
– J/Ψ rare decays. This channel has been studied in Ref. [162]. It relies on assuming that the X_{17} also couples to the charm quark. Therefore it basically constrain a flavour-universal X_{17}.

– $B^* \to B X_{17}$, $D^* \to D X_{17}$ rare decays. This channel provide loose limits on X_{17} quark couplings, which are complementary to those from π^0 decays [162].

If the X_{17} is instead an axial-vector, the leading limit from π^0 decays does not apply. However, since such an object cannot couple to a SM conserved current, other strong limits come into play [41,107,163,164].

If the X_{17} is a pseudo-scalar particle (ALP), several other mesonic decay channels become relevant:

– Direct ALP/π^0 mixing enhances the π^0 electromagnetic decay: $\pi^0 \to X_{17} \to e^+ e^-$ [59,60].
– $\pi^0 \to X_{17} X_{17} X_{17} \to 6e$ and other multi-lepton final states are also allowed, and can lead to significantly stronger constraints due to the reduced backgrounds [136].
– $K \to \pi X_{17}$, $K \to \mu\nu X_{17}$. Flavour-violating decays of heavier mesons also become enhanced, and can proceed even in absence of X_{17} flavour-violating couplings [58–60].

Finally, in the case where the X_{17} has additional flavour violating couplings, many additional channels become available both in lepton and in "standard" flavoured meson decays.

Production via X_{17}-lepton couplings The cm-scale of the ATOMKI apparatus provides an absolute lower bound on the X_{17} electron couplings (for our reference vector case, $g_e \gtrsim 10^{-6}$). Covering this region would provide a definite answer regarding the new physics origin of the anomaly. Additionally, the nature of the particle plays a smaller role in lepton-based production rates, allowing for more model independence. In practice, the lower limit on g_e is already covered by strong constraints from historical beam dump experiments as recast in [165,166]: in particular E141 [167], and two other experiments at KEK [168] and at the Orsay linac [169]. The main X_{17} production mechanism in these facilities is the bremsstrahlung process off a nucleus N,

$$eN \to eN X_{17}, \quad \text{with } \sigma_{\text{brem}} \propto \frac{g_e^2 \alpha_{em}}{16\pi^2} \frac{Z^2}{M_X^2}, \tag{34}$$

where Z is atomic number of the target atom, and we have left out order one coefficients. In this production process the X_{17} carries away a relevant fraction of the beam energy, and the typical propagation length before its decay is given by:

$$\gamma_{X_{17}} \ell_{X_{17}} \simeq 3 \text{ cm} \times \left(\frac{E_{X_{17}}}{100 \text{ GeV}}\right) \left(\frac{3 \cdot 10^{-4}}{g_e}\right)^2, \tag{35}$$

where we have assumed $E_{X_{17}} \sim E_{\text{beam}}$. This allows for a quite effective search strategy in which the X_{17} displaced

decays are search in a shielded detector. For the spin-1 X_{17} case one can be sensitive to couplings as large as $g_e \sim 10^{-5}$. The dominant constraint arises from the E141 experiment: $g_e \gtrsim 5.5 \cdot 10^{-5}$. However, this limit occurs near the mass threshold of the experimental sensitivity where the use of the Weizsäcker–Williams approximation in the recast [165,166] could have led to an overestimate of the experimental reach [170]. A more conservative approach then retains the somehow weaker limit $g_e \gtrsim 2 \cdot 10^{-5}$, corresponding to the KEK and Orsay constraints, which have been recast according to a theoretically more solid ground.

The same strategy has been exploited recently by the NA64 collaboration, that has repurposed its missing energy detector into a very short baseline beam dump experiment [15,138]. In particular, recent results of the collaboration exclude the g_e range $\sim 2 \cdot 10^{-4}$ to $3.5 \cdot 10^{-5}$ [15] for the case of a vector X_{17}. Note that if the X_{17} is instead a pseudo-scalar, the balance between the production rates and its lifetime is modified, weakening the NA64 exclusion [138].

The strongest upper limit on the coupling to electrons is obtained in e^+e^- colliders from the associate annihilation process

$$e^+e^- \to \gamma X_{17}, \quad \text{with } \sigma_{\gamma X_{17}} \propto \frac{g_e^2}{4\pi}\frac{1}{s}, \tag{36}$$

where $\sqrt{s}$ is the center-of-mass energy, and we have omitted order one factors. The analysis of the KLOE collaboration [171] has yielded the limit $g_e \lesssim 6 \cdot 10^{-4}$. Note that a somewhat stronger limit could be obtained from the anomalous magnetic moment of the electron, under the assumption of no additional compensating new physics (NP) contributions. However, the experimental situation for this observable is not currently clear, with two competing measurements disagreeing with the SM prediction at around 3σ, but in opposite directions [91,140]. Additionally, complete NP models realising the required protophobia for the X_{17} typically introduce a rich UV particle content, thus making any limit derived from $(g-2)_e$ strongly model dependent. We have summarised the current status of accelerator-based leptons search in Fig. 35 based on the data collated from DarkCast [172].

As a final comment, a somehow orthogonal experimental direction is to look for the X_{17} from μ decays in the Mu3e experiment [173]. Photo-production via the $\gamma N \to N e^+e^-$ has been also recently advocated in [174].

4.1.3 Resonant X_{17} production

In this section we focus on the resonant production of the X_{17} in positron beam dump experiments via the process:

$e^+e^- \to X_{17}$ (followed by $X_{17} \to e^+e^-$).
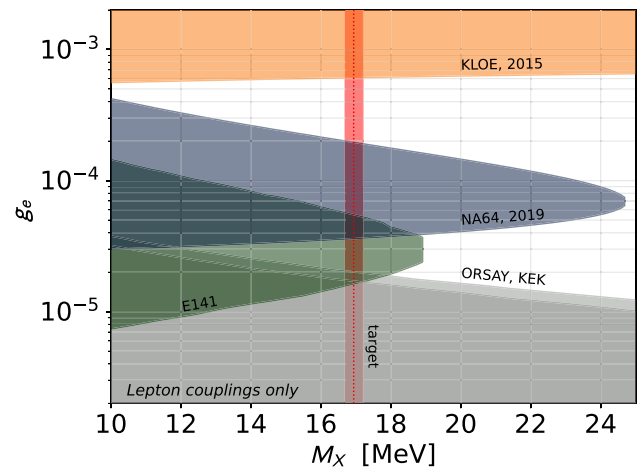
Fig. 35 Dominant constraints on the couplings of a new vector boson with $e^\pm$ from accelerator-based experiments only. We show the limits from KLOE [171] (orange region), NA64 [15] (blue region), E141 [167] (green region) and the KEK and Orsay experiments [168,169]. The red band represents the X_{17} mass target from [53]

Resonant production strategy In general, the use of positrons in a beam dump setup involves a trade-off. Indeed, producing and accelerating positrons implies certain losses in intensity and energy, since positrons are usually obtained from a primary electron beam via pair production of bremsstrahlung photons. On the other hand, the production rate increases dramatically if the CoM energy of the e^+e^- system matches precisely $M_X \sim 17$ MeV. For ultra-relativistic positrons impinging on target electrons assumed at rest, the resonant condition is achieved for a beam energy:

$$E_+ = \frac{M_X^2}{2m_e}. \tag{37}$$

The X_{17} is then produced with precisely E_+ of energy in the lab frame and a correspondingly relatively small boost:

$$\gamma_{X_{17}\text{res.}} = \frac{M_X}{2m_e} \sim 17. \tag{38}$$

This implies that resonantly produced X_{17} bosons will have a limited decay length, thus making displaced vertex searches quite challenging. Two experimental strategies can be considered to obtained positrons of the required energy:

– Use the energy loss and secondary e^+e^- production from electromagnetic showers in the target to "scan" various positron energies [175–179]. This requires a target with thickness of the order of one radiation length. However, while this strategy is particularly well-suited to study missing energy signatures when the light particle escape the detector, the background from the electromagnetic

shower will likely swamp the X_{17} prompt decay signature.

– Directly scan with the beam energy around the resonance. Since the mass of the X_{17} particle must lie in the rather limited range given in Eq. (31), according to Eq. (37) it is sufficient to vary the beam energy approximately within the range $[270-290]$ MeV. Since for resonant production the rate is strongly enhanced, very thin targets can be employed in order to reduce the background.

Focusing on this second approach, let us consider the case in which the particle width, although small, is not too narrow so that the energy distribution of the positrons in the beam can still be considered as continuous. In the CoM of the collision, this corresponds to the requirement

$$\frac{\Gamma_X M_X}{2m_e} \frac{1}{\delta E} N_{\text{tot}}(E) \sim \left(\frac{N_{\text{tot}}(E)}{4 \cdot 10^4}\right)\left(\frac{g_e}{2 \cdot 10^{-4}}\right)^2 \gg 1, \quad (39)$$

where $N_{\text{tot}}(E)$ is the total number of positron with energy E, and we have assumed a beam energy spread $\delta E \sim 0.7$ MeV. As long as the energy distribution of the positrons can be considered as continuous, in absence of additional photon radiation the resonant cross-section is given by:

$$\sigma_{\text{res}} = \frac{g_e^2}{2m_e} \delta(E_+ - E_{\text{res}}). \quad (40)$$

The delta-function directly encloses the suppression due to the narrow width. It is instructive however to estimate the peak cross-section for an incoming e^+ with precisely the X_{17} resonant energy $E_+ = E_{\text{res}}$. We obtain:

$$\sigma_{\text{peak}} \sim 50 \text{ b} \times \left(\frac{17 \text{ MeV}}{M_X}\right). \quad (41)$$

This value translates into a mean free path in a carbon target of around 200 μm. Thus, each positron with precisely the resonant energy will produce a X_{17} with near certainty, even in sub-millimetric targets. The g_e^2 suppression from Eq. (40) in fact arises because such "peak" positrons are exceedingly rare due to the narrow X_{17} width, highlighting the importance of the "continuous" condition, Eq. (39). All in all, the final number of produced X_{17} for N_{tot} positron-on-target is given by

$$\mathcal{N}_{X_{17}} = N_{\text{tot}} \frac{\mathcal{N}_A Z \rho}{A} L_{\text{tar}} \frac{g_e^2}{2m_e} \frac{df_{\text{beam}}}{dE}(E_{\text{res}}), \quad (42)$$

where L_{tar} and ρ are respectively the target thickness and density, and we have assumed that the target is sufficiently thin that the differential energy distribution $\frac{df_{\text{beam}}}{dE}$ is not significantly modified along the positrons path through it.
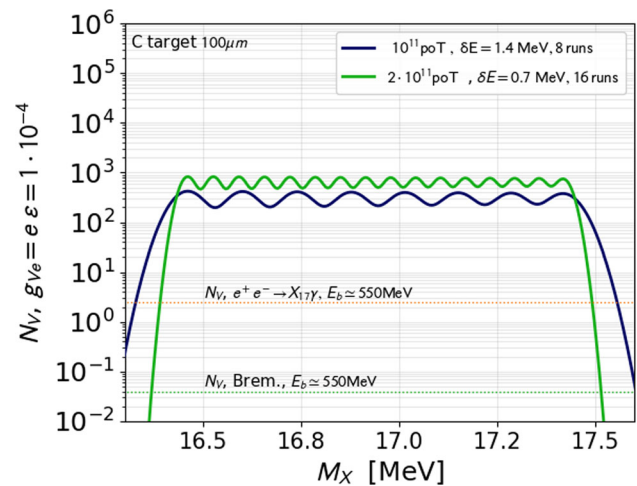
Fig. 36 Number of produced X_{17} boson in a PADME-like experimental setup, assuming either a beam spread δE of 0.7 MeV with an integrated $2 \cdot 10^{11}$ poT (green curve) or $\delta E = 1.4$ MeV with 10^{11} poT (blue curve). The X_{17} coupling with electron is fixed at $g_e = 10^{-4}$

Results: X_{17} resonant production search at LNF The DAΦNE beam facility at Laboratori Nazionali di Frascati (LNF) offers interesting prospects for a X_{17} search based on resonant production. In particular, the LNF accelerator complex can provide a positron beam and can vary its energy in the required range. Assuming a typical carbon target (with electron density of 10^{24} cm^{-3}) of 100 μm such as the one actually in use in the Positron Annihilation into Dark Matter Experiment (PADME) [180,181], the expected X_{17} production rate is approximately given by:

$$\mathcal{N}_{X_{17}}^{\text{per poT}} \simeq 3.8 \cdot 10^{-7} \times \left(\frac{g_e}{3 \cdot 10^{-4}}\right)^2 \left(\frac{1 \text{ MeV}}{\delta E}\right), \quad (43)$$

where we have assumed a beam energy centered on E_{res}.

We further illustrate this result in Fig. 36 in a more realistic scanning strategy, where a total number of poT of order 10^{11} is divided into several runs at different energies, in order to properly cover the X_{17} mass range. The number of runs needed to cover this range depends on the beam spread. Thus, while reducing δE would enhance the production, more runs are then required to scan the whole mass range, with the overall statistics for each energy bin accordingly reduced. Nevertheless, reducing δE as much as possible would still represent an important asset, in that it will increase the signal-to-noise ratio, and hence the experimental sensitivity. A thorough study including background estimations and projected limits can be found in [182].

4.1.4 Conclusion

The lightness of the X_{17} hypothetical NP particle hinted by the ATOMKI data implies that it can be produced in an very large number of processes. This offers a precious opportunity to provide an independent cross-check to the nuclear physics experiment. We have provided a short review of the various experimental analysis that constrain the X_{17} properties, recasting the existing limits depending on its couplings to quarks and leptons.

In this landscape, we have argued that electron/positron-based facilities are well-placed in that they provide a relatively model-independent way of testing the existence of the X_{17} solely via its coupling to $e^\pm$, which are unavoidably required for a particle physics interpretation of the ATOMKI anomaly. In particular, the resonant production mechanism can play an important role to help closing in a not-so-far future the remaining parameter space. In this regard we have presented an estimate of the production rate in an LNF-based facility, leveraging the current experimental setup.

4.2 Search for dark photon in π^0 decays by NA48/2 at CERN

Evgueni Goudzovski

School of Physics and Astronomy, University of Birmingham, Edgbaston, Birmingham, B15 2TT, UK

Abstract A sample of 1.69×10^7 fully reconstructed $\pi^0 \to \gamma e^+ e^-$ decay candidates collected by the NA48/2 experiment at CERN in 2003–2004 has been analysed to search for the dark photon (A') production in the $\pi^0 \to \gamma A'$ decay followed by the prompt $A' \to e^+ e^-$ decay. No signal has been observed, and an exclusion region in the plane of the dark photon mass $m_{A'}$ and mixing parameter ε^2 has been established in the mass range $9 \, \text{MeV}/c^2 < m_{A'} < 120 \, \text{MeV}/c^2$. The results can readily be interpreted in terms of the X17 particle production and decay.

4.2.1 Introduction

Kaons represent a source of tagged neutral pion decays, and high intensity kaon experiments provide opportunities for precision π^0 decay measurements. The NA48/2 experiment at the CERN SPS [183,184] collected a large sample of charged kaon ($K^\pm$) decays in flight, corresponding to about 2×10^{11} $K^\pm$ decays in the fiducial decay volume. This allows selecting a pure sample of Dalitz decays of the neutral pion, $\pi^0_D \to \gamma e^+ e^-$, through the reconstruction of $K^\pm \to \pi^\pm \pi^0$ and $K^\pm \to \pi^0 \mu^\pm \nu$ decays (denoted $K_{2\pi}$ and $K_{\mu 3}$). A search for dark photon production and prompt decay via the chain $\pi^0 \to \gamma A'$, $A' \to e^+ e^-$ based on the above sample, reported in detail in Ref. [185], is discussed

here. The expected branching fraction of the π^0 decay into the dark photon is [186]

$$\mathscr{B}(\pi^0 \to \gamma A') = 2\varepsilon^2 \left(1 - \frac{m_{A'}^2}{m_{\pi^0}^2}\right)^3 \mathscr{B}(\pi^0 \to \gamma\gamma), \quad (44)$$

where ε is the kinetic mixing parameter, and the search results in the mass range $9 \, \text{MeV}/c^2 < m_{A'} < 120 \, \text{MeV}/c^2$ are reported in terms of both the both the branching fraction $\mathscr{B}(\pi^0 \to \gamma A')$ and the corresponding ε value.

4.2.2 Beam, detector and data sample

The NA48/2 experiment [183,184] used simultaneous K^+ and K^- beams produced by 400 GeV/c primary CERN SPS protons impinging on a beryllium target. Charged particles with momenta of (60 ± 3) GeV/c were selected by an achromatic system of four dipole magnets which split the two beams in the vertical plane and recombined them on a common axis. The beams passed through collimators and quadrupole magnets, and entered a 114 m long cylindrical vacuum tank containing the fiducial decay region. Both beams had an angular divergence of about 0.05 mrad, a transverse size of about 1 cm, and were aligned with the longitudinal axis of the detector within 1 mm.

The vacuum tank was followed by a magnetic spectrometer housed in a vessel filled with helium at nearly atmospheric pressure, separated from the vacuum by a thin $(0.3\% X_0)$ Kevlar window. An aluminium beam pipe traversing the centre of the spectrometer (and all the following detectors) allowed the undecayed beam particles to continue their path in vacuum. The spectrometer consisted of four drift chambers (DCH): DCH1, DCH2 located upstream and DCH3, DCH4 downstream of a dipole magnet. The DCH momentum resolution was $\sigma_p/p = (1.02 \oplus 0.044 \cdot p)\%$, with p expressed in GeV/c. The spectrometer was followed by a plastic scintillator hodoscope (HOD) consisting of a plane of vertical and a plane of horizontal strip-shaped counters arranged in four quadrants. The HOD provided time measurements of charged particles with 150 ps resolution. It was followed by a liquid krypton electromagnetic calorimeter (LKr), an almost homogeneous $27 \, X_0$ deep ionisation chamber segmented transversally into 13,248 projective cells. The LKr energy resolution was $\sigma_E/E = (3.2/\sqrt{E} \oplus 9/E \oplus 0.42)\%$, with E expressed in GeV.

The NA48/2 experiment collected data in 2003–2004, with about 100 days of efficient data taking in total. A two-level trigger chain was employed to collect $K^\pm$ decays with at least three charged tracks in the final state. At the first level (L1), a coincidence of hits in the two planes of the HOD was required to occur in at least two of 16 non-overlapping regions. The second level (L2) performed online reconstruc-

tion of trajectories and momenta of charged particles based on the DCH information. The L2 logic was based on the multiplicities and kinematics of reconstructed tracks and two-track vertices.

4.2.3 Event reconstruction and selection

The two selections employed for $K_{2\pi}$ and $K_{\mu 3}$ decays followed by the prompt $\pi^0 \to \gamma A'$, $A' \to e^+ e^-$ decay chain are identical up to the momentum, invariant mass and particle identification conditions.

Three-track vertices are reconstructed by extrapolation of track segments from the upstream part of the spectrometer into the decay volume. Particle identification is based on energy deposition in the LKr calorimeter and momentum measured by the spectrometer, and the presence of a three-track vertex formed by a pion ($\pi^\pm$) or muon ($\mu^\pm$) candidate and two opposite sign electron ($e^\pm$) candidates is required. Tracks are required to be in the fiducial geometric acceptances of the DCH, HOD and LKr detectors, and well separated in the DCH1 plane to reject photon conversions. A single isolated LKr energy deposit cluster is considered as a photon candidate. The photon candidate is required to be compatible in time with the tracks, and separated from the electron (pion, muon) impact points.

An event is classified as a $K_{2\pi}$ or $K_{\mu 3}$ candidate based on the presence of a pion or a muon candidate, total and transverse momentum requirements, and mass and missing mass requirements. In particular, the reconstructed invariant mass of the $e^+ e^- \gamma$ system is required to be compatible with the nominal π^0 mass m_{π^0}: $|m_{ee\gamma} - m_{\pi^0}| < 8\,\mathrm{MeV}/c^2$, which corresponding to ± 5 times the resolution on $m_{ee\gamma}$. Finally, the search for resonances includes a $|m_{ee} - m_{A'}| < \Delta m(m_{A'})$ condition, where $m_{A'}$ is the assumed dark photon mass, and $\Delta m(m_{A'})$ is the half-width of the search window depending on the resolution.

4.2.4 Search for the dark photon signal

The number of $K^\pm$ decays in the 98 m long fiducial decay region is computed using the $K^\pm \to \pi^\pm \pi^0$ Dalitz decay selection to be

$$N_K = (1.57 \pm 0.05) \times 10^{11}, \tag{45}$$

where the uncertainty on N_K is dominated by the limited precision on $\mathcal{B}(\pi_D^0)$. The number of π_D^0 decay candidates reconstructed with the joint $K_{2\pi}$ and $K_{\mu 3}$ Dalitz decay selection is 1.69×10^7. The reconstructed spectra of invariant masses $m_{2\pi}$ and m_{ee} for data and simulated events passing the $K_{2\pi}$ Dalitz decay selection are shown in Figs. 37 and 38.

A scan for a dark signal in the mass range $9\,\mathrm{MeV}/c^2 \leq m_{A'} < 120\,\mathrm{MeV}/c^2$ has been performed. The lower bound-
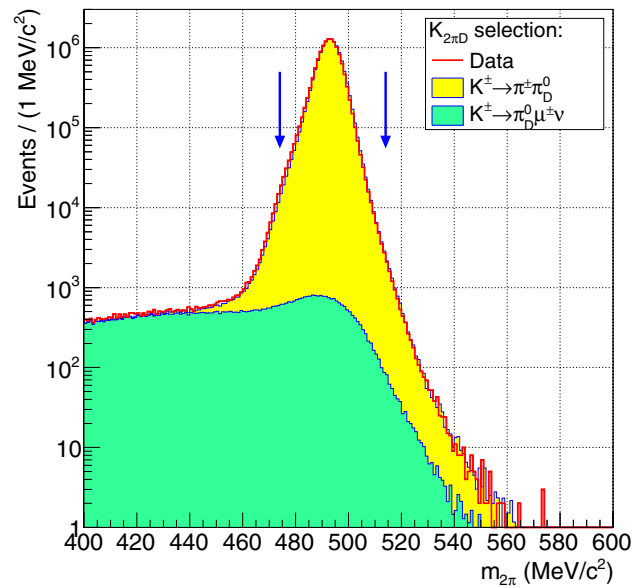
Fig. 37 Invariant mass ($m_{2\pi}$) distribution of data and MC events passing the $K_{2\pi}$ selection. The signal mass region is indicated with vertical arrows
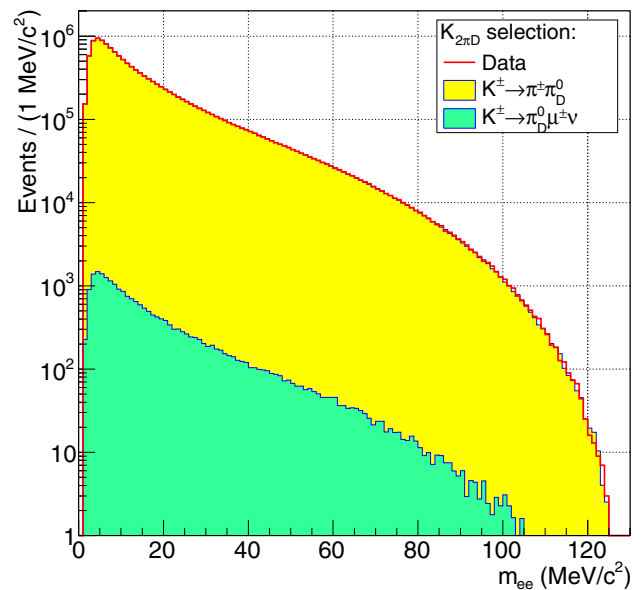

Fig. 38 Invariant mass (m_{ee}) distribution of data and MC events passing the $K_{2\pi}$ selection. A dark photon signal would correspond to a spike in the m_{ee} distributions

ary of the mass range is determined by the limited accuracy of the π_D^0 background simulation at low $e^+ e^-$ mass. The resolution on m_{ee} as a function of m_{ee} evaluated with simulations is parameterised as

$$\sigma_m(m_{ee}) = 0.067\,\mathrm{MeV}/c^2 + 0.0105 \cdot m_{ee}, \tag{46}$$

and varies in the range 0.16–$1.33\,\mathrm{MeV}/c^2$ over the mass range of the scan. For each considered mass value, the number
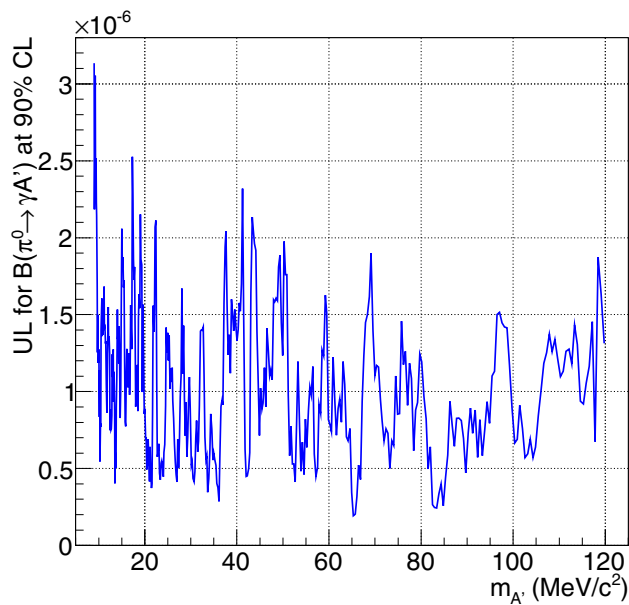
Fig. 39 Upper limits obtained for $\mathscr{B}(\pi^0 \to \gamma A')$ at 90% CL for each dark photon mass value $m_{A'}$

of observed data events N_{obs} is compared to the expected number of background events N_{exp} obtained using the full simulation of the π_D^0 background [187,188] shown in Fig. 38.

The local significance of the possible signal never exceeds 3σ, and upper limits at 90% CL for the number of $A' \to e^+e^-$ decay candidates for each dark photon mass hypothesis are obtained. Finally, upper limits at 90% CL of the branching fraction $\mathscr{B}(\pi^0 \to \gamma A')$ evaluated for each dark photon mass value, with the assumption of prompt decay and $\mathscr{B}(A' \to e^+e^-) = 1$, are shown in Fig. 39. These limits are $\mathscr{O}(10^{-6})$ and do not exhibit a strong dependence on $m_{A'}$, as the mass dependences of π_D^0 background level (Fig. 38) and signal acceptance largely compensate each other. It should be noted that the signal acceptance, and therefore the reported limits of $\mathscr{B}(\pi^0 \to \gamma A')$, depend on the assumed angular distribution of the $A' \to e^+e^-$ decay, which affects interpretations within alternative new physics models.

The sensitivity of this search is limited by the irreducible π_D^0 background. In particular, the upper limits of $\mathscr{B}(\pi^0 \to \gamma A')$ obtained are two to three orders of magnitude above the single event sensitivity. The achievable upper limit on $\mathscr{B}(\pi^0 \to \gamma A')$ scales as the inverse square root of the integrated beam flux, which means that the possible improvements to be made with this technique using for example a larger di-electron dataset collected by the NA62 experiment in 2016–2018 [189,190] are modest.

The details of this analysis are reported in Ref. [185]. A more recent review of the dark photon searches is available in Ref. [191]. Further prospects of hidden-sector searches in

kaon decays with the presently available and future datasets are discussed for a broad range of scenarios in Ref. [134].

4.2.5 Conclusions

A search for the dark photon production in the $\pi^0 \to \gamma A'$ decay followed by the prompt $A' \to e^+e^-$ decay has been performed using the data sample collected by the NA48/2 experiment in 2003–2004. No signal is observed, providing upper limits of $\mathscr{O}(10^{-6})$ the branching ratio $\mathscr{B}(\pi^0 \to \gamma A')$ in the mass range 9–120 MeV/c^2.

4.3 Prospects for dark photon searches in the Mu3e experiment

Ann-Kathrin Perrevoort, on behalf of the Mu3e Collaboration
Institute of Experimental Particle Physics, Karlsruhe Institute of Technology

Abstract The Mu3e experiment will search for the lepton-flavour violating decay $\mu^+ \to e^+e^-e^+$ with an unprecedented sensitivity of one in up to 10^{16} muon decays. The recorded data set will also be suited to search for e^+e^- resonances in $\mu^+ \to e^+e^-e^+\nu\nu$. In the following, a sensitivity study of the phase I Mu3e experiment to dark photons emitted in muon decays with prompt decay to e^+e^- pairs is presented.

4.3.1 The Mu3e experiment

In the Standard Model (SM), lepton flavour is conserved in all interactions. As there is no underlying global symmetry for this conservation, lepton flavour is violated in many extensions of the SM. While indeed the existence of lepton flavour violation (LFV) has already been proven by the observation of neutrino oscillations, in the charged lepton sector LFV has evaded observation so far.

The signature searched for by the Mu3e experiment [192] is the LFV decay $\mu^+ \to e^+e^-e^+$. Even if neutrino mixing is integrated in the SM, this decay is suppressed to unobservable branching fractions of $\mathscr{O}(10^{-54})$, and thus any observation of $\mu^+ \to e^+e^-e^+$ would be an unambiguous sign of physics beyond the SM.

The Mu3e experiment aims to search for $\mu^+ \to e^+e^-e^+$ down to branching fractions of 2×10^{-15} in the first and below 10^{-16} in the second and final phase of the experiment. The phase I experiment is currently being built at the Paul Scherrer Institute (PSI). It will be operated at muon stopping rates of 10^8 μ/s at an existing beamline. The phase II experiment will require rates in excess of 10^9 μ/s which will become available at the planned high intensity muon beam-

(a) Longitudinal view.
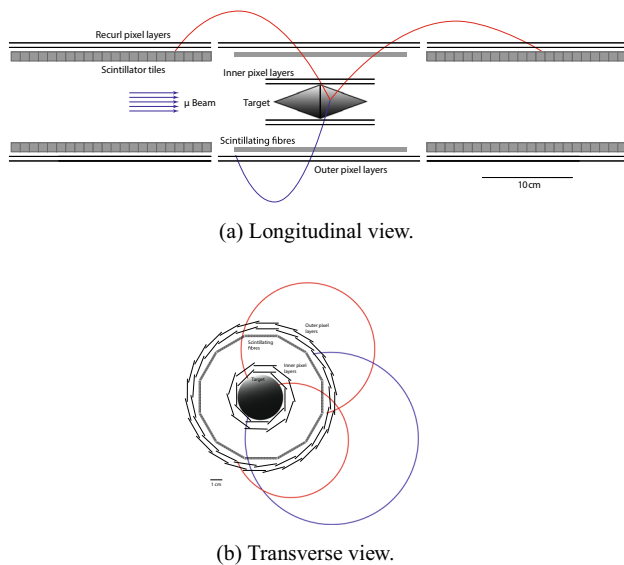
(b) Transverse view.

Fig. 40 Schematic of the phase I Mu3e detector [192] as seen **a** longitudinal and **b** transverse to the beamline with a potential $\mu^+ \to e^+ e^- e^+$ signal decay

line at PSI. In the following, only the phase I experiment is discussed.

The main backgrounds in Mu3e are the rare muon decay $\mu^+ \to e^+ e^- e^+ \nu\nu$ as well as accidental combinations mainly of Bhabha scattering events with positrons from another Michel decay. The first can only be distinguished from signal by the missing energy that is carried by the undetected neutrinos, and thus requires an excellent momentum measurement. The latter can be suppressed by precise tracking and timing measurements.

The Mu3e detector is constructed as a lightweight tracking detector in order to minimise uncertainties from multiple Coulomb scattering and to reduce the occurrence of accidental background. A schematic of the Mu3e experiment is shown in Fig. 40. The detector is placed in a 1 T solenoidal magnetic field. The incoming muons are stopped on the hollow target in the center of the experiment and decay at rest. The central tracking detector is constructed from four layers of ultra-thin pixel sensors with an additional scintillating fibre detector. In the large magnet bore, the electrons curl back to the detector and are measured again in the recurl stations up- and downstream of the central detector which are built from pixel sensors and scintillating tiles. Due to the increased lever arm, the momentum resolution of these recurling tracks is significantly improved. The detector is continuously read out. All events are reconstructed in the online filter farm but only events containing a potential $\mu \to eee$ candidate are kept for offline analysis.

It has been shown in simulation studies that the phase I Mu3e experiment can be operated free of background. A single-event sensitivity on the branching fraction of

$\mathscr{B}(\mu^+ \to e^+ e^- e^+) \approx 2 \times 10^{-15}$ can be achieved – pushing the current best limits obtained by SINDRUM [193] by three orders of magnitude.
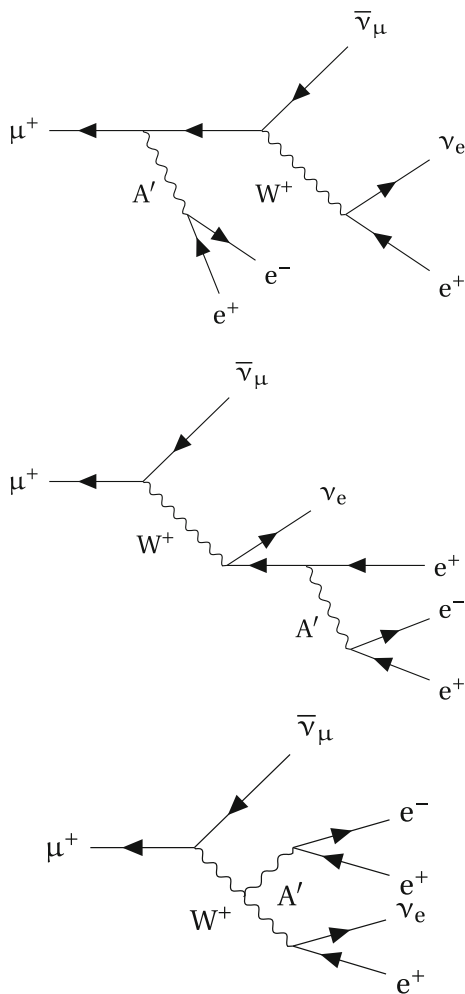
4.3.2 Dark photon searches

The Mu3e experiment will record an unprecedented data set of $\mathscr{O}(10^{15})$ muon decays with three electrons in the final state in phase I. As there is a priori no selection on the kinematics of $\mu \to eee$ candidates during data taking, this data set can be exploited for other BSM searches, e.g. on $e^+ e^-$-resonances in $\mu^+ \to e^+ e^- e^+ \nu\nu$.

The sensitivity to such processes has been estimated with a dark photon model [19]. The dark photon A' interacts through kinetic mixing with the photon and Z boson and thus couples to the electro-magnetic current. In Mu3e, this decay can only be detected if the dark photon subsequently decays into an $e^+ e^-$ pair. The respective Feynman diagrams are shown in Fig. 41.

In the sensitivity study presented here, prompt $A' \to e^+ e^-$ decays are investigated. Such a study has been performed previously [19] however with simplifications on the detector geometry and the expected backgrounds. In the following, signal events are generated with Mad-Graph5_aMC@NLO 2.4.3 [194] using the Lagrangian from [19], and the detector response is simulated with the full Geant4 [195] based Mu3e detector simulation. Signal events are simulated for dark photon masses $m_{A'}$ between 2 MeV and 80 MeV. Larger $m_{A'}$ in the reach of Mu3e are already excluded by existing experimental limits. The sources of background are the same as in the $\mu \to eee$ search. The same online and offline reconstruction is applied.

Selections on the quality of the track and vertex reconstruction as well as the distance of the reconstructed vertex to the target are applied which are especially effective against accidental background. The resulting spectra of the reconstructed invariant $e^+ e^-$ mass m_{ee} are shown in Fig. 42. The distribution of signal events features a clear peak around the simulated dark photon mass $m_{A'}$ while the distribution of background events is smoothly falling towards large m_{ee}. The broader underlying distribution in the signal spectra is caused by the wrong $e^+ e^-$ combination that does not stem from the $A' \to e^+ e^-$ decay. The sensitivity is enhanced by choosing the $e^+ e^-$ pair with the smaller m_{ee} for $m_{A'}$ up to 45 MeV, and the $e^+ e^-$ pair with the higher m_{ee} above.

The sensitivity is estimated by means of toy Monte Carlo studies for the full phase I of the Mu3e experiment. The expected upper limits on the branching fraction at 90% CL range from $\mathscr{O}(10^{-9})$ at low $m_{A'}$ down to $\mathscr{O}(10^{-12})$ at high $m_{A'}$ (see Fig. 43b). For $m_{A'} = 17$ MeV, the phase I Mu3e experiment is sensitive to branching fractions of a few 10^{-10}. These limits are translated to limits on the kinetic mixing parameter ϵ under the assumption that the dark photon decays

(a) Signal events from prompt dark photon decays with $m_{A'}$ of 20 MeV, 45 MeV and 70 MeV.

(b) Background events from rare muon decays and accidental combinations.

Fig. 42 Spectra of the reconstructed invariant mass m_{ee} of both e^+e^- combinations for signal prompt dark photons decays and background from rare muon decays and accidental combinations. The signal spectra are drawn normalized to one. For the background spectra, 300 days of data taking at 10^8 μ/s as expected in phase I of Mu3e are assumed

Fig. 41 Feynman diagrams of dark photons A' emitted in muon decays $\mu^+ \rightarrow A'e^+\nu\nu$. The dark photons decay visibly into an electron-positron pair $A' \rightarrow e^+e^-$
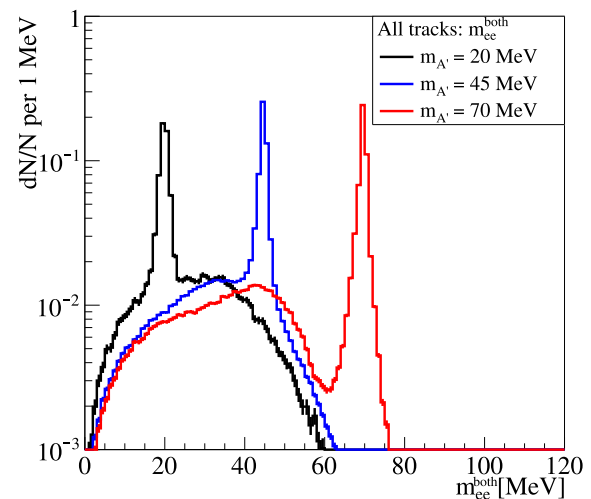
exclusively to an e^+e^- pair. A comparison with current limits from dark photon searches is shown in Fig. 43a.

4.4 Dark matter and X17 searches at MESA
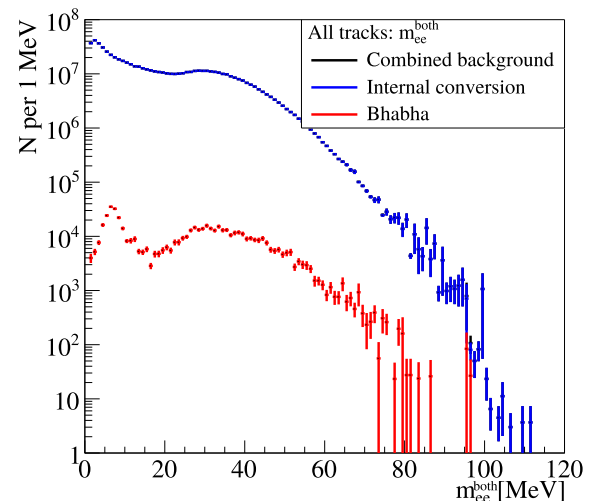
L. Doria (on behalf of the MAGIX/DarkMESA Collaboration)

Johannes Gutenberg-Universität Mainz, Johann-Joachim-Becher-Weg 45 D 55128 Mainz

Abstract Light dark matter searches with accelerators is currently a very active field with many running and planned experiments. Such experiments can also contribute to solve the question about the existence of X17, a postulated 17 MeV mass new particle for explaining different anomalies in nuclear and particle physics. In this contribution, we highlight in particular the contribution of the experiments being built at the new Mainz Energy-recovery Superconducting
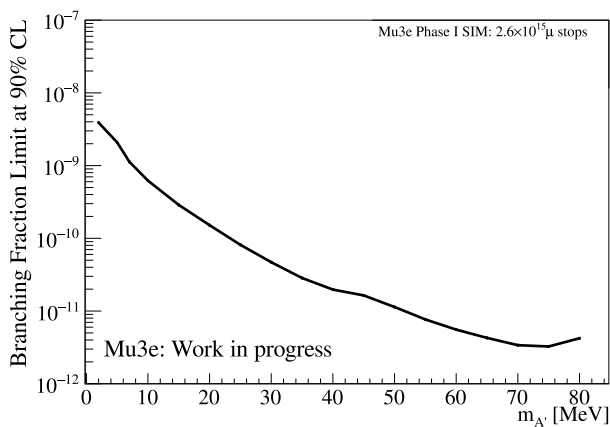
(a) Expected limits on the branching fraction of prompt dark photon decays at 90 % CL.
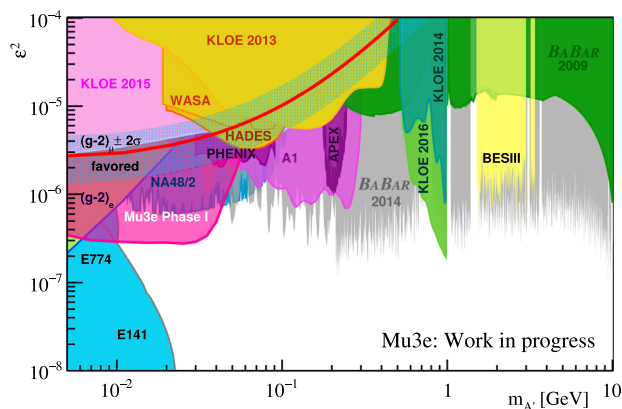
(b) Expected limits in the dark photon parameter space at 90 % CL assuming $\mathscr{B}(A' \to ee) = 1$. Adapted from [198].

Fig. 43 Expected sensitivity on dark photons emitted in $\mu \to A'e\nu\nu$ with prompt decay $A' \to ee$ in the phase I Mu3e experiment

Accelerator (MESA) facility. MESA will provide intense electron beams for hadron and nuclear physics, as well as for dark matter searches with competitive sensitivities.

4.4.1 Introduction

A variety of astrophysical and cosmological observations point to the existence of Dark Matter (DM). In the last decades, an effort was made for searching for DM with particle colliders, fixed-target experiments, indirect detection techniques, and underground direct detection experiments. Still, the nature of DM remains elusive, and more sensitive and diversified experiments are required. A large class of models describe DM as a relic from the early Universe where DM was in thermodynamic equilibrium with Standard Model (SM) particles. The DM abundance was set when its annihilation rate in SM particles became smaller than the expansion rate of the universe in a process known as *freeze-out*. While this mechanism is very compelling, it allows for a

broad range of DM masses (keV/c^2–TeV/c^2) and interaction cross-sections. The prime target of many experiments is a DM candidate called WIMP (Weakly-Interacting Massive Particle), motivated by models of physics beyond the SM (most notably supersymmetric models). This range can be effectively tackled by high-energy colliders and direct detection experiments. In the light dark matter ($< \text{GeV}/c^2$) range (LDM), these methods become less effective, and different techniques are needed. LDM production at accelerators can in principle overcome the limitations of direct detection experiments (the detection energy threshold) by producing DM particles with enough momentum to be detected, even if they are relatively light. High-energy colliders are not optimized for the low-mass range, and lower energy accelerators coupled with fixed targets can have an advantage in LDM searches. In this context, low-energy accelerator searches can also contribute to the "X17 puzzle", i.e. the existence of a new particle of mass ~ 17 MeV, as hinted by recent nuclear physics experiments [1].

4.4.2 Light dark matter

In the $< \text{GeV}/c^2$ range, for retaining a thermal origin of DM, the existence of additional interactions has to be postulated. For small masses, considering only electroweak-scale cross-sections, the annihilation rate would not be sufficient, leading to DM overproduction. A relevant class of LDM models is based on the idea that DM particles belong to a *dark sector* interacting with the SM via one (or more) mediator particle(s). Dark sector models can be classified by the type of mediator particle (the *portal*) and the type of DM particle. In general, the dark sector might contain more mediators and particles. A simple model which captures the essence of dark sector physics contains a massive vector mediator particle (a "dark photon") and one DM particle. The model's lagrangian is

$$\mathscr{L} \supseteq -\frac{1}{4}F'_{\mu\nu}F'^{\mu\nu} + \frac{\epsilon_Y}{2}F'_{\mu\nu}B^{\mu\nu}$$
$$+ \frac{m^2_{A'}}{2}A'_\mu A'^\mu + g_D A'_\mu J^\mu_\chi + g_Y B_\mu J^\mu_Y, \qquad (47)$$

where $F'_{\mu\nu} = \partial_\mu A'_\nu - \partial_\nu A'_\mu$ and $B_{\mu\nu} = \partial_\mu B_\nu - \partial_\nu B_\mu$ are the dark photon and the hypercharge fields, g_D is the dark gauge coupling, and J^μ_χ and J^μ_Y the DM and hypercharge currents, respectively. After electroweak symmetry breaking, the dark photon mixes with the SM photon and the Z boson

$$\frac{\epsilon_Y}{2}F'_{\mu\nu}B^{\mu\nu} \to \frac{\epsilon}{2}F'_{\mu\nu}F^{\mu\nu} + \frac{\epsilon_Z}{2}F'_{\mu\nu}Z^{\mu\nu}, \qquad (48)$$

where $\epsilon = \epsilon_Y/\cos\theta_W$, $\epsilon_Z = \epsilon_Y/\sin\theta_W$, and θ_W is the weak mixing angle. After diagonalization, the coupling of the dark
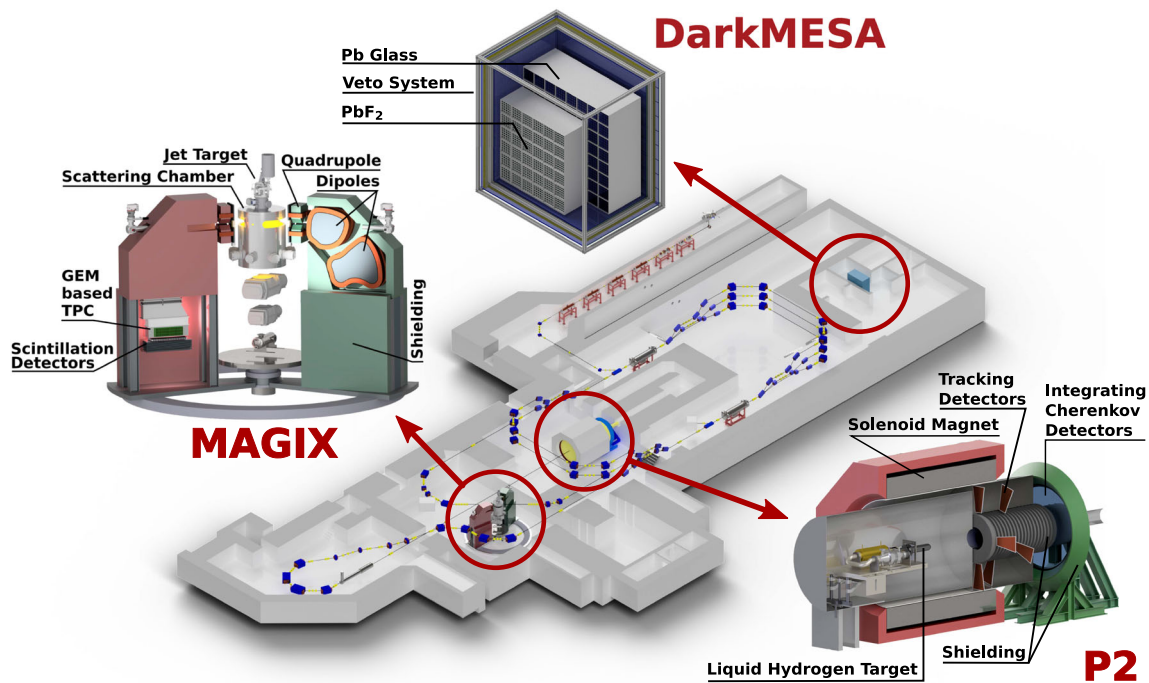
Fig. 44 The MESA accelerator with the three experiments: DarkMESA, MAGIX, and P2

photon with DM and the SM photon is

$$g_D A'_\mu J^\mu_\chi + g_Y B_\mu J^\mu_Y \rightarrow A'_\mu (g_D J^\mu_\chi + \epsilon e J^\mu_{EM}), \qquad (49)$$

where J^μ_{EM} is the SM electromagnetic current. The form of the DM current J^μ_χ depends on the exact nature of the DM particle. The coupling of the dark photon to SM particles happens via the coupling constant ϵe, while the dark fine structure constant $\alpha_D = \sqrt{4\pi g_D}$ describes the coupling with DM.

It is useful to define the dimensionless combination of the model parameters

$$y = \epsilon^2 \alpha_D \left(\frac{m_\chi}{m_{A'}} \right)^4, \qquad (50)$$

which is proportional to the thermally averaged DM annihilation rate.

4.4.3 The MESA accelerator

The Institute for Nuclear Physics at the Mainz University is building a new multi-turn, 100% duty-cycle, energy recovery linac for precision experiments with a beam energy of 100–200 MeV [24]. MESA (Mainz Energy-Recovering Superconducting Accelerator) will operate in two modes: energy recovery mode (ERM) and external beam mode (XBM).

In ERM, the accelerator will provide a beam current of up to 1 mA at 105 MeV for the MAGIX internal target experi-

ment with multi-turn energy recovery capability. In XBM, a polarized beam of 150 μA will be provided to the P2 experiment [196]. An additional experiment, DarkMESA, will be placed after the P2 beam dump, running in parallel to P2 and searching for LDM particles.

The MESA accelerator will consist of a polarized source followed by a low energy beam transport system containing a spin manipulation system and a chopper-buncher section. Normal conducting cavities will accelerate the beam up to 5 MeV before injection into the main linac equipped with a total of four ELBE-like 9-cell superconducting cavities [197] installed in two cryomodules. The linac will provide an energy gain of 50 MeV/pass.

4.4.4 The MAGIX experiment

The MAinz Gas Injection Target EXperiment (MAGIX) is a flexible experiment exploiting the unique combination of a supersonic gas-jet target and the MESA continuous beam in energy recovery mode. The experiment is based on two magnetic spectrometers ("STAR" and "PORT") which can be operated in coincidence with momentum resolution $\delta p / p \sim 10^{-4}$ and low-material budget focal plane detectors (Fig. 44). MAGIX will allow precision measurements in a variety of fields ranging from hadron physics to nuclear astrophysics and dark sector searches. The dark photon can be produced through a mechanism similar to bremsstrahlung on a heavy nuclear target Z via the reaction $e^- Z \rightarrow e^- Z \gamma'$. If the dark photon decays into SM particles, e.g. $\gamma' \rightarrow e^+ e^-$,
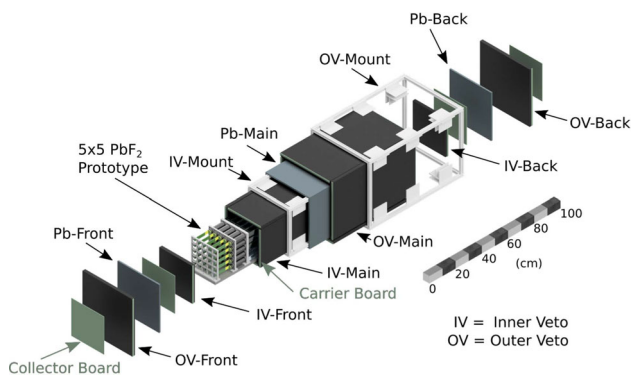
Fig. 45 Exploded view of the DarkMESA prototype detector

the electron/positron final state can be detected in coincidence in the two spectrometers and a peak-search on the QED background can be performed [198,199]. A similar strategy can be employed for the search for the X17 particle.

If the dark photon decays invisibly (e.g. into light dark matter particles $\gamma' \rightarrow \chi\bar{\chi}$), this will require the measurement of the recoil target nucleus for fully reconstructing the kinematics. A peak-search on the reconstructed missing mass $m_{\gamma'}^2 = (p_{beam} - p_Z - p_{e'})^2$ will be performed in this case with the addition of a silicon detector for detecting the recoil proton or nucleus.
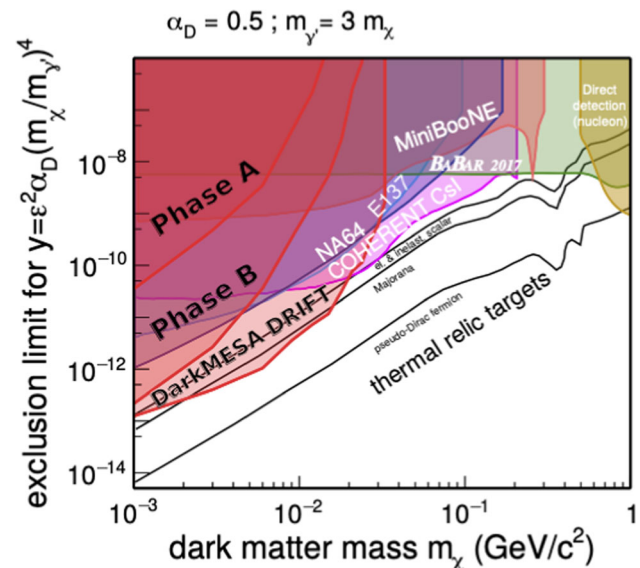
4.4.5 The DarkMESA experiment

DarkMESA (Fig. 45) is a beam-dump experiment, where the dark photon can be produced radiatively by the MESA electron beam on the P2 beam dump through the bremsstrahlung-like process $eZ \rightarrow eZ\gamma'$ [200]. In a simple DM model, it is assumed that the dark photon decays into pairs of DM particles ($\gamma' \rightarrow \chi\bar{\chi}$). Depending on the model, χ and $\bar{\chi}$ can be a particle/antiparticle couple or two different particles χ_1 and χ_2 (inelastic DM [201]).

After production, DM particles can be detected with a shielded detector downstream of the beam-dump.

The dark photon production yield scales as $Y_{\gamma'} \sim \alpha^3\epsilon^2/m_{A'}^2$ while the DM yield Y_χ in the detector is proportional to ϵ^2, giving a total number of detected DM particles scaling as $Y_{\gamma'} \cdot Y_\chi \sim \epsilon^4$. Although the yield does not have a favourable scaling, a beam dump experiment has unique advantages. The large number of electrons on target (EOT) deliverable in a reasonable amount of time by MESA can compensate for the small yield and reach high sensitivity. Another advantage is provided by the boost at which DM particles are produced, allowing for an improved reach at low masses. Moreover, such experiments can probe at the same time both the dark photon production/decay and DM interaction in the detector. At MESA, a radiation-shielded area is available 23 m downstream of the beam-dump of the
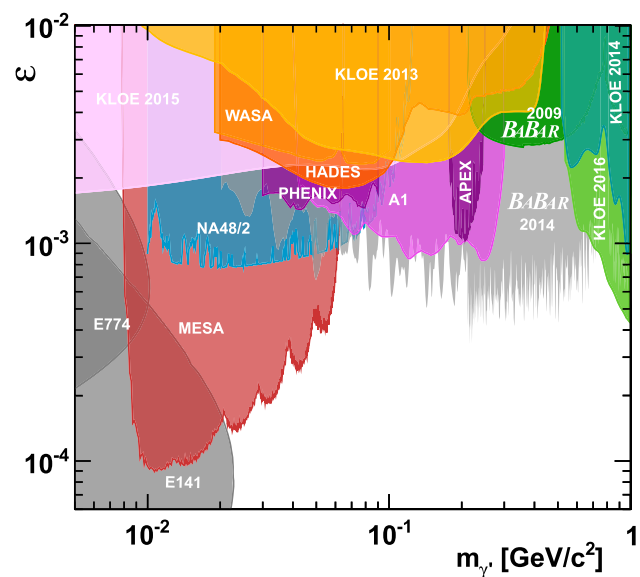
Fig. 46 MAGIX projected exclusion limits for ϵ as function of the dark photon mass for the $\gamma' \rightarrow e^+e^-$ decay

Fig. 47 DarkMESA projected exclusion limits for the y parameter as a function of the DM particle mass for the invisible dark photon decay $\gamma' \rightarrow \chi\bar{\chi}$ compared to existing limits [202–206]

P2 experiment, allowing for the installation of a detector for LDM searches (see Fig. 44).

4.4.6 Current plans

MAGIX The experiment is currently in an advanced design phase. The design of the magnets is complete and parts are being ordered.

The conceptual design of a GEM-based low-material budget time projection chamber has been finalized. The exper-

imental hall is almost completed. Significant progress has been achieved for the simulation and analysis software development, with a focus on the simulation of the dark photon production and astrophysical reactions. A key part of the experiment, the jet target, has been already built and tested at the A1 Collaboration experimental setup [207]. A preliminary simulation of the exclusion limits for visible dark photon decays achievable with MAGIX are shown in Fig. 46. MAGIX will be able to explore new territories in the dark sector parameter space and exploit its reach for searching also for the X17 particle.

DarkMESA The beam dump experiment is currently actively developed [208–211]. The current plan for the construction of the experiment is divided into two phases. Phase-A consists in the construction of a prototype calorimeter module comprised by a matrix of 5×5 PbF$_2$ Cherenkov crystals for a total volume of ~ 4 dm^3 surrounded by a hermetic cosmic ray veto system built with two plastic scintillator layers and one lead layer (Fig. 45). The design follows successful tests by the BDX Collaboration, which is proposing a similar experiment at Jefferson Lab [212].

In particular, a dedicated electronics has been developed for the readout of silicon photomultipliers optically coupled to the veto plastic scintillator planes. In Phase-B, the full volume available in the experimental hall will be exploited with the construction of a PbF$_2$, 0.12 m^2 calorimeter and a lead-glass, 0.58 m^3 calorimeter. The advantage of Cherenkov crystals is their speed and relatively low sensitivity to background neutrons. Exploiting the 2.2×10^{22} (6600 hours) electrons on target delivered to the P2 experiment at 150 µA of beam current, a total charge of ~ 5400 C will be deposited in the beam-dump and will be available for DarkMESA.

Besides the calorimeters, it is under study also the opportunity to add a negative-ion time projection chamber to the experimental setup. In particular, the chamber will leverage on the technology of the DRIFT experiment optimized for dark matter searches with 20keV nuclear recoil detection threshold [213].

In Fig. 47, simulated 90% exclusion limits for the two experimental phases and for the DRIFT detector technology are showed.

4.4.7 Conclusions

The MESA accelerator will deliver high-current beams for experiments in low-energy precision particle and nuclear physics experiments. The new facility will be exploited also for the search for light dark matter and other particles like axions and the X17. In particular, the MAGIX and Dark-MESA experiments will be well suited for these tasks, allowing the exploration of new territories in the theory parameter space and contributing to the solution of the X17 puzzle.

4.5 A direct detection search for hidden sector new particles in the 3–60 MeV mass range

A. Gasparian

North Carolina A&T State University, Greensboro, NC 27411

Abstract In our quest for investigating the nature of dark matter from the way its constituents interact with ordinary matter, we propose an experiment using a PbWO$_4$ calorimeter to search for or set new limits on the production rate of (i) hidden sector dark matter mediator in the 3–60 MeV mass range via their e^+e^- decay (or $\gamma\gamma$ decay with limited tracking), and (ii) the hypothetical X17 particle, claimed in two recent experiments. The search for these particles is motivated by new dark matter models and candidates introduced to account for the small-scale structure in astrophysical observations and anomalies such as the 4.2σ disagreement between experiments and the standard model prediction for the muon anomalous magnetic moment, and the excess of e^+e^- pairs from the ^{8}Be M1 nuclear transition to its ground state observed by the ATOMKI group. In these models the 1–100 MeV mass range is particularly well-motivated and the lower part of this range still remains unexplored. The proposed direct detection experiment will use a magnetic-spectrometer-free setup (the PRad apparatus) to detect all three final state particles in the visible decay of the dark matter mediator allowing for an effective control of the background and will cover the mass range in a single setting. The use of the well-demonstrated PRad setup allows for an essentially ready-to-run and uniquely cost-effective search for dark matter mediator in the 3–60 MeV mass range with a sensitivity of 7.2×10^{-8}–5.9×10^{-9} to ϵ^2 the square of kinetic mixing interaction coupling constant.

4.5.1 Introduction

The remarkable fact that $\sim 85\%$ of the matter in the Universe is of unknown origin – dark matter (DM) – is inferred from astronomical measurements over a wide range of distance scales, from the solar neighborhood to the largest cosmological scales. There are many candidate theories for dark matter and dark mediators that span a very large mass range, from 10^{-22} eV up to 100 solar masses. Several recent observations and anomalies have brought forth new dark matter models and candidates such as the hidden sector dark matter (HSDM) [214] models that point to the $1-100$ MeV/c^2 region as one that is of high priority to search [215]. We have proposed a search of the $3-60$ MeV/c^2 using the magnetic-spectrometer-free PRad setup in Hall B. This setup provides an essentially ready-to-run and uniquely cost effective method for a search experiment.
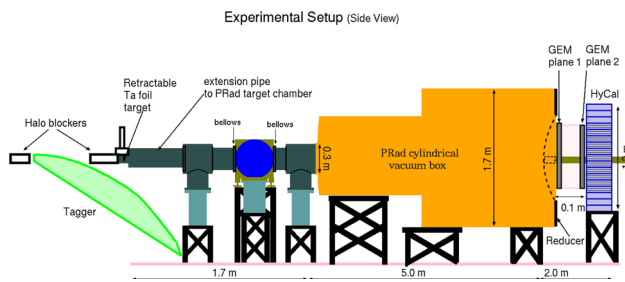
Fig. 48 Schematic of the experimental setup
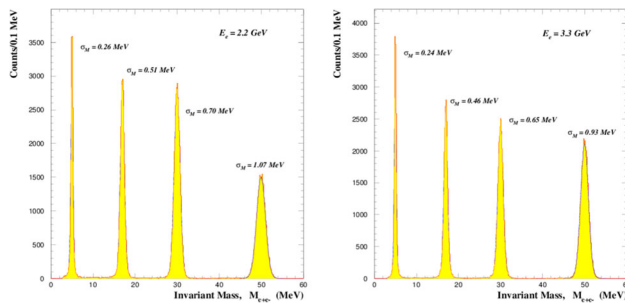
Fig. 49 The e^+e^- invariant mass resolution at 2.2 GeV (left) and 3.3 GeV (right)

4.5.2 Experimental setup

The proposed experiment plans to reuse the PRad [216,217] setup (shown in Fig. 48) but with a Tantalum foil target placed 7.5 m upstream of the calorimeter. Only the high resolution PbWO$_4$ crystal part of the electromagnetic calorimeter will be used together with a new fADC based readout system for the calorimeter. The scattered electrons will travel through the 5 m long vacuum chamber, which matches the geometrical acceptance of the calorimeter, with a thin window to minimize multiple scattering and backgrounds. An extension piece will be added to the upstream end to couple the PRad target chamber to the super-harp which will now hold the target foil. A reducer ring will be attached to the downstream exit of the PRad vacuum chamber and a new 1 mm thick Al exit window will be used such that it matches the PbWO$_4$ portion of the calorimeter. Two layers of GEM detectors will add a modest tracking capability to help reduce the photon background and to reduce the background originating from the vacuum chamber exit window.

4.5.3 Monte Carlo simulations of the background

A comprehensive simulation of the experiment was carried out using the Geant simulation package developed for the PRad experiment. This simulation takes into account realistic geometry of the experimental setup, and detector resolutions. The generated scattering events were propagated
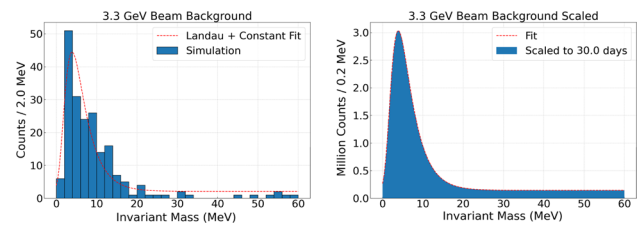
Fig. 50 (Left) The simulated background for 3.5 s of 100 nA beam at 3.3 GeV (corresponding to 2.2×10^{12} electrons on target) and a fit to a sum of Landau + constant distribution. (right) The background counts are scaled to the beam time according to the fit, the number of events are sampled bin-by-bin

within the Geant simulation package, which included the detector geometry and materials of the PRad setup.

The *ep* elastic and $e - e$ Møller generators developed for the PRad experiments were used to verify that these background processes are kinematically suppressed. We have also simulated the Bethe–Heitler and the radiative background processes. The Bethe–Heitler background process is kinematically suppressed and the radiative process is the irreducible background. The background was simulated for about 3.5 s of 3.3 GeV electron beam with a current of 100 nA (corresponding to 2.2×10^{12} electrons on target). The reconstructed invariant mass $M_{e^+e^-}$ spectrum for these simulated events are shown in Fig. 49. A fit of this simulation was used to scale the background by sampling the number of events bin-by-bin to give the expected background for 30 days of 3.3 GeV beam at 100 nA, as shown in Fig. 50. The shape of the background can be validated by comparing it to the background using similar event selection of PRad data.

4.5.4 Conclusions

We have proposed a direct detection search for hidden sector particles in the $3-60$ MeV mass range with a sensitivity of 7.2×10^{-8}–5.9×10^{-9} to the kinetic mixing interaction coupling constant ϵ^2 using the magnetic-spectrometer-free PRad setup in Hall-B. This experiment will exploit the well-demonstrated PRad setup to perform a ready-to-run and cost-effective search. This search experiments is timely as well as urgent given the recent confirmation of the muon $(g-2)$ anomaly [218,219] and the 17-MeV particle proposed to account for the excess e^+e^- pairs found in a nuclear transition in ^{8}Be from one of its 1^+ resonance to its ground state [1], and the electromagnetically forbidden M0 transition in ^{4}He [6]. In particular, the $3-60$ MeV mass range remains relatively unexplored (Fig. 51).

4.6 Searching X17 with positrons at PADME

V. Kozhuharov[a,b]
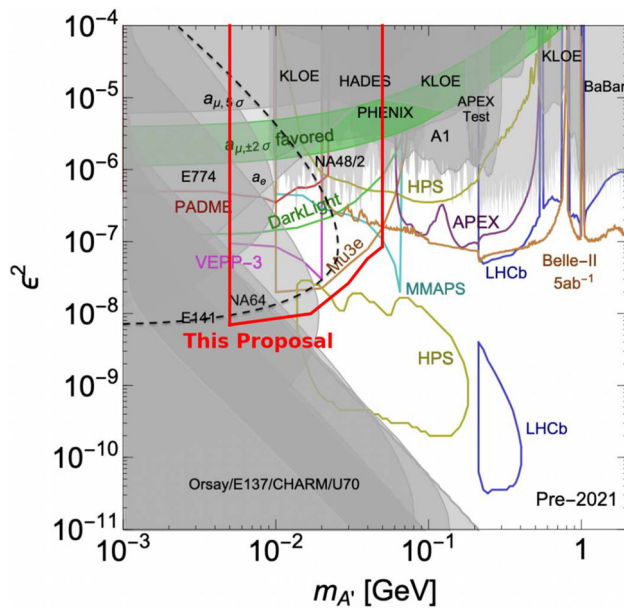
Fig. 51 Projected coverage of the square of the coupling constant (ϵ^2) and mass (m_X) parameter space by this proposed experiment is shown as the thick red lines for the combined statistics of the two beam energies. The projections are superimposed on top of the constraints plot which was adapted from Ref. [214]

^{a} Faculty of Physics, Sofia University, 5 J. Bourchier Blvd., 1164 Sofia, Bulgaria

^{b} LNF-INFN, Via Enrico Fermi 54, 00044 Frascati (RM), Italy

4.6.1 Positron-on-target technique

The ability to exclusively reconstruct the reaction is highly beneficial when searching for unknown new physics states. This is particularly true for the X17 quest where the particle mass is limited to a narrow region and additional information exists for the strength of the interaction.

The positron-on-target technique employs positrons from a beam with a well-defined energy E_{beam} annihilating with the atomic electrons inside a thin target. The process under consideration is $e^+ + e^- \rightarrow X + Y$, where X is the unknown new state and Y denotes all accompanying Standard model particles, including also none as a possibility. Two possible scenarios are viable for X:

– X does not decay to SM particles within the experimental setup. X it is either invisible or long lived. In the simplest case when Y is a single photon the missing mass, M_X, can be determined as

$$M_{miss}^2 = (\bar{P}_{e^+} + \bar{P}_{e^-} - \bar{P}_\gamma)^2, \qquad (51)$$
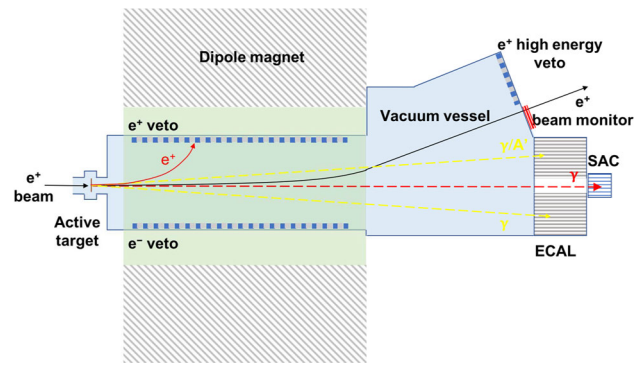
Fig. 52 A layout of the PADME detector system

where $\bar{P}_{e^+}$ and $\bar{P}_{e^-} = (m_e, \vec{0})$ are the beam positron and the target electron 4-momenta. The 4-momentum of the recoil photon should be reconstructed by measuring its energy and impact position in an electromagnetic calorimeter.

– X decays into lepton or photon pairs. In this scenario the process can be fully reconstructed, even if Y is none, as long as the decay products of X are measured. In the case of a lepton pair the natural detector choice is a magnetic spectrometer, while an electromagnetic calorimeter is required for the photon pairs. If Y represents an additional SM particles, the kinematics can be overconstrained to highly reduce the background contribution.

Several experiments, VEPP3, PADME, MMAPS, etc., aimed at positron-on-target technique with beam energy ranging from O(100 MeV) to O(1 GeV). At present only PADME was approved and constructed.

4.6.2 The PADME experiment at LNF-INFN

The PADME experiment at LNF-INFN [180] (schematically shown in Fig. 52) was constructed to search for the associate production of new light particles in the process $e^+ + e^- \rightarrow \gamma + A'$, with A' usually considered to be a dark photon.

The positron beam, obtained from the DAΦNE Linac (either primary or secondary), has an energy up to 550 MeV [220]. The Linac provided 50 bunches per second, one of which is used for monitoring while rest were directed towards the experimental setup. To increase duty cycle, the LINAC bunch length was extended for the PADME data taking, and varied from 100 ns up to about 320 ns. The maximum number of positrons, delivered to the PADME setup, is limited by the detector pile-up to about 100 e^+ per 1 ns. The beam is transported in vacuum through almost the whole setup using a large two-section vacuum chamber. The upstream section of the chamber is placed inside a dipole magnet able to provide 0.6 T magnetic field in a large volume. The downstream

section geometry follows the deflected beam and covers the acceptance of the PADME detectors.

Beam positrons traverse a 100 μm thick active diamond target with transverse dimensions of 20×20 mm^2 [221]. Horizontal and vertical 1 mm wide graphite strips are used to extract the ionization signal from the traversing beam and to determine the bunch position and multiplicity.

The final state photons are detected by the PADME calorimetric system. It consists of a ring-shaped crystal calorimeter, composed by 616 assemblies of BGO inorganic crystal and an HZC XP1911 photomultipliers, the so-called ECal [222]. The central hole of the ECal is covered by a Cherenkov calorimeter, the SAC, based on PbF$_2$ and Hamamatsu R13478UV photomultipliers [223]. SAC is able to withstand the high photon rate due to bremsstrahlung in the target while the ECal provides better energy resolution for photons in the range 50 MeV $< E_\gamma <$ 450 MeV. Three modules of segmented plastic scintillator detectors (PVeto, EVeto, HEPVeto) equipped with silicon photomultipliers and custom designed front-end electronics are located inside the vacuum chamber of the experiment [224]. They detect the positrons (electrons) with momentum in the approximate range 50 MeV $< E_{e^+} <$ 450 MeV for the PVeto (EVeto) and 450 MeV $< E_{e^+} <$ 500 MeV for the HEPVeto. Both the EVeto and PVeto are placed inside the magnetic field while the HEPVeto is close to the beam exit window.

4.6.3 Data taking periods and data analysis

PADME took data with its nominal setup in the autumn/winter 2018/19 (RUN I), two test runs in summer 2019 and 2020, and ∼ 90 days physics run in the autumn, 2020 (RUN II). Data from several different dedicated test runs were also recorded for special purposes. The preliminary data analysis showed that the amount of beam induced background is largely reduced by using the primary positron target of the Linac.

In all data taking scenarios the search for X17 follows the main design goal of PADME – bump searches in the missing mass spectrum. The X17 is produced in association with a photon, which is measured by the PADME calorimetric system. The expected sensitivity is thus consistent entirely with the nominal dark photon limit on the interaction strength and is of the order of 10^{-6} in ϵ^2.

In addition, the EVeto and the PVeto could detect the decay products of X17, which will further reduce the background. Despite being hodoscopes, the charged particle detectors provide also momentum measurement due to their placement inside the magnetic field. However the precision is of the order of O(5%) and the absence of the track angles measurement doesn't allow invariant mass reconstruction.

4.6.4 Prospects for X17 searches

Several directions were identified in the efforts to optimize the sensitivity of PADME to the X17.

Short term detector upgrades and running scenarios The PADME collaboration decided to attempt a search for X17 in resonant production mode $e^+ + e^- \to X17$ inside the target, with a subsequent decay of X17 to e^+e^- pair. The resonant mode exhibits much higher production cross-section and can be competitive even with relatively low statistics – O(10^{11}–10^{12}) positrons on target.

In contrary to the usual technique for measurement of the charged particles by employing a magnetic spectrometer, PADME will rely entirely on calorimetric approach to determine the energy of the outgoing electron and positron. The magnetic field will be switched off and the opening angle of the e^+e^- pair will be used to reconstruct the invariant mass of the event, under the assumption of prompt X17 decay.

The dominant backgrounds to $e^+ + e^- \to X17 \to e^+ + e^-$ are the t-channel and t-channel scattering $e^+ + e^- \to \gamma^* \to e^+ + e^-$ and the two photon annihilation $e^+ + e^- \to \gamma\gamma$. Despite the higher cross-section the t-channel scattering contribution can be suppressed due to the requirement that both e^+ and e^- carry significant amount of the initial beam momentum (i.e. the requirement that the event is quasi-symmetric).

The s-channel scattering through virtual photon represents the insuppressible background since it entirely resembles the X17 on-shell production. To cope with the two- (and multi-) photon annihilation PADME has decided to install a new particle identification detector just in front of the electromagnetic calorimeter. The hodoscope will be based on plastic scintillator bars, with scintillation light detected by silicon photomultipliers and the custom SiPM electronics, used for the PVeto and EVeto. The detector will positively identify the charged particle pairs and its efficiency is expected to be higher than 99%.

After the assembly and installation of the tagger hodoscope in front of the electromagnetic calorimeter, PADME will resume data taking during its Run III (in the autumn/winter of 2022), to search for X17 using the resonant mode production. Positrons with energy ∼ 282 MeV will interact in a target (either the nominal PADME diamond target or a different one) to explore the center of mass region in between 16.4 and 17.4 MeV with an unprecedented sensitivity. The resonant mode production however requires an extremely precise determination of beam energy scale and resolution, while profiting from the much lower beam induced background.

Reconstruction optimizations Present PADME reconstruction profits from the largely common readout electronics of the different detectors, based on CAEN V1742 digitizer

board. This will allow the collaboration to exploit digitized signal to adapt the calorimeter reconstruction to the lower cluster energies expected during Run III. In addition, the ECal PMT gain was set to intermediate values which can be increased if necessary. Reconstruction optimizations are faced at the two consequent stages – pulse reconstruction and cluster reconstruction. Currently PADME collaboration studies the possibility to employ deep machine learning techniques to both stages. Preliminary results show that sub nanosecond time resolution and higher than 95% identification efficiency is achievable for pulses with sufficient amplitude.

Setup modifications While for RUN III PADME will use its present beamline and largely unmodified setup, the best sensitivity to X17 can be achieved in a dedicated setup, which allows to acquire high statistic positron interaction sample of data. A possibility would be to operate PADME detector in a continuous mode with positron beam extracted from a storage ring. This will overcome the limit of 49 bunches per second and will allow to operate in a mode of measurement of every single positron interacting in the target. Even with similar statistics, the sensitivity will be much higher due to the background free measurement.

4.6.5 Conclusions

The PADME experiment aims at testing the X17 hypothesis using positron beams in resonant production mode. The experiment is preparing the detector optimization for Run III which will start in autumn of 2022. The aim of PADME Run III is to explore the center of mass region 16.4 MeV $\leq M_{X17} \leq 17.4$ MeV with unprecedented precision to exclude or possibly confirm the existence of the X17 particle. Other possibilities are also studied, however they require modification of the accelerator and beam storage setup at LNF-INFN.

Acknowledgements

5 Conclusions

^{8}Be and more recently ^{4}He anomalies constitute an open question in nuclear and low energy particle physics. Independent confirmation will be very welcome in strengthening the Atomki observation, and possibly confirming the particle-like explanation of the anomalous angular distributions observed so far.

Several experimental efforts are ongoing in different international laboratories in order to reproduce the observation using the same or similar techniques. Future initiatives are proposing alternative approaches based on different production mechanisms.

A wide and diverse theoretical approaches have been proposed in order to, either explain the anomaly as nuclear physics, or as a beyond the Standard Model effect. Vector, scalar, and pseudo-scalar new particle have been postulated to explain the observed data.

On the basis of theoretical models several searches have been carried out by particle physics experiments, in order to find the new postulated particles. However, no new particle observation can be definitively claimed so far.

References

1. A.J. Krasznahorkay, M. Csatlós, L. Csige, Z. Gácsi, J. Gulyás, M. Hunyadi, I. Kuti, B.M. Nyakó, L. Stuhl, J. Timár, T.G. Tornyi, Z. Vajta, T.J. Ketel, A. Krasznahorkay, Phys. Rev. Lett. **116**, 042501 (2016). https://doi.org/10.1103/PhysRevLett.116.042501
2. J. Gulyás, T. Ketel, A. Krasznahorkay, M. Csatlós, L. Csige, Z. Gácsi, M. Hunyadi, A. Krasznahorkay, A. Vitéz, T. Tornyi, Nucl. Instrum. Methods Phys. Res. Sect. A: Accel. Spectrom. Detect. Assoc. Equip. **808**, 21 (2016). https://doi.org/10.1016/j.nima.2015.11.009

3. M.E. Rose, Phys. Rev. **76**, 678 (1949). https://doi.org/10.1103/PhysRev.76.678

4. A.J. Krasznahorkay, M. Csatlós, L. Csige, J. Gulyás, T.J. Ketel, A. Krasznahorkay, I. Kuti, Á. Nagy, B.M. Nyakó, N. Sas, J. Timár, EPJ Web Conf. **142**, 01019 (2017). https://doi.org/10.1051/epjconf/201714201019

5. A. Krasznahorkay, M. Csatlós, L. Csige, J. Gulyás, M. Hunyadi, T. Ketel, A. Krasznahorkay, I. Kuti, B.N. Á. Nagy, N. Sas, J. Timár, I. Vajda, New results on the Be-8 anomaly, in *Proceedings, 55th International Winter Meeting on Nuclear Physics, January 23–27, 2017* (2017)

6. A.J. Krasznahorkay, M. Csatlos, L. Csige, J. Gulyas, M. Koszta, B. Szihalmi, J. Timar, D.S. Firak, A. Nagy, N.J. Sas, A. Krasznahorkay, New evidence supporting the existence of the hypothetic x17 particle (2019). arXiv:1910.10459

7. A. Aleksejevs, S. Barkanova, Y.G. Kolomensky, B. Sheff, A standard model explanation for the ätomki anomalÿ (2021). arXiv:2102.01127

8. J.L. Feng, B. Fornal, I. Galon, S. Gardner, J. Smolinsky, T.M.P. Tait, P. Tanedo, Phys. Rev. Lett. **117**, 071803 (2016). https://doi.org/10.1103/PhysRevLett.117.071803

9. A.M. Baldini, E. Baracchini, C. Bemporad, F. Berg, M. Biasotti, G. Boca, P.W. Cattaneo, G. Cavoto, F. Cei, M. Chiappini, G. Chiarello, C. Chiri, G. Cocciolo, A. Corvaglia, A. de Bari, M. De Gerone, A. D'Onofrio, M. Francesconi, Y. Fujii, L. Galli, F. Gatti, F. Grancagnolo, M. Grassi, D.N. Grigoriev, M. Hildebrandt, Z. Hodge, K. Ieki, F. Ignatov, R. Iwai, T. Iwamoto, D. Kaneko, K. Kasami, P.R. Kettle, B.I. Khazin, N. Khomutov, A. Korenchenko, N. Kravchuk, T. Libeiro, M. Maki, N. Matsuzawa, S. Mihara, M. Milgie, W. Molzon, T. Mori, F. Morsani, A. Mtchedilishvili, M. Nakao, S. Nakaura, D. Nicolò, H. Nishiguchi, M. Nishimura, S. Ogawa, W. Ootani, M. Panareo, A. Papa, A. Pepino, G. Piredda, A. Popov, F. Raffaelli, F. Renga, E. Ripiccini, S. Ritt, M. Rossella, G. Rutar, R. Sawada, G. Signorelli, M. Simonetta, G.F. Tassielli, Y. Uchiyama, M. Usami, M. Venturini, C. Voena, K. Yoshida, Y.V. Yudin, Y. Zhang, Eur. Phys. J. C **78**(5), 380 (2018). https://doi.org/10.1140/epjc/s10052-018-5845-6

10. Institute of Experimental and Applied Physics, Czech Technical University in Prague. http://www.utef.cvut.cz/ieap

11. INFN National Laboratory of Legnaro. https://www.lnl.infn.it/en/

12. M. Sabaté-Gilarte, M. Barbagallo, N. Colonna, F. Gunsing, P. Žugec, V. Vlachoudis, Y.H. Chen, A. Stamatopoulos, J. Lerendegui-Marco, M.A. Cortés-Giraldo, A. Villacorta, C. Guerrero, L. Damone, L. Audouin, E. Berthoumieux, L. Cosentino, M. Diakaki, P. Finocchiaro, A. Musumarra, T. Papaevangelou, M. Piscopo, L. Tassan-Got, O. Aberle, J. Andrzejewski, V. Bécares, M. Bacak, R. Baccomi, J. Balibrea, S. Barros, F. Bečvář, C. Beinrucker, F. Belloni, J. Billowes, D. Bosnar, M. Brugger, M. Caamaño, F. Calviño, M. Calviani, D. Cano-Ott, R. Cardella, A. Casanovas, D.M. Castelluccio, F. Cerutti, E. Chiaveri, G. Cortés, K. Deo, C. Domingo-Pardo, R. Dressler, E. Dupont, I. Durán, B. Fernández-Domínguez, A. Ferrari, P. Ferreira, R.J.W. Frost, V. Furman, K. Göbel, A.R. García, A. Gawlik, I. Gheorghe, T. Glodariu, I.F. Gonçalves, E. González, A. Goverdovski, E. Griesmayer, H. Harada, T. Heftrich, S. Heinitz, A. Hernández-Prieto, J. Heyse, D.G. Jenkins, E. Jericha, F. Käppeler, Y. Kadi, T. Katabuchi, P. Kavrigin, V. Ketlerov, V. Khryachkov, A. Kimura, N. Kivel, M. Kokkoris, M. Krtička, E. Leal-Cidoncha, C. Lederer, H. Leeb, M. Licata, S. Lo Meo, S.J. Lonsdale, R. Losito, D. Macina, J. Marganiec, T. Martínez, C. Massimi, P. Mastinu, P. Mastromarco, F. Matteucci, E.A. Maugeri, E. Mendoza, A. Mengoni, P.M. Milazzo, F. Mingrone, M. Mirea, S. Montesano, R. Nolte, A. Oprea, F.R. Palomo-Pinto, C. Paradela, N. Patronis, A. Pavlik, J. Perkowski, J.I. Porras, J. Praena, J.M. Quesada, K. Rajeev, T. Rauscher, R. Reifarth, A. Riego-Perez, M.S. Robles, P.C. Rout, C. Rubbia, J.A. Ryan, A. Saxena, P. Schillebeeckx, S. Schmidt, D. Schumann, P. Sedyshev, A.G. Smith, S.V. Suryanarayana, G. Tagliente, J.L. Tain, A. Tarifeño-Saldivia, A. Tsinganis, S. Valenta, G. Vannini, V. Variale, P. Vaz, A. Ventura, R. Vlastou, A. Wallner, S. Warren, M. Weigand, C. Wolf, P.J. Woods, C. Weiss, T. Wright, Eur. Phys. J. A **53**(10), 210 (2017). https://doi.org/10.1140/epja/i2017-12392-4

13. Laboratory for Underground Nuclear Astrophysics. https://luna.lngs.infn.it/

14. G. Azuelos et al. (2022). https://doi.org/10.48550/arXiv.2211.11900

15. D. Banerjee et al., Phys. Rev. D **101**(7), 071101 (2020). https://doi.org/10.1103/PhysRevD.101.071101

16. V. Fanti et al., Nucl. Instrum. Methods Phys. Res. Sect. A: Accel. Spectrom. Detect. Assoc. Equip. **574**(3), 433 (2007). https://doi.org/10.1016/j.nima.2007.01.178

17. M. Raggi, Nuovo Cim. C **38**(4), 132 (2016). https://doi.org/10.48550/arXiv.1508.01307

18. A.P. Caricato, M. Martino, I. Oceano, F. Oliva, S. Spagnolo, G. Chiodini, F. Bossi, B. Buonomo, R.D. Sangro, C.D. Giulio, D. Domenici, G. Finocchiaro, L.G. Foggetta, M. Garattini, A. Ghigo, F. Giacchino, P. Gianotti, I. Sarra, B. Sciascia, T. Spadaro, E. Spiriti, C. Taruggi, E. Vilucchi, F. Ferrarotto, E. Leonardi, F.S. Tehrani, P. Valente, S. Fiore, G. Georgiev, S. Ivanov, R. Simeonov, V. Kozhuharov, B. Liberti, E. Long, G.C. Organtini, G. Piperno, M. Raggi, M. Martini, V. Capirossi, F. Iazzi, F. Pinna, J. Alexander, A. Frankenthal, Phys. Scr. **97**(2), 024003 (2022). https://doi.org/10.1088/1402-4896/ac41eb

19. B. Echenard, R. Essig, Y.M. Zhong, JHEP **01**, 113 (2015). https://doi.org/10.1007/JHEP01(2015)113

20. FASER Collaboration, A. Ariga, T. Ariga, J. Boyd, F. Cadoux, D.W. Casper, F. Cerutti, S. Danzeca, L. Dougherty, Y. Favre, J.L. Feng, D. Ferrere, J. Gall, I. Galon, S. Gonzalez-Sevilla, S.C. Hsu, G. Iacobucci, E. Kajomovitz, F. Kling, S. Kuehn, M. Lamont, L. Levinson, H. Otono, J. Osborne, B. Petersen, O. Sato, M. Sabate-Gilarte, M. Schott, A. Sfyrla, J. Smolinsky, A.M. Soffa, Y. Takubo, P. Thonet, E. Torrence, S. Trojanowski, G. Zhang. Technical proposal for FASER: forward search experiment at the LHC (2018). arXiv:1812.09139

21. R. Corliss et al., Nucl. Instrum. Methods Phys. Res. Sect. A: Accel. Spectrom. Detect. Assoc. Equip. **865**, 125 (2017). https://doi.org/10.1016/j.nima.2016.07.053

22. O. Moreno (2013) The heavy photon search experiment at Jefferson Lab. https://doi.org/10.48550/arXiv.1310.2060

23. B. Wojtsekhowski et al., J. Instrum. **13**(02), P02021 (2018). https://doi.org/10.48550/arXiv.1708.07901

24. F. Hug, K. Aulenbacher, R. Heine, B. Ledroit, D. Simon, in *LINAC2016, Conference Proceedings MOP106012* (JACoW, 2017), pp. 313–315. https://doi.org/10.18429/JACoW-LINAC2016-MOP106012

25. G.L. Castro, N. Quintero (2021) Tests of the Atomki anomaly in lepton pair decays of heavy mesons. https://doi.org/10.48550/arXiv.2101.01865

26. K. Ban et al. (2020) Search for new light vector boson using J/Ψ at BESIII and Belle II. https://doi.org/10.48550/arXiv.2012.04190

27. X. Zhang, G.A. Miller, Phys. Lett. B **773**, 159 (2017). https://doi.org/10.1016/j.physletb.2017.08.013

28. B. Koch, Nucl. Phys. A **1008**, 122143 (2021). https://doi.org/10.1016/j.nuclphysa.2021.122143

29. H.X. Chen, Is the $X17$ composed of four bare quarks? (2020). arXiv:2006.01018 [hep-ph]

30. V. Kubarovsky, J.R. West, S.J. Brodsky, Quantum chromodynamics resolution of the ATOMKI anomaly in ^{4}He nuclear transitions (2022). arXiv:2206.14441 [hep-ph]

31. C.Y. Wong, QED meson description of the X17 and other anomalous particles, in *Shedding Light on X17* (2022). arXiv:2201.09764 [hep-ph]

32. D.S.M. Alves, N. Weiner, JHEP **07**, 092 (2018). https://doi.org/10.1007/JHEP07(2018)092

33. D.S.M. Alves, Phys. Rev. D **103**(5), 055018 (2021). https://doi.org/10.1103/PhysRevD.103.055018

34. T. Nomura, P. Sanyal, JHEP **05**, 232 (2021). https://doi.org/10.1007/JHEP05(2021)232

35. P Tie Du, N Ai. Viet, N. Van Dat, J. Phys. Conf. Ser. **1506**(1), 012004 (2020). https://doi.org/10.1088/1742-6596/1506/1/012004

36. Y. Liang, L.B. Chen, C.F. Qiao, Chin. Phys. C **41**(6), 063105 (2017). https://doi.org/10.1088/1674-1137/41/6/063105

37. J.L. Feng, B. Fornal, I. Galon, S. Gardner, J. Smolinsky, T.M.P. Tait, P. Tanedo, Phys. Rev. Lett. **117**(7), 071803 (2016). https://doi.org/10.1103/PhysRevLett.117.071803

38. J.L. Feng, B. Fornal, I. Galon, S. Gardner, J. Smolinsky, T.M.P. Tait, P. Tanedo, Phys. Rev. D **95**(3), 035017 (2017). https://doi.org/10.1103/PhysRevD.95.035017

39. J.L. Feng, T.M.P. Tait, C.B. Verhaaren, Phys. Rev. D **102**(3), 036016 (2020). https://doi.org/10.1103/PhysRevD.102.036016

40. X. Zhang, G.A. Miller, Phys. Lett. B **813**, 136061 (2021). https://doi.org/10.1016/j.physletb.2021.136061

41. J. Kozaczuk, D.E. Morrissey, S.R. Stroberg, Phys. Rev. D **95**(11), 115024 (2017). https://doi.org/10.1103/PhysRevD.95.115024

42. U. Ellwanger, S. Moretti, JHEP **11**, 039 (2016). https://doi.org/10.1007/JHEP11(2016)039

43. D. Barducci, C. Toni, An updated view on the ATOMKI nuclear anomalies (2022). arXiv:2212.06453 [hep-ph]

44. L. Delle Rose, S. Khalil, S.J.D. King, S. Moretti, A.M. Thabt, Phys. Rev. D **99**(5), 055022 (2019). https://doi.org/10.1103/PhysRevD.99.055022

45. S. Weinberg, Phys. Rev. Lett. **40**, 223 (1978). https://doi.org/10.1103/PhysRevLett.40.223

46. F. Wilczek, Phys. Rev. Lett. **40**, 279 (1978). https://doi.org/10.1103/PhysRevLett.40.279

47. R.D. Peccei, H.R. Quinn, Phys. Rev. Lett. **38**, 1440 (1977). https://doi.org/10.1103/PhysRevLett.38.1440

48. R.D. Peccei, H.R. Quinn, Phys. Rev. D **16**, 1791 (1977). https://doi.org/10.1103/PhysRevD.16.1791

49. T.W. Donnelly, S.J. Freedman, R.S. Lytel, R.D. Peccei, M. Schwartz, Phys. Rev. D **18**, 1607 (1978). https://doi.org/10.1103/PhysRevD.18.1607

50. F.W.N. de Boer, R. van Dantzig, Phys. Rev. Lett. **62**, 2639 (1989). https://doi.org/10.1103/PhysRevLett.62.2639

51. F.W.N. de Boer, K. Bethge, H. Bokemeyer, R. van Dantzig, J. van Klinken, V. Mironov, K.A. Müller, K.E. Stiebing, J. Phys. G: Nucl. Part. Phys. **27**(4), L29 (2001). https://doi.org/10.1088/0954-3899/27/4/102

52. K.E. Stiebing, F.W.N. de Boer, O. Fröhlich, H. Bokemeyer, K.A. Müller, K. Bethge, J. van Klinken, J. Phys. G: Nucl. Part. Phys. **30**(2), 165 (2004). https://doi.org/10.1088/0954-3899/30/2/014

53. A.J. Krasznahorkay, M. Csatlós, L. Csige, J. Gulyás, A. Krasznahorkay, B.M. Nyakó, I. Rajta, J. Timár, I. Vajda, N.J. Sas, Phys. Rev. C **104**, 044003 (2021). https://doi.org/10.1103/PhysRevC.104.044003

54. N.J. Sas, A.J. Krasznahorkay, M. Csatlós, J. Gulyás, B. Kertész, A. Krasznahorkay, J. Molnár, I. Rajta, J. Timár, I. Vajda, M.N. Harakeh, Observation of the x17 anomaly in the ^{7}li(p,e^+e^-)^{8}be direct proton-capture reaction (2022). arXiv:2205.07744

55. W. Verkerke, D. Kirkby, in *Computing in High Energy and Nuclear Physics* (arXiv, 2003). arXiv:physics/0306116

56. A. Datta, J.L. Feng, S. Kamali, J. Kumar, Phys. Rev. D **101**, 035010 (2020). https://doi.org/10.1103/PhysRevD.101.035010

57. J.L. Feng, B. Fornal, I. Galon, S. Gardner, J. Smolinsky, T.M.P. Tait, P. Tanedo, Phys. Rev. D **95**, 035017 (2017). https://doi.org/10.1103/PhysRevD.95.035017

58. U. Ellwanger, S. Moretti, J. High Energy Phys. **2016**, 39 (2016). https://doi.org/10.1007/JHEP11(2016)039

59. D. Alves, N.A. Weiner, J. High Energy Phys. **2018**, 92 (2018). https://doi.org/10.1007/JHEP07(2018)092

60. D.S.M. Alves, Phys. Rev. D **103**, 055018 (2021). https://doi.org/10.1103/PhysRevD.103.055018

61. J. Liu, N. McGinnis, C.E.M. Wagner, X.P. Wang, J. High Energy Phys. **2021**, 138 (2021). https://doi.org/10.1007/JHEP05(2021)138

62. A.J. Krasznahorkay, M. Csatlós, L. Csige, Z. Gácsi, J. Gulyás, Á. Nagy, N. Sas, J. Timár, T.G. Tornyi, I. Vajda, A.J. Krasznahorkay, J. Phys.: Conf. Ser. **1056**, 012028 (2018). https://doi.org/10.1088/1742-6596/1056/1/012028

63. A.J. Krasznahorkay, M. Csatlós, L. Csige, D. Firak, J. Gulyás, Á. Nagy, N. Sas, J. Timár, T.G. Tornyi, Acta Phys. Pol. B **50**, 675 (2019). https://doi.org/10.5506/APhysPolB.50.675

64. A.J. Krasznahorkay, M. Csatlós, L. Csige, J. Gulyás, M. Hunyadi, T.J. Ketel, A. Krasznahorkay, I. Kuti, Á. Nagy, B.M. Nyakó, N. Sas, J. Timár, I. Vajda, EPJ Web Conf. **137**, 08010 (2017). https://doi.org/10.1051/epjconf/201713708010

65. D.S. Firak, A.J. Krasznahorkay, M. Csatlós, L. Csige, J. Gulyás, M. Koszta, B. Szihalmi, J. Timár, Á. Nagy, N.J. Sas, A. Krasznahorkay, EPJ Web Conf. **232**, 04005 (2020). https://doi.org/10.1051/epjconf/202023204005

66. A.J. Krasznahorkay et al., J. Phys.: Conf. Ser. **1**, 012028 (2018)

67. M. Viviani, E. Filandri, L. Girlanda, C. Gustavino, A. Kievsky, L.E. Marcucci, R. Schiavilla, Phys. Rev. C **105**, 014001 (2022). https://doi.org/10.1103/PhysRevC.105.014001

68. X. Zhang, G.A. Miller, Phys. Lett. B **813**, 136061 (2021). https://doi.org/10.1016/j.physletb.2021.136061

69. A.C. Hayes, J.L. Friar, G. Hale, G. Garvey, The angular correlations in the e^+e^- decay of excited states in 8be (2021). arXiv:2106.06834

70. A. Baldini et al., Eur. Phys. J. C **76**, 434 (2016). https://doi.org/10.1140/epjc/s10052-016-4271-x

71. J. Adam, X. Bai, A. Baldini, E. Baracchini, C. Bemporad, G. Boca, P. Cattaneo, G. Cavoto, F. Cei, C. Cerri, M. Corbo, N. Curalli, A. de Bari, M. De Gerone, T. Doke, S. Dussoni, J. Egger, K. Fratini, Y. Fujii, L. Galli, G. Gallucci, F. Gatti, B. Golden, M. Grassi, D. Grigoriev, T. Haruyama, M. Hildebrandt, F. Ignatov, T. Iwamoto, P.R. Kettle, B. Khazin, O. Kiselev, A. Korenchenko, N. Kravchuk, A. Maki, S. Mihara, W. Molzon, T. Mori, D. Mzavia, H. Natori, D. Nicolò, H. Nishiguchi, Y. Nishimura, W. Ootani, M. Panareo, A. Papa, R. Pazzi, G. Piredda, A. Popov, F. Renga, S. Ritt, M. Rossella, R. Sawada, F. Sergiampietri, G. Signorelli, F. Tenchini, C. Topchyan, Y. Uchiyama, R. Valle, C. Voena, F. Xiao, A. Yamamoto, Y. Yudin, D. Zanello, Nucl. Instrum. Methods Phys. Res. Sect. A: Accel. Spectrom. Detect. Assoc. Equip. **641**(1), 19 (2011). https://doi.org/10.1016/j.nima.2011.03.048

72. S. Agostinelli, J. Allison, K. Amako, J. Apostolakis, H. Araujo, P. Arce, M. Asai, D. Axen, S. Banerjee, G. Barrand, F. Behner, L. Bellagamba, J. Boudreau, L. Broglia, A. Brunengo, H. Burkhardt, S. Chauvie, J. Chuma, R. Chytracek, G. Cooperman, G. Cosmo, P. Degtyarenko, A. Dell'Acqua, G. Depaola, D. Dietrich, R. Enami, A. Feliciello, C. Ferguson, H. Fesefeldt, G. Folger, F. Foppiano, A. Forti, S. Garelli, S. Giani, R. Giannitrapani, D. Gibin, J. Gómez Cadenas, I. González, G. Gracia Abril, G. Greeniaus, W. Greiner, V. Grichine, A. Grossheim, S. Guatelli, P. Gumplinger, R. Hamatsu, K. Hashimoto, H. Hasui, A. Heikkinen, A. Howard, V. Ivanchenko, A. Johnson, F. Jones, J. Kallenbach, N. Kanaya, M. Kawabata, Y. Kawabata, M. Kawaguti, S. Kelner, P. Kent, A. Kimura, T. Kodama, R. Kokoulin, M. Kossov, H. Kurashige, E. Lamanna, T. Lampén, V. Lara,

V. Lefebure, F. Lei, M. Liendl, W. Lockman, F. Longo, S. Magni, M. Maire, E. Medernach, K. Minamimoto, P. Mora de Freitas, Y. Morita, K. Murakami, M. Nagamatu, R. Nartallo, P. Nieminen, T. Nishimura, K. Ohtsubo, M. Okamura, S. O'Neale, Y. Oohata, K. Paech, J. Perl, A. Pfeiffer, M. Pia, F. Ranjard, A. Rybin, S. Sadilov, E. Di Salvo, G. Santin, T. Sasaki, N. Savvas, Y. Sawada, S. Scherer, S. Sei, V. Sirotenko, D. Smith, N. Starkov, H. Stoecker, J. Sulkimo, M. Takahata, S. Tanaka, E. Tcherniaev, E. Safai Tehrani, M. Tropeano, P. Truscott, H. Uno, L. Urban, P. Urban, M. Verderi, A. Walkden, W. Wander, H. Weber, J. Wellisch, T. Wenaus, D. Williams, D. Wright, T. Yamada, H. Yoshida, D. Zschiesche, Nucl. Instrum. Methods Phys. Res. Sect. A: Accel. Spectrom. Detect. Assoc. Equip. **506**(3), 250 (2003). https://doi.org/10.1016/S0168-9002(03)01368-8

73. N.J. Carron, *An Introduction to the Passage of Energetic Particles through Matter* (Taylor & Francis, Milton Park, 2007)

74. T. Poikela, J. Plosila, T. Westerlund, M. Campbell, M.D. Gaspari, X. Llopart, V. Gromov, R. Kluit, M. van Beuzekom, F. Zappon, V. Zivkovic, C. Brezina, K. Desch, Y. Fu, A. Kruth, J. Instrum. **9**(05), C05013 (2014). https://doi.org/10.1088/1748-0221/9/05/c05013

75. B. Bergmann, M. Pichotka, S. Pospisil, J. Vycpalek, P. Burian, P. Broulim, J. Jakubek, EPJ C **77**(6), 421 (2017). https://doi.org/10.1140/epjc/s10052-017-4993-4

76. M. Filipenko, T. Gleixner, G. Anton, T. Michel, EPJ C **74**(8), 3013 (2014). https://doi.org/10.1140/epjc/s10052-014-3013-1

77. G. Charpak, R. Bouclier, T. Bressani, J. Favier, C. Zupancic, Nucl. Instrum. Methods **62**(3), 262 (1968). https://doi.org/10.1016/0029-554X(68)90371-6

78. D. Nygren, PEP-198-1975 (b) 1976 proposal for a PEP facility based on the TPC. PEP4, December 30

79. F. Sauli, Nucl. Instrum. Methods A **386**(2), 531 (1997). https://doi.org/10.1016/S0168-9002(96)01172-2

80. F. Sauli, Nucl. Instrum. Methods A **805**, 2 (2016). https://doi.org/10.1016/j.nima.2015.07.060. Special Issue in memory of Glenn F. Knoll

81. S. Bachmann, S. Kappler, B. Ketzer, T. Müller, L. Ropelewski, F. Sauli, E. Schulte, Nucl. Instrum. Methods A **478**, 104 (2002)

82. G.G. de Souza, H.N. da Luz, Nucl. Instrum. Methods A **937**, 141 (2019). https://doi.org/10.1016/j.nima.2019.05.058

83. S. Bachmann, A. Bressan, M. Capeáns, M. Deutel, S. Kappler, B. Ketzer, A. Polouektov, L. Ropelewski, F. Sauli, E. Schulte, L. Shekhtman, A. Sokolov, Nucl. Instrum. Methods A **479**(2), 294 (2002). https://doi.org/10.1016/S0168-9002(01)00931-7

84. P. Gasik, A. Mathis, L. Fabbietti, J. Margutti, Nucl. Instrum. Methods A **870**, 116 (2017). https://doi.org/10.1016/j.nima.2017.07.042

85. The ALICE Collaboration, Upgrade of the ALICE time projection chamber. Technical Report. CERN-LHCC-2013-020, ALICE-TDR-016 (2013). https://cds.cern.ch/record/1622286

86. A. Colaleo, A. Safonov, A. Sharma, M. Tytgat, CMS technical design report for the muon endcap GEM upgrade. Technical Report. CERN-LHCC-2015-012, CMS-TDR-013 (2015). https://cds.cern.ch/record/2021453

87. M. Usman, Scalable readout system. Technical Report. CERN-Note-2018-087 (2018). http://cds.cern.ch/record/2636697

88. L. Scharenberg, J. Bortfeldt, F. Brunbauer, K. Desch, F. Garcia, M. Hracek, D. Janssens, M. Lisowska, M. Lupberger, H. Muller, H. Natal da Luz, E. Oliveri, D. Pfeiffer, H. Pulkkinen, L. Ropelewski, J. Samarati, M. van Stenis, A. Utrobicic, R. Veenhof, Nucl. Instrum. Methods A **1011**, 165576 (2021). https://doi.org/10.1016/j.nima.2021.165576

89. F.M. Brunbauer, F. Garcia, T. Korkalainen, A. Lugstein, M. Lupberger, E. Oliveri, D. Pfeiffer, L. Ropelewski, P. Thuiner, M. Schinnerl, IEEE Trans. Nucl. Sci. **65**(3), 913 (2018). https://doi.org/10.1109/TNS.2018.2800775

90. H. Hernández, B.C. de Souza Sanches, D. Carvalho, M. Bregant, A.A. Pabon, R.W. da Silva, R.A. Hernandez, T.O. Weber, A.L. do Couto, A. Campos, H.A. Cubas, T.A. Martins, M.G. Munhoz, W. Van Noije, IEEE Trans. Instrum. Meas. **69**(6), 2686 (2020). https://doi.org/10.1109/TIM.2019.2931016

91. L. Morel, Z. Yao, P. Cladé, S. Guellati-Khélifa, Nature **588**, 61 (2020). https://doi.org/10.1038/s41586-020-2964-7

92. E. Cisbani, N. Colonna, P. Finocchiaro, S. Fiore, G. Gervino, C. Gustavino, C. Massimi, P. Mastinu, A. Mazzone, F. Renga, M. Viviani, X17 boson through neutron-induced reactions: feasibility test at n_TOF EAR2. Technical report. CERN, Geneva (2021). https://cds.cern.ch/record/2766541. Measurement/test of the detection system

93. M. Barbagallo, A. Musumarra, L. Cosentino, E. Maugeri, S. Heinitz, A. Mengoni, R. Dressler, D. Schumann, F. Käppeler, N. Colonna, P. Finocchiaro, M. Ayranov, L. Damone, N. Kivel, O. Aberle, S. Altstadt, J. Andrzejewski, L. Audouin, M. Bacak, J. Balibrea-Correa, S. Barros, V. Bécares, V. Bečvář, C. Beinrucker, E. Berthoumieux, J. Billowes, D. Bosnar, M. Brugger, M. Caamaño, M. Calviani, F. Calviño, D. Cano-Ott, R. Cardella, A. Casanovas, D.M. Castelluccio, F. Cerutti, Y.H. Chen, E. Chiaveri, G. Cortés, M.A. Cortés-Giraldo, S. Cristallo, M. Diakaki, C. Domingo-Pardo, E. Dupont, I. Duran, B. Fernandez-Dominguez, A. Ferrari, P. Ferreira, W. Furman, S. Ganesan, A. García-Rios, A. Gawlik, T. Glodariu, K. Göbel, I.F. Gonçalves, E. González-Romero, E. Griesmayer, C. Guerrero, F. Gunsing, H. Harada, T. Heftrich, J. Heyse, D.G. Jenkins, E. Jericha, T. Katabuchi, P. Kavrigin, A. Kimura, M. Kokkoris, M. Krtička, E. Leal-Cidoncha, J. Lerendegui, C. Lederer, H. Leeb, S. Lo Meo, S.J. Lonsdale, R. Losito, J. Macina, J. Marganiec, T. Martínez, C. Massimi, P. Mastinu, M. Mastromarco, A. Mazzone, E. Mendoza, P.M. Milazzo, F. Mingrone, M. Mirea, S. Montesano, R. Nolte, A. Oprea, A. Pappalardo, N. Patronis, A. Pavlik, J. Perkowski, M. Piscopo, A. Plompen, I. Porras, J. Praena, J. Quesada, K. Rajeev, T. Rauscher, R. Reifarth, A. Riego-Perez, P. Rout, C. Rubbia, J. Ryan, M. Sabate-Gilarte, A. Saxena, P. Schillebeeckx, S. Schmidt, P. Sedyshev, A.G. Smith, A. Stamatopoulos, G. Tagliente, J.L. Tain, A. Tarifeño Saldivia, L. Tassan-Got, A. Tsinganis, S. Valenta, G. Vannini, V. Variale, P. Vaz, A. Ventura, V. Vlachoudis, R. Vlastou, J. Vollaire, A. Wallner, S. Warren, M. Weigand, C. Weiß, C. Wolf, P.J. Woods, T. Wright, P. Žugec, Phys. Rev. Lett. **117**, 152701 (2016). https://doi.org/10.1103/PhysRevLett.117.152701

94. A.J. Krasznahorkay, M. Csatlós, L. Csige, J. Gulyás, A. Krasznahorkay, B.M. Nyakó, I. Rajta, J. Timár, I. Vajda, N.J. Sas, Phys. Rev. C **104**(4), 044003 (2021). https://doi.org/10.1103/PhysRevC.104.044003

95. Available online. https://eljentechnology.com/products/plastic-scintillators/ej-200-ej-204-ej-208-ej-212

96. A. Ferri, F. Acerbi, A. Gola, G. Paternoster, C. Piemonte, N. Zorzi, EJNMMI Phys. **1**(1), 1 (2014). https://doi.org/10.1186/2197-7364-1-S1-A14

97. J. Allison, K. Amako, J. Apostolakis, P. Arce, M. Asai, T. Aso, E. Bagli, A. Bagulya, S. Banerjee, G. Barrand, B. Beck, A. Bogdanov, D. Brandt, J. Brown, H. Burkhardt, P. Canal, D. Cano-Ott, S. Chauvie, K. Cho, G. Cirrone, G. Cooperman, M. Cortés-Giraldo, G. Cosmo, G. Cuttone, G. Depaola, L. Desorgher, X. Dong, A. Dotti, V. Elvira, G. Folger, Z. Francis, A. Galoyan, L. Garnier, M. Gayer, K. Genser, V. Grichine, S. Guatelli, P. Guèye, P. Gumplinger, A. Howard, I. Hřivnáčová, S. Hwang, S. Incerti, A. Ivanchenko, V. Ivanchenko, F. Jones, S. Jun, P. Kaitaniemi, N. Karakatsanis, M. Karamitros, M. Kelsey, A. Kimura, T. Koi, H. Kurashige, A. Lechner, S. Lee, F. Longo, M. Maire, D. Mancusi, A. Mantero, E. Mendoza, B. Morgan, K. Murakami, T. Nikitina, L. Pandola, P. Paprocki, J. Perl, I. Petrović, M. Pia, W. Pokorski, J. Quesada, M. Raine, M. Reis, A. Ribon, A. Ristić

Fira, F. Romano, G. Russo, G. Santin, T. Sasaki, D. Sawkey, J. Shin, I. Strakovsky, A. Taborda, S. Tanaka, B. Tomé, T. Toshito, H. Tran, P. Truscott, L. Urban, V. Uzhinsky, J. Verbeke, M. Verderi, B. Wendt, H. Wenzel, D. Wright, D. Wright, T. Yamashita, J. Yarba, H. Yoshida, Nucl. Instrum. Methods Phys. Res. Sect. A: Accel. Spectrom. Detect. Assoc. Equip. **835**, 186 (2016). https://doi.org/10.1016/j.nima.2016.06.125

98. D. Barducci, G. Cavoto, M. Nardecchia, G. Organtini, G. Piperno, M. Raggi, C. Toni, P. Valente, C. Voena, Shedding light on X17 conference proceedings. Eur. Phys. J. C. These proceedings

99. P. Tanedo, The delirium over beryllium (2016). https://www.quantumdiaries.org/2016/08/25/the-delirium-over-beryllium

100. J.L. Feng, J. Kumar, Phys. Rev. Lett. **101**, 231301 (2008). https://doi.org/10.1103/PhysRevLett.101.231301

101. J.L. Feng, H. Tu, H.B. Yu, J. Cosmol. Astropart. Phys. **2008**, 043 (2008). https://doi.org/10.1088/1475-7516/2008/10/043

102. P.H. Gu, X.G. He, Nucl. Phys. B **919**, 209 (2017). https://doi.org/10.1016/j.nuclphysb.2017.03.023

103. L.B. Jia, X.Q. Li, Eur. Phys. J. C **76**(12), 706 (2016). https://doi.org/10.1140/epjc/s10052-016-4561-3

104. C.S. Chen, G.L. Lin, Y.H. Lin, F. Xu, Int. J. Mod. Phys. A **32**(31), 1750178 (2017). https://doi.org/10.1142/S0217751X17501780

105. T. Kitahara, Y. Yamamoto, Phys. Rev. D **95**(1), 015008 (2017). https://doi.org/10.1103/PhysRevD.95.015008

106. L. Delle Rose, S. Khalil, S. Moretti, Phys. Rev. D **96**(11), 115024 (2017). https://doi.org/10.1103/PhysRevD.96.115024

107. Y. Kahn, G. Krnjaic, S. Mishra-Sharma, T.M.P. Tait, JHEP **05**, 002 (2017). https://doi.org/10.1007/JHEP05(2017)002

108. B. Fornal, Int. J. Mod. Phys. A **32**, 1730020 (2017). https://doi.org/10.1142/S0217751X17300204

109. B. Abi, T. Albahri, S. Al-Kilani, D. Allspach, L.P. Alonzi, A. Anastasi, A. Anisenkov, F. Azfar, K. Badgley, S. Baeßler, I. Bailey, V.A. Baranov, E. Barlas-Yucel, T. Barrett, E. Barzi, A. Basti, F. Bedeschi, A. Behnke, M. Berz, M. Bhattacharya, H.P. Binney, R. Bjorkquist, P. Bloom, J. Bono, E. Bottalico, T. Bowcock, D. Boyden, G. Cantatore, R.M. Carey, J. Carroll, B.C.K. Casey, D. Cauz, S. Ceravolo, R. Chakraborty, S.P. Chang, A. Chapelain, S. Chappa, S. Charity, R. Chislett, J. Choi, Z. Chu, T.E. Chupp, M.E. Convery, A. Conway, G. Corradi, S. Corrodi, L. Cotrozzi, J.D. Crnkovic, S. Dabagov, P.M. De Lurgio, P.T. Debevec, S. Di Falco, P. Di Meo, G. Di Sciascio, R. Di Stefano, B. Drendel, A. Driutti, V.N. Duginov, M. Eads, N. Eggert, A. Epps, J. Esquivel, M. Farooq, R. Fatemi, C. Ferrari, M. Fertl, A. Fiedler, A.T. Fienberg, A. Fioretti, D. Flay, S.B. Foster, H. Friedsam, E. Frlež, N.S. Froemming, J. Fry, C. Fu, C. Gabbanini, M.D. Galati, S. Ganguly, A. Garcia, D.E. Gastler, J. George, L.K. Gibbons, A. Gioiosa, K.L. Giovanetti, P. Girotti, W. Gohn, T. Gorringe, J. Grange, S. Grant, F. Gray, S. Haciomeroglu, D. Hahn, T. Halewood-Leagas, D. Hampai, F. Han, E. Hazen, J. Hempstead, S. Henry, A.T. Herrod, D.W. Hertzog, G. Hesketh, A. Hibbert, Z. Hodge, J.L. Holzbauer, K.W. Hong, R. Hong, M. Iacovacci, M. Incagli, C. Johnstone, J.A. Johnstone, P. Kammel, M. Kargiantoulakis, M. Karuza, J. Kaspar, D. Kawall, L. Kelton, A. Keshavarzi, D. Kessler, K.S. Khaw, Z. Khechadoorian, N.V. Khomutov, B. Kiburg, M. Kiburg, O. Kim, S.C. Kim, Y.I. Kim, B. King, N. Kinnaird, M. Korostelev, I. Kourbanis, E. Kraegeloh, V.A. Krylov, A. Kuchibhotla, N.A. Kuchinskiy, K.R. Labe, J. LaBounty, M. Lancaster, M.J. Lee, S. Lee, S. Leo, B. Li, D. Li, L. Li, I. Logashenko, A. Lorente Campos, A. Lucà, G. Lukicov, G. Luo, A. Lusiani, A.L. Lyon, B. MacCoy, R. Madrak, K. Makino, F. Marignetti, S. Mastroianni, S. Maxfield, M. McEvoy, W. Merritt, A.A. Mikhailichenko, J.P. Miller, S. Miozzi, J.P. Morgan, W.M. Morse, J. Mott, E. Motuk, A. Nath, D. Newton, H. Nguyen, M. Oberling, R. Osofsky, J.F. Ostiguy, S. Park, G. Pauletta, G.M. Piacentino, R.N. Pilato, K.T. Pitts, B. Plaster, D. Počanić, N. Pohlman, C.C. Polly, M. Popovic,

J. Price, B. Quinn, N. Raha, S. Ramachandran, E. Ramberg, N.T. Rider, J.L. Ritchie, B.L. Roberts, D.L. Rubin, L. Santi, D. Sathyan, H. Schellman, C. Schlesier, A. Schreckenberger, Y.K. Semertzidis, Y.M. Shatunov, D. Shemyakin, M. Shenk, D. Sim, M.W. Smith, A. Smith, A.K. Soha, M. Sorbara, D. Stöckinger, J. Stapleton, D. Still, C. Stoughton, D. Stratakis, C. Strohman, T. Stuttard, H.E. Swanson, G. Sweetmore, D.A. Sweigart, M.J. Syphers, D.A. Tarazona, T. Teubner, A.E. Tewsley-Booth, K. Thomson, V. Tishchenko, N.H. Tran, W. Turner, E. Valetov, D. Vasilkova, G. Venanzoni, V.P. Volnykh, T. Walton, M. Warren, A. Weisskopf, L. Welty-Rieger, M. Whitley, P. Winter, A. Wolski, M. Wormald, W. Wu, C. Yoshikawa, Phys. Rev. Lett. **126**, 141801 (2021). https://doi.org/10.1103/PhysRevLett.126.141801

110. A. Ariga, T. Ariga, J. Boyd, F. Cadoux, D.W. Casper, Y. Favre, J.L. Feng, H. Ferrere, I. Galon, S. Gonzalez-Sevilla, S.C. Hsu, G. Iacobucci, E. Kajomovitz, F. Kling, S. Kuehn, L. Levinson, H. Otono, B. Petersen, O. Sato, M. Schott, A. Sfyrla, J. Smolinsky, A.M. Soffa, Y. Takubo, E. Torrence, S. Trojanowski, G. Zhang, Phys. Rev. D **99**, 095011 (2019). https://doi.org/10.1103/PhysRevD.99.095011

111. J.L. Feng, I. Galon, F. Kling, S. Trojanowski, Phys. Rev. D **97**, 035001 (2018). https://doi.org/10.1103/PhysRevD.97.035001

112. L.B. Chen, Y. Liang, C.F. Qiao, X(16.7) Production in electron–positron collision (2016). arXiv:1607.03970 [hep-ph]

113. O. Seto, T. Shimomura, Phys. Rev. D **95**(9), 095032 (2017). https://doi.org/10.1103/PhysRevD.95.095032

114. M.J. Neves, J.A. Helayël-Neto, A unified hidden-sector-electroweak model, paraphotons and the X-Boson (2016). arXiv:1611.07974 [hep-ph]

115. C.W. Chiang, P.Y. Tseng, Phys. Lett. B **767**, 289 (2017). https://doi.org/10.1016/j.physletb.2017.02.022

116. J.R. Batley et al., Phys. Lett. B **746**, 178 (2015). https://doi.org/10.1016/j.physletb.2015.04.068

117. P. Fayet, Nucl. Phys. B **187**, 184 (1981). https://doi.org/10.1016/0550-3213(81)90122-X

118. P. Fayet, Phys. Lett. **95B**, 285 (1980). https://doi.org/10.1016/0370-2693(80)90488-8

119. P. Fayet, Nucl. Phys. B **347**, 743 (1990). https://doi.org/10.1016/0550-3213(90)90381-M

120. P. Fayet, Phys. Rev. D **75**, 115017 (2007). https://doi.org/10.1103/PhysRevD.75.115017

121. P. Fayet, Phys. Lett. B **675**, 267 (2009). https://doi.org/10.1016/j.physletb.2009.03.078

122. P. Fayet, Eur. Phys. J. C **77**(1), 53 (2017). https://doi.org/10.1140/epjc/s10052-016-4568-9

123. L. Delle Rose, S. Khalil, S.J.D. King, S. Moretti, Front. Phys. **7**, 73 (2019). https://doi.org/10.3389/fphy.2019.00073

124. P. Ko, Y. Omura, C. Yu, Phys. Lett. B **717**, 202 (2012). https://doi.org/10.1016/j.physletb.2012.09.019

125. P. Ko, Y. Omura, C. Yu, JHEP **01**, 016 (2014). https://doi.org/10.1007/JHEP01(2014)016

126. R. MacCoun, S. Perlmutter, Nature **526**, 187 (2015). https://doi.org/10.1038/526187a

127. E. Abouzaid, M. Arenton, A.R. Barker, L. Bellantoni, A. Bellavance, E. Blucher, G.J. Bock, E. Cheu, R. Coleman, M.D. Corcoran, B. Cox, A.R. Erwin, C.O. Escobar, A. Glazov, A. Golossanov, R.A. Gomes, P. Gouffon, K. Hanagaki, Y.B. Hsiung, H. Huang, D.A. Jensen, R. Kessler, K. Kotera, A. Ledovskoy, P.L. McBride, E. Monnier, K.S. Nelson, H. Nguyen, R. Niclasen, D.G. Phillips, H. Ping, X.R. Qi, E.J. Ramberg, R.E. Ray, M. Ronquest, E. Santos, J. Shields, W. Slater, D. Smith, N. Solomey, E.C. Swallow, P.A. Toale, R. Tschirhart, C. Velissaris, Y.W. Wah, J. Wang, H.B. White, J. Whitmore, M.J. Wilking, B. Winstein, R. Winston, E.T. Worcester, M. Worcester, T. Yamanaka, E.D. Zimmerman, R.F. Zukanovich, Phys. Rev. D **75**, 012004 (2007). https://doi.org/10.1103/PhysRevD.75.012004

128. R. Eichler, L. Felawka, N. Kraus, C. Niebuhr, H. Walter, S. Egli, R. Engfer, C. Grab, E. Hermes, H. Pruys, A. van der Schaaf, D. Vermeulen, W. Bertl, N. Lordong, U. Bellgardt, G. Otter, T. Kozlowski, J. Martino, Phys. Lett. B **175**(1), 101 (1986). https://doi.org/10.1016/0370-2693(86)90339-4

129. W.A. Bardeen, S.H. Tye, J. Vermaseren, Phys. Lett. B **76**(5), 580 (1978). https://doi.org/10.1016/0370-2693(78)90859-6

130. Constraints on variant axions models. Phys. Lett. B **279**, 401 (1987)

131. M. Bauer, M. Neubert, S. Renner, M. Schnubel, A. Thamm, Phys. Rev. Lett. **127**, 081803 (2021). https://doi.org/10.1103/PhysRevLett.127.081803

132. A. Barroso, N.C. Mukhopadhyay, Phys. Rev. C **24**, 2382 (1981). https://doi.org/10.1103/PhysRevC.24.2382

133. M.J. Savage, B.W. Filippone, L.W. Mitchell, Phys. Rev. D **37**, 1134 (1988). https://doi.org/10.1103/PhysRevD.37.1134

134. E. Goudzovski, D. Redigolo, K. Tobioka, J. Zupan, G. Alonso-Alvarez, D.S.M. Alves, S. Bansal, M. Bauer, J. Brod, V. Chobanova, G. D'Ambrosio, A. Datta, A. Dery, F. Dettori, B.A. Dobrescu, B. Dobrich, D. Egana-Ugrinovic, G. Elor, M. Escudero, M. Fabbrichesi, B. Fornal, P.J. Fox, E. Gabrielli, L.S. Geng, V.V. Gligorov, M. Gorbahn, S. Gori, B. Grinstein, Y. Grossman, D. Guadagnoli, S. Homiller, M. Hostert, K.J. Kelly, T. Kitahara, S. Knapen, G. Krnjaic, A. Kupsc, S. Kvedaraite, G. Lanfranchi, D. Marfatia, J.M. Camalich, D.M. Santos, K. Massri, P. Mead, M. Moulson, H. Nanjo, M. Neubert, M. Pospelov, S. Renner, S. Schacht, M. Schnubel, R.X. Shi, B. Shuve, T. Spadaro, Y. Soreq, E. Stamou, O. Sumensari, M. Tammaro, J. Terol-Calvo, A. Thamm, Y.C. Tung, D. Wang, K. Yamamoto, R. Ziegler (2022). arXiv:2201.0785

135. REDTOP Collaboration, The REDTOP experiment: rare η/η' decays to probe new physics (2022). arXiv:2203.07651 [hep-ex]

136. M. Hostert, M. Pospelov, Novel multi-lepton signatures of dark sectors in light meson decays (2020). arXiv:2012.02142

137. N.P. Samios, R. Plano, A. Prodell, M. Schwartz, J. Steinberger, Phys. Rev. **126**, 1844 (1962). https://doi.org/10.1103/PhysRev.126.1844

138. Y.M. Andreev, D. Banerjee, J. Bernhard, V.E. Burtsev, N. Charitonidis, A.G. Chumakov, D. Cooke, P. Crivelli, E. Depero, A.V. Dermenev, S.V. Donskov, R.R. Dusaev, T. Enik, A. Feshchenko, V.N. Frolov, A. Gardikiotis, S.G. Gerassimov, S.N. Gninenko, M. Hösgen, M. Jeckel, V.A. Kachanov, A.E. Karneyeu, G. Kekelidze, B. Ketzer, D.V. Kirpichnikov, M.M. Kirsanov, V.N. Kolosov, I.V. Konorov, S.G. Kovalenko, V.A. Kramarenko, L.V. Kravchuk, N.V. Krasnikov, S.V. Kuleshov, V.E. Lyubovitskij, V. Lysan, V.A. Matveev, Y.V. Mikhailov, L. Molina Bueno, D.V. Peshekhonov, V.A. Polyakov, B. Radics, R. Rojas, A. Rubbia, V.D. Samoylenko, H. Sieber, D. Shchukin, V.O. Tikhomirov, I. Tlisova, A.N. Toropin, A.Y. Trifonov, B.I. Vasilishin, G. Vasquez Arenas, P.V. Volkov, V.Y. Volkov, P. Ulloa, Phys. Rev. D **104**, L111102 (2021). https://doi.org/10.1103/PhysRevD.104.L111102

139. J. Liu, N. McGinnis, C.E.M. Wagner, X.P. Wang, J. High Energy Phys. **2021**, 138 (2021). https://doi.org/10.1007/JHEP05(2021)138

140. R.H. Parker, C. Yu, W. Zhong, B. Esteyand, H. Müller, Science **360**, 191 (2018). https://doi.org/10.1126/science.aap7706

141. H. Müller, Nature **588**, 37 (2020). https://doi.org/10.1038/d41586-020-03314-0

142. K.U. Abraamyan, A.B. Anisimov, M.I. Baznat, K.K. Gudima, M.A. Nazarenko, S.G. Reznikov, A.S. Sorin, Observation of the e(38)-boson (2012). arXiv:1208.3829

143. K. Abraamyan, C. Austin, M. Baznat, K. Gudima, M. Kozhin, S. Reznikov, A. Sorin, EPJ Web Conf. **204**, 08004 (2019). https://doi.org/10.1051/epjconf/201920408004

144. P. Chliapnikov, E. De Wolf, A. Fenyuk, L. Gerdyukov, Y. Goldschmidt-Clermont, V. Ronjin, A. Weigend, Phys.

145. F. Botterweck, M.M. Chapkin, M. Charlet, P.V. Chliapnikov, A. De Roeck, E.A. De Wolf, K. Dziunikowska, A. Eskreys, Z.C. Garutchava, G.R. Gulkanyan, T. Haupt, L.P. Kishinevskaya, W. Kittel, I.V. Nikolaenko, K. Olkiewicz, V.M. Ronjin, L.N. Smirnova, O.G. Tchikilev, L.A. Tikhonova, V.A. Uvarov, F. Verbeure, R. Wischnewski, S.A. Zotkin, Zeitschrift für Physik C Part. Fields **51**(4), 541 (1991). https://doi.org/10.1007/BF01565578

146. A. Belogianni, W. Beusch, T. Brodbeck, F. Dzheparov, B. French, P. Ganoti, J. Kinson, A. Kirk, V. Lenti, I. Minashvili, V. Perepelitsa, N. Russakovich, A. Singovsky, P. Sonderegger, M. Spyropoulou-Stassinaki, O. Villalobos Baillie, Phys. Lett. B **548**(3), 129 (2002). https://doi.org/10.1016/S0370-2693(02)02837-X

147. V.F. Perepelitsa, Nonlinear Phenom. Complex Syst. **12**, 343 (2009)

148. J. Abdallah, P. Abreu, W. Adam, P. Adzic, T. Albrecht, R. Alemany-Fernandez, T. Allmendinger, P.P. Allport, U. Amaldi, N. Amapane, S. Amato, E. Anashkin, A. Andreazza, S. Andringa, N. Anjos, P. Antilogus, W.D. Apel, Y. Arnoud, S. Ask, B. Asman, J.E. Augustin, A. Augustinus, P. Baillon, A. Ballestrero, P. Bambade, R. Barbier, D. Bardin, G.J. Barker, A. Baroncelli, M. Battaglia, M. Baubillier, K.H. Becks, M. Begalli, A. Behrmann, E. Ben-Haim, N. Benekos, A. Benvenuti, C. Berat, M. Berggren, D. Bertrand, M. Besancon, N. Besson, D. Bloch, M. Blom, M. Bluj, M. Bonesini, M. Boonekamp, P.S.L. Booth, G. Borisov, O. Botner, B. Bouquet, T.J.V. Bowcock, I. Boyko, M. Bracko, R. Brenner, E. Brodet, P. Bruckman, J.M. Brunet, B. Buschbeck, P. Buschmann, M. Calvi, T. Camporesi, V. Canale, F. Carena, N. Castro, F. Cavallo, M. Chapkin, P. Charpentier, P. Checchia, R. Chierici, P. Chliapnikov, J. Chudoba, S.U. Chung, K. Cieslik, P. Collins, R. Contri, G. Cosme, F. Cossutti, M.J. Costa, D. Crennell, J. Cuevas, J. D'Hondt, T. da Silva, W. Da Silva, G. Della Ricca, A. De Angelis, W. De Boer, C. De Clercq, B. De Lotto, N. De Maria, A. De Min, L. de Paula, L. Di Ciaccio, A. Di Simone, K. Doroba, J. Drees, G. Eigen, T. Ekelof, M. Ellert, M. Elsing, M.C. Espirito Santo, G. Fanourakis, D. Fassouliotis, M. Feindt, J. Fernandez, A. Ferrer, F. Ferro, U. Flagmeyer, H. Foeth, E. Fokitis, F. Fulda-Quenzer, J. Fuster, M. Gandelman, C. Garcia, P. Gavillet, E. Gazis, R. Gokieli, B. Golob, G. Gomez-Ceballos, P. Goncalves, E. Graziani, G. Grosdidier, K. Grzelak, J. Guy, C. Haag, A. Hallgren, K. Hamacher, K. Hamilton, S. Haug, F. Hauler, V. Hedberg, M. Hennecke, J. Hoffman, S.O. Holmgren, P.J. Holt, M.A. Houlden, J.N. Jackson, G. Jarlskog, P. Jarry, D. Jeans, E.K. Johansson, P. Jonsson, C. Joram, L. Jungermann, F. Kapusta, S. Katsanevas, E. Katsoufis, G. Kernel, B.P. Kersevan, U. Kerzel, B.T. King, N.J. Kjaer, P. Kluit, P. Kokkinias, C. Kourkoumelis, O. Kouznetsov, Z. Krumstein, M. Kucharczyk, J. Lamsa, G. Leder, F. Ledroit, L. Leinonen, R. Leitner, J. Lemonne, V. Lepeltier, T. Lesiak, W. Liebig, D. Liko, A. Lipniacka, J.H. Lopes, J.M. Lopez, D. Loukas, P. Lutz, L. Lyons, J. MacNaughton, A. Malek, S. Maltezos, F. Mandl, J. Marco, R. Marco, B. Marechal, M. Margoni, J.C. Marin, C. Mariotti, A. Markou, C. Martinez-Rivero, J. Masik, N. Mastroyiannopoulos, F. Matorras, C. Matteuzzi, F. Mazzucato, M. Mazzucato, R. Mc Nulty, C. Meroni, E. Migliore, W. Mitaroff, U. Mjoernmark, T. Moa, M. Moch, K. Moenig, R. Monge, J. Montenegro, D. Moraes, S. Moreno, P. Morettini, U. Mueller, K. Muenich, M. Mulders, L. Mundim, W. Murray, B. Muryn, G. Myatt, T. Myklebust, M. Nassiakou, F. Navarria, K. Nawrocki, S. Nemecek, R. Nicolaidou, M. Nikolenko, A. Oblakowska-Mucha, V. Obraztsov, A. Olshevski, A. Onofre, R. Orava, K. Osterberg, A. Ouraou, A. Oyanguren, M. Paganoni, S. Paiano, J.P. Palacios, H. Palka, T.D. Papadopoulou, L. Pape, C. Parkes, F. Parodi, U. Parzefall, A. Passeri, O. Passon, L. Per-

Lett. B **141**(3), 276 (1984). https://doi.org/10.1016/0370-2693(84)90216-8

alta, V. Perepelitsa, A. Perrotta, A. Petrolini, J. Piedra, L. Pieri, F. Pierre, M. Pimenta, E. Piotto, T. Podobnik, V. Poireau, M.E. Pol, G. Polok, V. Pozdniakov, N. Pukhaeva, A. Pullia, D. Radojicic, P. Rebecchi, J. Rehn, D. Reid, R. Reinhardt, P. Renton, F. Richard, J. Ridky, M. Rivero, D. Rodriguez, A. Romero, P. Ronchese, P. Roudeau, T. Rovelli, V. Ruhlmann-Kleider, D. Ryabtchikov, A. Sadovsky, L. Salmi, J. Salt, C. Sander, A. Savoy-Navarro, U. Schwickerath, R. Sekulin, M. Siebel, A. Sisakian, G. Smadja, O. Smirnova, A. Sokolov, A. Sopczak, R. Sosnowski, T. Spassov, M. Stanitzki, A. Stocchi, J. Strauss, B. Stugu, M. Szczekowski, M. Szeptycka, T. Szumlak, T. Tabarelli, F. Tegenfeldt, J. Timmermans, L. Tkatchev, M. Tobin, S. Todorovova, B. Tome, Eur. Phys. J. C **67**, 343 (2010)

149. C.Y. Wong, Phys. Rev. C **81**, 064903 (2010). https://doi.org/10.1103/PhysRevC.81.064903

150. C.Y. Wong, J. High Energy Phys. **2020**(8) (2020). https://doi.org/10.1007/jhep08(2020)165

151. C.Y. Wong, On the stability of the open-string QED neutron and dark matter (2020). arXiv:2010.13948

152. C.Y. Wong, EPJ Web Conf. **259**, 13016 (2022). https://doi.org/10.1051/epjconf/202225913016

153. C.Y. Wong, A.V. Koshelkin, Dynamics of quarks and gauge fields in the lowest-energy states in QCD and QED (2021). arXiv:2111.14933

154. J. Schwinger, Phys. Rev. **128**, 2425 (1962). https://doi.org/10.1103/PhysRev.128.2425

155. J. Schwinger, Gauge theories of vector particles (1963). The general topic of this paper is the vector theory of gauge fields, but I like to think that these lectures are really concerned with the future of the relativistic field theory as an effective force in the development of fundamental physics. Two basic positions are at present under investigation as the possible organizing forces for the rapidly growing empirical data on elementary particles. To put it as extremely as possible, we might call these two positions: (i) The particle point of view, (ii) The field point of view. By the particle point of view, I mean those investigations in which the physical particles, as we see them, are the basic elements. This is the whole line of development associated with the S-matrix, with the idea that the only function of the theory is to compute and to correlate the results of scattering measurements. It also underlies those further attempts intended to give a physical content to this essentially empty framework, such as dispersion relations, Regge poles, etc. And, to adopt this point of view systematically, one must necessarily accept the Orwellian philosophy that no particle is more fundamental than any other. That is the strict particle point of view; the particles are unanalysable. To our mind it is an extremely conservative position. IAEA

156. A. Polyakov, Nucl. Phys. B **120**(3), 429 (1977). https://doi.org/10.1016/0550-3213(77)90086-4

157. A. Polyakov, *Gauge Fields and Strings* (Routledge, London, 1987). https://doi.org/10.1201/9780203755082

158. S.D. Drell, H.R. Quinn, B. Svetitsky, M. Weinstein, Phys. Rev. D **19**, 619 (1979). https://doi.org/10.1103/PhysRevD.19.619

159. C.N. Yang, Phys. Rev. D **1**, 2360 (1970). https://doi.org/10.1103/PhysRevD.1.2360

160. C.Y. Wong, *Introduction to High-Energy Heavy-Ion Collisions* (World Scientific, Singapore, 1994)

161. V.B. Berestetskii, E.M. Lifshitz, L.P. Pitsevskii, *Quantum Electrodynamics* (Pergamon Press, Oxford, 1982)

162. K. Ban, Y. Jho, Y. Kwon, S.C. Park, S. Park, P.Y. Tseng, JHEP **04**, 091 (2021). https://doi.org/10.1007/JHEP04(2021)091

163. J.A. Dror, R. Lasenby, M. Pospelov, Phys. Rev. D **96**(7), 075036 (2017). https://doi.org/10.1103/PhysRevD.96.075036

164. J.A. Dror, R. Lasenby, M. Pospelov, Phys. Rev. Lett. **119**(14), 141803 (2017). https://doi.org/10.1103/PhysRevLett.119.141803

165. J.D. Bjorken, R. Essig, P. Schuster, N. Toro, Phys. Rev. D **80**, 075018 (2009). https://doi.org/10.1103/PhysRevD.80.075018

166. S. Andreas, C. Niebuhr, A. Ringwald, Phys. Rev. D **86**, 095019 (2012). https://doi.org/10.1103/PhysRevD.86.095019

167. E.M. Riordan et al., Phys. Rev. Lett. **59**, 755 (1987). https://doi.org/10.1103/PhysRevLett.59.755

168. A. Konaka et al., Phys. Rev. Lett. **57**, 659 (1986). https://doi.org/10.1103/PhysRevLett.57.659

169. M. Davier, H. Nguyen Ngoc, Phys. Lett. B **229**, 150 (1989). https://doi.org/10.1016/0370-2693(89)90174-3

170. Y.S. Liu, G.A. Miller, Phys. Rev. D **96**(1), 016004 (2017). https://doi.org/10.1103/PhysRevD.96.016004

171. A. Anastasi et al., Phys. Lett. B **750**, 633 (2015). https://doi.org/10.1016/j.physletb.2015.10.003

172. P. Ilten, Y. Soreq, M. Williams, W. Xue, JHEP **06**, 004 (2018). https://doi.org/10.1007/JHEP06(2018)004

173. A. Blondel et al., Research proposal for an experiment to search for the decay $\mu \to eee$ (2013). arXiv:1301.6113 [physics.ins-det]

174. J. Backens, M. Vanderhaeghen, X17 discovery potential in the $\gamma N \to e^+ e^- N$ process at electron scattering facilities (2021). arXiv:2110.06055 [hep-ph]

175. E. Nardi, C.D.R. Carvajal, A. Ghoshal, D. Meloni, M. Raggi, Phys. Rev. D **97**(9), 095004 (2018). https://doi.org/10.1103/PhysRevD.97.095004

176. L. Marsicano, M. Battaglieri, M. Bondi', C.D.R. Carvajal, A. Celentano, M. De Napoli, R. De Vita, E. Nardi, M. Raggi, P. Valente, Phys. Rev. D **98**(1), 015031 (2018). https://doi.org/10.1103/PhysRevD.98.015031

177. L. Marsicano, M. Battaglieri, M. Bondí, C.D.R. Carvajal, A. Celentano, M. De Napoli, R. De Vita, E. Nardi, M. Raggi, P. Valente, Phys. Rev. Lett. **121**(4), 041802 (2018). https://doi.org/10.1103/PhysRevLett.121.041802

178. A. Celentano, L. Darmé, L. Marsicano, E. Nardi, Phys. Rev. D **102**(7), 075026 (2020). https://doi.org/10.1103/PhysRevD.102.075026

179. M. Battaglieri et al., Eur. Phys. J. A **57**(8), 253 (2021). https://doi.org/10.1140/epja/s10050-021-00524-6

180. M. Raggi, V. Kozhuharov, Adv. High Energy Phys. **2014**, 959802 (2014). https://doi.org/10.1155/2014/959802

181. M. Raggi, V. Kozhuharov, P. Valente, EPJ Web Conf. **96**, 01025 (2015). https://doi.org/10.1051/epjconf/20159601025

182. L. Darmé, M. Mancini, E. Nardi, M. Raggi, Phys. Rev. D **106**(11), 115036 (2022). https://doi.org/10.1103/PhysRevD.106.115036

183. V. Fanti, A. Lai, D. Marras, L. Musa, A. Nappi, R. Batley, A. Bevan, R. Dosanjh, R. Galik, T. Gershon, B. Hay, G. Kalmus, S. Katvars, C. Lazzeroni, R. Moore, D. Munday, M. Needham, E. Olaiya, M. Parker, M. Patel, M. Slater, S. Takach, T. White, S. Wotton, F. Bal, G. Barr, G. Bocquet, J. Bremer, P. Brodier-Yourstone, P. Buchholz, M. Burns, A. Ceccucci, M. Clément, T. Cuhadar-Dönzelsmann, D. Cundy, N. Doble, V. Falaleev, F. Formenti, W. Funk, L. Gatignon, A. Gonidec, P. Grafström, B. Hallgren, P. Kapusta, G. Kesseler, W. Kubischta, W. Iwanski, A. Lacourt, G. Laverriere, G. Linser, C. Ljuslin, A. Marchioro, M. Mast, J. Matheys, M. Morel, A. Norton, J. Orlic, B. Panzer-Steindel, D. Schinzel, W. Seidl, H. Taureg, J.C. Tarle, M. Velasco, O. Vossnack, H. Wahl, P. Wertelaers, J. Weterings, C. Cheshkov, A. Gaponenko, E. Goudzovski, P. Hristov, A. Kalinin, V. Kekelidze, Y. Kozhevnikov, D. Madigozhin, N. Molokanova, Y. Potrebenikov, A. Tkatchev, A. Zinchenko, O. Boyle, I. Knowles, V. Martin, H. Parsons, K. Peach, R. Sacco, E. Veitch, A. Walker, V. Carassiti, M. Contalbrigo, A. Cotta Ramusino, P. Dalpiaz, C. Damiani, J. Duclos, P. Ferretti, P. Frabetti, A. Gianoli, M. Martini, F. Petrucci, M. Porcu, F. Rossi, M. Savrie, M. Scarpa, C. Simani, A. Bizzeti, M. Calvetti, G. Collazuol, G. Graziani, E. Iacopini, M. Lenti, F. Martelli, A. Michetti, G. Ruggiero, M. Veltri, H. Becker, M. Behler, H. Blümer, D. Cow-

ard, C. Ebersberger, K. Eppard, M. Eppard, H. Fox, K. Geib, A. Hirstius, A. Kalter, K. Kleinknecht, U. Koch, L. Köpke, P. Lopes da Silva, S. Luitz, P. Marouelli, L. Masetti, I. Melzer-Pellmann, U. Moosbrugger, C. Morales, A. Peters, B. Renk, J. Scheidt, J. Schmidt, S. Schmidt, V. Schönharting, Y. Schué, J. Staeck, R. Wanke, R. Wilhelm, A. Winhart, M. Wittgen, O. Zeitnitz, A. Dabrowski, T. Fonseca Martin, J. Chollet, S. Crépé, C. De La Taille, L. Fayard, L. Iconomidou-Fayard, G. Martin-Chassard, J. Ocariz, G. Unal, I. Wingerter-Seez, G. Anzivino, F. Bordacchini, P. Cenci, E. Imbergamo, P. Lariccia, P. Lubrano, A. Mestvirishivili, A. Papi, M. Pepe, M. Piccini, M. Punturo, C. Talamonti, F. Tondini, L. Bertanza, P. Calafiura, R. Carosi, R. Casali, C. Cerri, M. Cirilli, F. Costantini, R. Fantechi, F. Fidecaro, L. Fiorini, S. Giudici, B. Gorini, F. Laico, G. Lamanna, I. Mannelli, V. Marzulli, D. Passuello, G. Pierazzini, F. Raffaelli, M. Sozzi, R. Tripiccione, S. Anvar, D. Béderède, F. Bugeon, J. Chèze, J. Cogan, M. De Beer, P. Debu, D. Durand, S. Edard, J. Fallou, A. Formica, L. Gosset, R. Granier de Cassagnac, J. Heitzmann, H. Le Provost, F. Louis, I. Mandzhavidze, E. Mazzucato, A. Migliori, M. Mur, B. Peyaud, S. Schanne, O. Steinkamp, G. Tarte, R. Turlay, B. Vallage, M. Holder, I. Augustin, M. Bender, A. Maier, I. Schwarz, M. Ziolkowski, R. Arcidiacono, P. Barberis, F. Benotto, F. Bertolino, C. Biino, O. Brunasso, N. Cartiglia, M. Clemencic, D. Dattola, S. Goy Lopez, G. Govi, R. Guida, F. Marchetto, E. Menichetti, S. Palestini, N. Pastrone, A. Chlopik, Z. Guzik, J. Nassalski, E. Rondio, M. Szleper, W. Wislicki, S. Wronka, H. Dibon, G. Fischer, M. Jeitler, M. Markytan, I. Mikulec, G. Neuhofer, M. Pernicka, A. Taurok, L. Widhalm, Nucl. Instrum. Methods Phys. Res. Sect. A: Accel. Spectrom. Detect. Assoc. Equip. **574**(3), 433 (2007). https://doi.org/10.1016/j.nima.2007.01.178

184. J. Batley, A. Culling, G. Kalmus, C. Lazzeroni, D. Munday, M. Slater, S. Wotton, R. Arcidiacono, G. Bocquet, N. Cabibbo, A. Ceccucci, D. Cundy, V. Falaleev, M. Fidecaro, L. Gatignon, A. Gonidec, W. Kubischta, A. Norton, A. Maier, M. Patel, A. Peters, S. Balev, P. Frabetti, E. Goudzovski, P. Hristov, V. Kekelidze, V. Kozhuharov, L. Litov, D. Madigozhin, E. Marinova, N. Molokanova, I. Polenkevich, Y. Potrebenikov, S. Stoynev, A. Zinchenko, E. Monnier, E. Swallow, R. Winston, P. Rubin, A. Walker, W. Baldini, A. Cotta Ramusino, P. Dalpiaz, C. Damiani, M. Fiorini, A. Gianoli, M. Martini, F. Petrucci, M. Savrié, M. Scarpa, H. Wahl, A. Bizzeti, M. Calvetti, E. Celeghini, E. Iacopini, M. Lenti, F. Martelli, G. Ruggiero, M. Veltri, M. Behler, K. Eppard, K. Kleinknecht, P. Marouelli, L. Masetti, U. Moosbrugger, C. Morales Morales, B. Renk, M. Wache, R. Wanke, A. Winhart, D. Coward, A. Dabrowski, T. Fonseca Martin, M. Shieh, M. Szleper, M. Velasco, M. Wood, G. Anzivino, P. Cenci, E. Imbergamo, A. Nappi, M. Pepe, M. Petrucci, M. Piccini, M. Raggi, M. Valdata-Nappi, C. Cerri, G. Collazuol, F. Costantini, L. DiLella, N. Doble, R. Fantechi, L. Fiorini, S. Giudici, G. Lamanna, I. Mannelli, A. Michetti, G. Pierazzini, M. Sozzi, B. Bloch-Devaux, C. Cheshkov, J. Chèze, M. De Beer, J. Derré, G. Marel, E. Mazzucato, B. Peyaud, B. Vallage, M. Holder, M. Ziolkowski, S. Bifani, C. Biino, N. Cartiglia, M. Clemencic, S. Goy Lopez, F. Marchetto, H. Dibon, M. Jeitler, M. Markytan, I. Mikulec, G. Neuhofer, L. Widhalm, Eur. Phys. J. C **52**(4), 875 (2007). https://doi.org/10.1140/epjc/s10052-007-0456-7

185. J. Batley, G. Kalmus, C. Lazzeroni, D. Munday, M. Slater, S. Wotton, R. Arcidiacono, G. Bocquet, N. Cabibbo, A. Ceccucci, D. Cundy, V. Falaleev, M. Fidecaro, L. Gatignon, A. Gonidec, W. Kubischta, A. Norton, A. Maier, M. Patel, A. Peters, S. Balev, P. Frabetti, E. Gersabeck, E. Goudzovski, P. Hristov, V. Kekelidze, V. Kozhuharov, L. Litov, D. Madigozhin, N. Molokanova, I. Polenkevich, Y. Potrebenikov, S. Stoynev, A. Zinchenko, E. Monnier, E. Swallow, R. Winston, P. Rubin, A. Walker, W. Baldini, A. Cotta Ramusino, P. Dalpiaz, C. Damiani, M. Fiorini, A. Gianoli, M. Martini, F. Petrucci, M. Savrié, M. Scarpa, H. Wahl, A. Bizzeti, M. Lenti, M. Veltri, M. Calvetti, E. Celeghini, E. Iacopini, G. Ruggiero, M. Behler, K. Eppard, K. Kleinknecht, P. Marouelli, L. Masetti, U. Moosbrugger, C. Morales Morales, B. Renk, M. Wache, R. Wanke, A. Winhart, D. Coward, A. Dabrowski, T. Fonseca Martin, M. Shieh, M. Szleper, M. Velasco, M. Wood, P. Cenci, M. Pepe, M. Petrucci, G. Anzivino, E. Imbergamo, A. Nappi, M. Piccini, M. Raggi, M. Valdata-Nappi, C. Cerri, R. Fantechi, G. Collazuol, L. DiLella, G. Lamanna, I. Mannelli, A. Michetti, F. Costantini, N. Doble, L. Fiorini, S. Giudici, G. Pierazzini, M. Sozzi, S. Venditti, B. Bloch-Devaux, C. Cheshkov, J. Chèze, M. De Beer, J. Derré, G. Marel, E. Mazzucato, B. Peyaud, B. Vallage, M. Holder, M. Ziolkowski, C. Biino, N. Cartiglia, F. Marchetto, S. Bifani, M. Clemencic, S. Goy Lopez, H. Dibon, M. Jeitler, M. Markytan, I. Mikulec, G. Neuhofer, L. Widhalm, Phys. Lett. B **746**, 178 (2015). https://doi.org/10.1016/j.physletb.2015.04.068

186. B. Batell, M. Pospelov, A. Ritz, Phys. Rev. D **80**, 095024 (2009). https://doi.org/10.1103/PhysRevD.80.095024

187. T. Husek, K. Kampf, J. Novotný, Phys. Rev. D **92**, 054027 (2015)

188. C. Lazzeroni, N. Lurkin, A. Romano, T. Blazek, M. Koval, A. Ceccucci, H. Danielsson, V. Falaleev, L. Gatignon, S. Goy Lopez, B. Hallgren, A. Maier, A. Peters, M. Piccini, P. Riedler, P. Frabetti, E. Gersabeck, V. Kekelidze, D. Madigozhin, M. Misheva, N. Molokanova, S. Movchan, Y. Potrebenikov, S. Shkarovskiy, A. Zinchenko, P. Rubin, W. Baldini, A. Cotta Ramusino, P. Dalpiaz, M. Fiorini, A. Gianoli, A. Norton, F. Petrucci, M. Savrié, H. Wahl, A. Bizzeti, F. Bucci, E. Iacopini, M. Lenti, M. Veltri, A. Antonelli, M. Moulson, M. Raggi, T. Spadaro, K. Eppard, M. Hita-Hochgesand, K. Kleinknecht, B. Renk, R. Wanke, A. Winhart, R. Winston, V. Bolotov, V. Duk, E. Gushchin, F. Ambrosino, D. Di Filippo, P. Massarotti, M. Napolitano, V. Palladino, G. Saracino, G. Anzivino, E. Imbergamo, R. Piandani, A. Sergi, P. Cenci, M. Pepe, F. Costantini, N. Doble, S. Giudici, G. Pierazzini, M. Sozzi, S. Venditti, S. Balev, G. Collazuol, L. DiLella, S. Gallorini, E. Goudzovski, G. Lamanna, I. Mannelli, G. Ruggiero, C. Cerri, R. Fantechi, S. Kholodenko, V. Kurshetsov, V. Obraztsov, V. Semenov, O. Yushchenko, G. D'Agostini, E. Leonardi, M. Serra, P. Valente, A. Fucci, A. Salamon, B. Bloch-Devaux, B. Peyaud, J. Engelfried, D. Coward, V. Kozhuharov, L. Litov, R. Arcidiacono, S. Bifani, C. Biino, G. Dellacasa, F. Marchetto, T. Numao, F. Retière, Phys. Lett. B **768**, 38 (2017). https://doi.org/10.1016/j.physletb.2017.02.042

189. E.C. Gil, E.M. Albarrán, E. Minucci, G. Nüssle, S. Padolski, P. Petrov, N. Szilasi, B. Velghe, G. Georgiev, V. Kozhuharov, L. Litov, T. Husek, K. Kampf, M. Zamkovsky, R. Aliberti, K.H. Geib, G. Khoriauli, K. Kleinknecht, J. Kunze, D. Lomidze, R. Marchevski, L. Peruzzo, M. Vormstein, R. Wanke, A. Winhart, M. Bolognesi, V. Carassiti, S. Chiozzi, A.C. Ramusino, A. Gianoli, R. Malaguti, P. Dalpiaz, M. Fiorini, E. Gamberini, I. Neri, A. Norton, F. Petrucci, M. Statera, H. Wahl, F. Bucci, R. Ciaranfi, M. Lenti, F. Maletta, R. Volpe, A. Bizzeti, A. Cassese, E. Iacopini, A. Antonelli, E. Capitolo, C. Capoccia, A. Cecchetti, G. Corradi, V. Fascianelli, F. Gonnella, G. Lamanna, R. Lenci, G. Mannocchi, S. Martellotti, M. Moulson, C. Paglia, M. Raggi, V. Russo, M. Santoni, T. Spadaro, D. Tagnani, S. Valeri, T. Vassilieva, F. Cassese, L. Roscilli, F. Ambrosino, T. Capussela, D.D. Filippo, P. Massarotti, M. Mirra, M. Napolitano, G. Saracino, M. Barbanera, P. Cenci, B. Checcucci, V. Duk, L. Farnesini, E. Gersabeck, M. Lupi, A. Papi, M. Pepe, M. Piccini, G. Scolieri, D. Aisa, G. Anzivino, M. Bizzarri, C. Campeggi, E. Imbergamo, A. Piluso, C. Santoni, L. Berretta, S. Bianucci, A. Burato, C. Cerri, R. Fantechi, S. Galeotti, G. Magazzu', M. Minuti, A. Orsini, G. Petragnani, L. Pontisso, F. Raffaelli, F. Spinella, G. Collazuol, I. Mannelli,

C. Avanzini, F. Costantini, L.D. Lella, N. Doble, M. Giorgi, S. Giudici, E. Pedreschi, R. Piandani, G. Pierazzini, J. Pinzino, M. Sozzi, L. Zaccarelli, A. Biagioni, E. Leonardi, A. Lonardo, P. Valente, P. Vicini, G. D'Agostini, R. Ammendola, V. Bonaiuto, N.D. Simone, L. Federici, A. Fucci, G. Paoluzzi, A. Salamon, G. Salina, F. Sargeni, C. Biino, G. Dellacasa, S. Garbolino, F. Marchetto, S. Martoiu, G. Mazza, A. Rivetti, R. Arcidiacono, B. Bloch-Devaux, M. Boretto, L. Iacobuzio, E. Menichetti, D. Soldi, J. Engelfried, N. Estrada-Tristan, A.M. Bragadireanu, O.E. Hutanu, N. Azorskiy, V. Elsha, T. Enik, V. Falaleev, L. Glonti, Y. Gusakov, S. Kakurin, V. Kekelidze, S. Kilchakovskaya, E. Kislov, A. Kolesnikov, D. Madigozhin, M. Misheva, S. Movchan, I. Polenkevich, Y. Potrebenikov, V. Samsonov, S. Shkarovskiy, S. Sotnikov, L. Tarasova, M. Zaytseva, A. Zinchenko, V. Bolotov, S. Fedotov, E. Gushin, A. Khotjantsev, A. Khudyakov, A. Kleimenova, Y. Kudenko, A. Shaikhiev, A. Gorin, S. Kholodenko, V. Kurshetsov, V. Obraztsov, A. Ostankov, V. Rykalin, V. Semenov, V. Sugonyaev, O. Yushchenko, L. Bician, T. Blazek, V. Cerny, M. Koval, R. Lietava, G.A. Rinella, J.A. Garcia, S. Balev, M. Battistin, J. Bendotti, F. Bergsma, S. Bonacini, F. Butin, A. Ceccucci, P. Chiggiato, H. Danielsson, J. Degrange, N. Dixon, B. Döbrich, P. Farthouat, L. Gatignon, P. Golonka, S. Girod, A.G.M.D. Oliveira, R. Guida, F. Hahn, E. Harrouch, M. Hatch, P. Jarron, O. Jamet, B. Jenninger, J. Kaplon, A. Kluge, G. Lehmann-Miotto, P. Lichard, G. Maire, A. Mapelli, J. Morant, M. Morel, J. Noël, M. Noy, V. Palladino, A. Pardons, F. Perez-Gomez, L. Perktold, M. Perrin-Terrin, P. Petagna, K. Poltorak, P. Riedler, G. Romagnoli, G. Ruggiero, T. Rutter, J. Rouet, V. Ryjov, A. Saputi, T. Schneider, G. Stefanini, C. Theis, S. Tiuraniemi, F.V. Rodriguez, S. Venditti, M. Vergain, H. Vincke, P. Wertelaers, M.B. Brunetti, S. Edwards, E. Goudzovski, B. Hallgren, M. Krivda, C. Lazzeroni, N. Lurkin, D. Munday, F. Newson, C. Parkinson, S. Pyatt, A. Romano, X. Serghi, A. Sergi, R. Staley, A. Sturgess, H. Heath, R. Page, B. Angelucci, D. Britton, D. Protopopescu, I. Skillicorn, P. Cooke, J.B. Dainton, J.R. Fry, L. Fulton, D. Hutchcroft, E. Jones, T. Jones, K. Massri, E. Maurice, K. McCormick, P. Sutcliffe, B. Wrona, A. Conovaloff, P. Cooper, D. Coward, P. Rubin, R. Winston, J. Instrum. **12**(05), P05025 (2017). https://doi.org/10.1088/1748-0221/12/05/p05025

190. NA62 Collaboration, Searches for lepton number violating $k^+ \rightarrow \pi^- (\pi^0) e^+ e^+$ decays (2022). arXiv:2202.00331
191. G.L. Marco Fabbrichesi, E. Gabrielli, *The Physics of the Dark Photon* (Springer, Berlin, 2021)
192. K. Arndt et al., Nucl. Instrum. Methods A **1014**, 165679 (2021). https://doi.org/10.1016/j.nima.2021.165679
193. U. Bellgardt et al., Nucl. Phys. B **299**, 1 (1988). https://doi.org/10.1016/0550-3213(88)90462-2
194. J. Alwall et al., JHEP **07**, 079 (2014). https://doi.org/10.1007/JHEP07(2014)079
195. S. Agostinelli et al., Nucl. Instrum. Methods A **506**(3), 250 (2003). https://doi.org/10.1016/S0168-9002(03)01368-8
196. D. Becker, R. Bucoveanu, C. Grzesik, K. Imai, R. Kempf, M. Molitor, A. Tyukin, M. Zimmermann, D. Armstrong, K. Aulenbacher, S. Baunack, R. Beminiwattha, N. Berger, P. Bernhard, A. Brogna, L. Capozza, S. Covrig Dusa, W. Deconinck, J. Diefenbach, J. Dunne, J. Erler, C. Gal, M. Gericke, B. Gläser, M. Gorchtein, B. Gou, W. Gradl, Y. Imai, K.S. Kumar, F. Maas, J. Mammei, J. Pan, P. Pandey, K. Paschke, I. Perić, M. Pitt, S. Rahman, S. Riordan, D. Rodríguez Piñeiro, C. Sfienti, I. Sorokin, P. Souder, H. Spiesberger, M. Thiel, V. Tyukin, Q. Weitzel, Eur. Phys. J. A **54**(11), 208 (2018). https://doi.org/10.1140/epja/i2018-12611-6
197. T. Stengler, K. Aulenbacher, R. Heine, M. Pekeler, F. Schlander, D. Simon, D. Trompetter, in *Proc. of International Conference on RF Superconductivity (SRF2015), Whistler, BC, Canada, Sept. 13–18, 2015*, ed. by R.E.L. (TRIUMF, Vancouver, BC, Canada), J.T. (TRIUMF, Vancouver, BC, Canada), V.R.S. (GSI, Darmstadt, Germany), JACoW (JACoW, Geneva, Switzerland, 2015), no. 17 in International Conference on RF Superconductivity, pp. 1413–1416. https://doi.org/10.18429/JACoW-SRF2015-THPB116. http://srf2015.vrws.de/papers/thpb116.pdf
198. H. Merkel, P. Achenbach, C. Ayerbe Gayoso, J.C. Bernauer, R. Böhm, D. Bosnar, L. Debenjak, A. Denig, M.O. Distler, A. Esser, H. Fonvieille, I. Friščić, D.G. Middleton, U. Müller, L. Nungesser, J. Pochodzalla, M. Rohrbeck, S. Sánchez Majos, B.S. Schlimme, M. Schoth, S. Širca, M. Weinriefer, Phys. Rev. Lett. **106**, 251802 (2011). https://doi.org/10.1103/PhysRevLett.106.251802
199. H. Merkel, P. Achenbach, C. Ayerbe Gayoso, T. Beranek, J. Beričič, J.C. Bernauer, R. Böhm, D. Bosnar, L. Correa, L. Debenjak, A. Denig, M.O. Distler, A. Esser, H. Fonvieille, I. Friščić, H. Gómez Rodríguez de la Paz, M. Hoek, S. Kegel, Y. Kohl, D.G. Middleton, M. Mihovilovič, U. Müller, L. Nungesser, J. Pochodzalla, M. Rohrbeck, G. Ron, S. Sánchez Majos, B.S. Schlimme, M. Schoth, F. Schulz, C. Sfienti, S. Širca, M. Thiel, A. Tyukin, A. Weber, M. Weinriefer, Phys. Rev. Lett. **112**, 221802 (2014). https://doi.org/10.1103/PhysRevLett.112.221802
200. J.D. Bjorken, R. Essig, P. Schuster, N. Toro, Phys. Rev. D **80**, 075018 (2009). https://doi.org/10.1103/PhysRevD.80.075018
201. E. Izaguirre, G. Krnjaic, P. Schuster, N. Toro, Phys. Rev. Lett. **115**, 251301 (2015). https://doi.org/10.1103/PhysRevLett.115.251301
202. S.N. Gninenko, N.V. Krasnikov, V.A. Matveev, Phys. Part. Nucl. **51** (2020). https://doi.org/10.1134/S1063779620050044
203. J.P. Lees, V. Poireau, V. Tisserand, E. Grauges, A. Palano, G. Eigen, D.N. Brown, M. Derdzinski, A. Giuffrida, Y.G. Kolomensky, M. Fritsch, H. Koch, T. Schroeder, C. Hearty, T.S. Mattison, J.A. McKenna, R.Y. So, V.E. Blinov, A.R. Buzykaev, V.P. Druzhinin, V.B. Golubev, E.A. Kravchenko, A.P. Onuchin, S.I. Serednyakov, Y.I. Skovpen, E.P. Solodov, K.Y. Todyshev, A.J. Lankford, J.W. Gary, O. Long, A.M. Eisner, W.S. Lockman, W. Panduro Vazquez, D.S. Chao, C.H. Cheng, B. Echenard, K.T. Flood, D.G. Hitlin, J. Kim, T.S. Miyashita, P. Ongmongkolkul, F.C. Porter, M. Röhrken, Z. Huard, B.T. Meadows, B.G. Pushpawela, M.D. Sokoloff, L. Sun, J.G. Smith, S.R. Wagner, D. Bernard, M. Verderi, D. Bettoni, C. Bozzi, R. Calabrese, G. Cibinetto, E. Fioravanti, I. Garzia, E. Luppi, V. Santoro, A. Calcaterra, R. de Sangro, G. Finocchiaro, S. Martellotti, P. Patteri, I.M. Peruzzi, M. Piccolo, M. Rotondo, A. Zallo, S. Passaggio, C. Patrignani, H.M. Lacker, B. Bhuyan, U. Mallik, C. Chen, J. Cochran, S. Prell, H. Ahmed, A.V. Gritsan, N. Arnaud, M. Davier, F. Le Diberder, A.M. Lutz, G. Wormser, D.J. Lange, D.M. Wright, J.P. Coleman, E. Gabathuler, D.E. Hutchcroft, D.J. Payne, C. Touramanis, A.J. Bevan, F. Di Lodovico, R. Sacco, G. Cowan, S. Banerjee, D.N. Brown, C.L. Davis, A.G. Denig, W. Gradl, K. Griessinger, A. Hafner, K.R. Schubert, R.J. Barlow, G.D. Lafferty, R. Cenci, A. Jawahery, D.A. Roberts, R. Cowan, S.H. Robertson, B. Dey, N. Neri, F. Palombo, R. Cheaib, L. Cremaldi, R. Godang, D.J. Summers, P. Taras, G. De Nardo, C. Sciacca, G. Raven, C.P. Jessop, J.M. LoSecco, K. Honscheid, R. Kass, A. Gaz, M. Margoni, M. Posocco, G. Simi, F. Simonetto, R. Stroili, S. Akar, E. Ben-Haim, M. Bomben, G.R. Bonneaud, G. Calderini, J. Chauveau, G. Marchiori, J. Ocariz, M. Biasini, E. Manoni, A. Rossi, G. Batignani, S. Bettarini, M. Carpinelli, G. Casarosa, M. Chrzaszcz, F. Forti, M.A. Giorgi, A. Lusiani, B. Oberhof, E. Paoloni, M. Rama, G. Rizzo, J.J. Walsh, A.J.S. Smith, F. Anulli, R. Faccini, F. Ferrarotto, F. Ferroni, A. Pilloni, G. Piredda, C. Bünger, S. Dittrich, O. Grünberg, M. Heß, T. Leddig, C. Voß, R. Waldi, T. Adye, F.F. Wilson, S. Emery, G. Vasseur, D. Aston, C. Cartaro, M.R. Convery, J. Dorfan, W. Dunwoodie, M. Ebert, R.C. Field, B.G. Fulsom, M.T. Gra-

ham, C. Hast, W.R. Innes, P. Kim, D.W.G.S. Leith, S. Luitz, D.B. MacFarlane, D.R. Muller, H. Neal, B.N. Ratcliff, A. Roodman, M.K. Sullivan, J. Va'vra, W.J. Wisniewski, M.V. Purohit, J.R. Wilson, A. Randle-Conde, S.J. Sekula, M. Bellis, P.R. Burchat, E.M.T. Puccio, M.S. Alam, J.A. Ernst, R. Gorodeisky, N. Guttman, D.R. Peimer, A. Soffer, S.M. Spanier, J.L. Ritchie, R.F. Schwitters, J.M. Izen, X.C. Lou, F. Bianchi, F. De Mori, A. Filippi, D. Gamba, L. Lanceri, L. Vitale, F. Martinez-Vidal, A. Oyanguren, J. Albert, A. Beaulieu, F.U. Bernlochner, G.J. King, R. Kowalewski, T. Lueck, I.M. Nugent, J.M. Roney, R.J. Sobie, N. Tasneem, T.J. Gershon, P.F. Harrison, T.E. Latham, R. Prepost, S.L. Wu, Phys. Rev. Lett. **119**, 131804 (2017). https://doi.org/10.1103/PhysRevLett.119.131804

204. A.A. Aguilar-Arevalo, M. Backfish, A. Bashyal, B. Batell, B.C. Brown, R. Carr, A. Chatterjee, R.L. Cooper, P. deNiverville, R. Dharmapalan, Z. Djurcic, R. Ford, F.G. Garcia, G.T. Garvey, J. Grange, J.A. Green, W. Huelsnitz, I.L. de Icaza Astiz, G. Karagiorgi, T. Katori, W. Ketchum, T. Kobilarcik, Q. Liu, W.C. Louis, W. Marsh, C.D. Moore, G.B. Mills, J. Mirabal, P. Nienaber, Z. Pavlovic, D. Perevalov, H. Ray, B.P. Roe, M.H. Shaevitz, S. Shahsavarani, I. Stancu, R. Tayloe, C. Taylor, R.T. Thornton, R. Van de Water, W. Wester, D.H. White, J. Yu, Phys. Rev. Lett. **118**, 221803 (2017). https://doi.org/10.1103/PhysRevLett.118.221803

205. D. Akimov, P. An, C. Awe, P.S. Barbeau, B. Becker, V. Belov, I. Bernardi, M.A. Blackston, C. Bock, A. Bolozdynya, J. Browning, B. Cabrera-Palmer, D. Chernyak, E. Conley, J. Daughhetee, J. Detwiler, K. Ding, M.R. Durand, Y. Efremenko, S.R. Elliott, L. Fabris, M. Febbraro, A.G. Rosso, A. Galindo-Uribarri, M.P. Green, M.R. Heath, S. Hedges, D. Hoang, M. Hughes, T. Johnson, A. Khromov, A. Konovalov, E. Kozlova, A. Kumpan, L. Li, J.M. Link, J. Liu, K. Mann, D.M. Markoff, J. Mastroberti, P.E. Mueller, J. Newby, D.S. Parno, S.I. Penttila, D. Pershey, R. Rapp, H. Ray, J. Raybern, O. Razuvaeva, D. Reyna, G.C. Rich, J. Ross, D. Rudik, J. Runge, D.J. Salvat, A.M. Salyapongse, K. Scholberg, A. Shakirov, G. Simakov, G. Sinev, W.M. Snow, V. Sosnovstsev, B. Suh, R. Tayloe, K. Tellez-Giron-Flores, I. Tolstukhin, E. Ujah, J. Vanderwerp, R.L. Varner, C.J. Virtue, G. Visser, T. Wongjirad, Y.R. Yen, J. Yoo, C.H. Yu, J. Zettlemoyer, First probe of sub-GeV dark matter beyond the cosmological expectation with the coherent CsI detector at the SNS (2021). arXiv:2110.11453

206. G. Angloher, P. Bauer, A. Bento, C. Bucci, L. Canonica, X. Defay, A. Erb, F.v. Feilitzsch, N.F. Iachellini, P. Gorla, A. Gütlein, D. Hauff, J. Jochum, M. Kiefer, H. Kluck, H. Kraus, J.C. Lanfranchi, J.Loebell, M. Mancuso, A. Münster, C. Pagliarone, F. Petricca, W. Potzel, F. Pröbst, R. Puig, F. Reindl, K. Schäffner, J. Schieck, S. Schönert, W. Seidel, L. Stodolsky, C. Strandhagen, R. Strauss, A. Tanzke, H.H.T. Thi, C. Türkoğlu, M. Uffinger, A. Ulrich, I. Usherov, S. Wawoczny, M. Willers, M. Wüstrich, A. Zöller, Eur. Phys. J. C **77**, 299 (2017). https://doi.org/10.1140/epjc/s10052-017-4878-6

207. B. Schlimme, S. Aulenbacher, P. Brand, M. Littich, Y. Wang, P. Achenbach, M. Ball, J. Bernauer, M. Biroth, D. Bonaventura, D. Bosnar, S. Caiazza, M. Christmann, E. Cline, A. Denig, M. Distler, L. Doria, P. Eckert, A. Esser, I. Friščić, S. Gagneur, J. Geimer, S. Grieser, P. Gülker, P. Herrmann, M. Hoek, S. Kegel, J. Kelsey, P. Klag, A. Khoukaz, M. Kohl, T. Kolar, M. Lauß, L. Leßmann, S. Lunkenheimer, J. Mareković, D. Markus, M. Mauch, H. Merkel, M. Mihovilovič, R. Milner, J. Müller, U. Müller, T. Petrović, J. Pochodzalla, J. Rausch, J. Schlaadt, H. Schürg, C. Sfienti, S. Širca, R. Spreckels, S. Stengel, Y. Stöttinger, C. Szyszka, M. Thiel, S. Vestrick, C. Vidal, Nucl. Instrum. Methods Phys. Res. Sect. A: Accel. Spectrom. Detect. Assoc. Equip. **1013**, 165668 (2021). https://doi.org/10.1016/j.nima.2021.165668

208. L. Doria, P. Achenbach, M. Christmann, A. Denig, P. Guelker, H. Merkel, Search for light dark matter with the mesa accelerator (2018). arXiv:1809.07168

209. M. Lauß, P. Achenbach, S. Aulenbacher, M. Ball, I. Beltschikow, M. Biroth, P. Brand, S. Caiazza, M. Christmann, O. Corell, A. Denig, L. Doria, P. Drexler, J. Geimer, P. Gülker, T. Kolar, W. Lauth, M. Littich, M. Lupberger, S. Lunkenheimer, D. Markus, M. Mauch, H. Merkel, M. Mihovilovič, J. Müller, B. Schlimme, C. Sfienti, S. Širca, S. Stengel, C. Szyszka, S. Vestrick, Nucl. Instrum. Methods Phys. Res. Sect. A: Accel. Spectrom. Detect. Assoc. Equip. **1012**, 165617 (2021). https://doi.org/10.1016/j.nima.2021.165617

210. M. Christmann, P. Burger, P. Achenbach, S. Aulenbacher, M. Ball, S. Baunack, J. Bernauer, M. Biroth, P. Brand, S. Caiazza, E. Cline, A. Denig, L. Doria, I. Friščić, J. Geimer, P. Gülker, A. Khoukaz, M. Kohl, T. Kolar, M. Lauß, W. Lauth, M. Littich, M. Lupberger, S. Lunkenheimer, F. Maas, M. Mauch, H. Merkel, M. Mihovilovič, R. Milner, J. Müller, J. Rausch, B. Schlimme, C. Sfienti, S. Širca, S. Stengel, C. Szyszka, S. Vestrick, Y. Wang, Nucl. Instrum. Methods Phys. Res. Sect. A: Accel. Spectrom. Detect. Assoc. Equip. **960**, 163665 (2020). https://doi.org/10.1016/j.nima.2020.163665

211. M. Christmann, P. Achenbach, S. Baunack, P. Burger, A. Denig, L. Doria, F. Maas, H. Merkel, Nucl. Instrum. Methods Phys. Res. Sect. A: Accel. Spectrom. Detect. Assoc. Equip. **958**, 162398 (2020). https://doi.org/10.1016/j.nima.2019.162398. Proceedings of the Vienna Conference on Instrumentation 2019

212. M. Battaglieri, A. Bersani, G. Bracco, B. Caiffi, A. Celentano, R. De Vita, L. Marsicano, P. Musico, M. Osipenko, F. Panza, M. Ripani, E. Santopinto, M. Taiuti, V. Bellini, M. Bondi', P. Castorina, M. De Napoli, A. Italiano, V. Kuznetzov, E. Leonora, F. Mammoliti, N. Randazzo, L. Re, G. Russo, M. Russo, A. Shahinyan, M. Sperduto, S. Spinali, C. Sutera, F. Tortorici, N. Baltzell, M. Dalton, A. Freyberger, F.X. Girod, G. Kharashvili, V. Kubarovsky, E. Pasyuk, E.S. Smith, S. Stepanyan, M. Ungaro, T. Whitlatch, E. Izaguirre, G. Krnjaic, D. Snowden-Ifft, D. Loomba, M. Carpinelli, D. D'Urso, A. Gabrieli, G. Maccioni, M. Sant, V. Sipala, F. Ameli, E. Cisbani, F. De Persio, A. Del Dotto, F. Garibaldi, F. Meddi, C.A. Nicolau, G.M. Urciuoli, T. Chiarusi, M. Manzali, C. Pellegrino, P. Schuster, N. Toro, R. Essig, M.H. Wood, M.H.R. Paremuzyan, G. De Cataldo, R. De Leo, D. Di Bari, L. Lagamba, E. Nappi, R. Perrino, I. Balossino, L. Barion, G. Ciullo, M. Contalbrigo, A. Drago, P. Lenisa, A. Movsisyan, L. Pappalardo, F. Spizzo, M. Turisini, D. Hasch, V. Lucherini, M. Mirazita, S. Pisano, P. Rossi, S. Tomassini, G. Simi, A. D'Angelo, L. Lanza, A. Rizzo, C. Schaerf, I. Zonta, A. Filippi, M. Genovese, S. Fegan, M. Kunkel, M. Bashkanov, A. Murphy, G. Smith, D. Watts, N. Zachariou, L. Zana, D. Glazier, D. Ireland, B. McKinnon, D. Sokhan, L. Colaneri, S.A. Pereira, A. Afanasev, B. Briscoe, I. Strakovsky, N. Kalantarians, L. Weinstein, K.P. Adhikari, J.A. Dunne, D. Dutta, L.E. Fassi, L. Ye, K. Hicks, P. Cole, S. Dobbs, C. Fanelli, P.T.M. Murthy, Dark matter search in a beam-dump experiment (BDX) at Jefferson lab: an update on PR12-16-001 (2017). arXiv:1712.01518

213. J. Battat, A. Ezeribe, J.L. Gauvreau, J. Harton, R. Lafler, E. Law, E. Lee, D. Loomba, A. Lumnah, E. Miller, A. Monte, F. Mouton, S. Paling, N. Phan, M. Robinson, S. Sadler, A. Scarff, F. Schuckman II., D. Snowden-Ifft, N. Spooner, N. Waldram, Astropart. Phys. **91**, 65 (2017). https://doi.org/10.1016/j.astropartphys.2017.03.007

214. J. Alexander et al., Dark sectors 2016 workshop: community report (2016). arXiv:1608.08632 [hep-ph]

215. M. Battaglieri et al., US cosmic visions: new ideas in dark matter 2017: community report, in *U.S. Cosmic Visions: New Ideas in Dark Matter.* FERMILAB-CONF-17-282-AE-PPD-T (2017). arXiv:1707.04591 [hep-ph]

216. W. Xiong et al., Nature **575**(7781), 147 (2019). https://doi.org/10.1038/s41586-019-1721-2
217. A. Gasparian et al. (PRad), PRad-II: a new upgraded high precision measurement of the proton charge radius (2020). arXiv:2009.10510 [nucl-ex]
218. T. Albahri et al., Phys. Rev. A **103**(4), 042208 (2021). https://doi.org/10.1103/PhysRevA.103.042208
219. G.W. Bennett et al., Phys. Rev. D **73**, 072003 (2006). https://doi.org/10.1103/PhysRevD.73.072003
220. L. Foggetta et al., in *12th International Particle Accelerator Conference* (2021). https://doi.org/10.18429/JACoW-IPAC2021-THPAB113
221. F. Oliva, Nucl. Instrum. Methods A 162354 (2019). https://doi.org/10.1016/j.nima.2019.162354
222. P. Albicocco et al., JINST **15**(10), T10003 (2020). https://doi.org/10.1088/1748-0221/15/10/T10003
223. A. Frankenthal et al., Nucl. Instrum. Methods A **919**, 89 (2019). https://doi.org/10.1016/j.nima.2018.12.035
224. F. Ferrarotto et al., IEEE Trans. Nucl. Sci. **65**(8), 2029 (2018). https://doi.org/10.1109/TNS.2018.2822724